Dynamic Performance of Magnetically Levitated Rotors

by

Benny Wahjudi Tjahjono

Submitted to the Department of Mechanical Engineering
in partial fulfillment of the requirements for the degree of

Master of Science in Mechanical Engineering

at the

MASSACHUSETTS INSTITUTE OF TECHNOLOGY

May 1995

© Massachusetts Institute of Technology 1995. All rights reserved.

Author .....
Department of Mechanical Engineering
May 12, 1995

Certified by .....
Kamal Youcef-Toumi
Associate Professor
Thesis Supervisor

Accepted by .....
Ain Sonin
Chairman, Departmental Committee on Graduate Students

MASSACHUSETTS INSTITUTE
OF TECHNOLOGY

AUG 31 1995

LIBRARIES Barker Eng

Dynamic Performance of Magnetically Levitated Rotors

by

Benny Wahjudi Tjahjono

Submitted to the Department of Mechanical Engineering
on May 12, 1995, in partial fulfillment of the
requirements for the degree of
Master of Science in Mechanical Engineering

Abstract

Magnetic bearings are selected as the physical systems because of the recent tremendous research activity in their use in high performance machines. The input-output characteristic makes such a system inherently nonlinear and unstable, so it is necessary to implement a desired control to it. However, if the system dynamic behavior and the limitations from the control system hardware as a whole are not incorporated into the electro-mechanical and the control system design, the desired system performance may not be realizable.

This thesis treats the equations of motion of a rigid, horizontal rotor magnetic bearing system. Through LQ feedback linearization and describing function methodology to approximate the saturation nonlinearity at the input level, the open-loop system characteristic is analized. This system is then simulated to demonstrate disturbance rejection properties and its robustness to parameter uncertainty and unmodelled dynamics. Such procedure results in the information of the performance limitation of a magnetic bearing system for the purpose of any further implementation of its control design.

Thesis Supervisor: Kamal Youcef-Toumi
Title: Associate Professor

Acknowledgments

I am very grateful to my thesis supervisor, *Prof. Kamal Youcef- Toumi* for his advice and assistance throughout my thesis work. His ideas, comments, and suggestions have helped me a great deal.

Students involved in collaboration during my thesis work need to be acknowledged (in alphabetical order): *Mr. Ali Yurdun Orbak*, a graduate student has been helpful in assisting me with using LaTex; *Mr. Jake Wetzel*, a graduate student is continuing experiments with control of magnetic bearings; *Mr. T-J. Yeh*, a graduate student whose paper got me started with the project and has been a helpful lab partner.

Most of all, I thank God for His continuing love and assistance for me.

Contents

1 Introduction **8**

1.1 Advantages and Disadvantages 9

1.2 Types of magnetic bearings 10

2 Rotor Dynamics **13**

2.1 Introduction 13

2.2 Imbalance 13

2.3 Balancing 14

2.3.1 Static Balancing 14

2.3.2 Dynamic Balancing 15

2.3.3 Flexible Shaft Balancing 19

2.4 Gravity Effect 20

2.5 Gyroscopic Effect 20

2.6 System Identification 23

2.7 Asymmetry Of Rotating Shaft Parts 26

2.7.1 The Free Vibration 29

2.7.2 The Forced Vibration 31

2.8 Shaft and Mount 32

2.8.1 Flexibility 32

2.8.2 Damping 32

2.9 Instability 33

2.10 Critical Speed 35

2.10.1 Coupled Critical Speed 37

2.11 Whirling 39

3 Performance Analysis **42**

3.1 Nonlinear System 42

3.1.1 Current Limitation 42

3.1.2 Magnetic Saturation 44

3.2 System Identification 46

3.3 Summary 57

4 Simulation and Results **59**

4.1 Introduction 59

4.2 System Parameters 59

4.3 LQ Regulator 62

4.3.1 LQR Design with Relative Stability 71

4.4 Saturation Limit 76

4.4.1 Results 79

4.5 Stability: Popov method 81

4.6 Stiffness 83

4.6.1 Results 84

4.7 Disturbance 86

4.7.1 Results 87

4.8 Summary 90

5 Conclusion and Recommendation **91**

A The Describing Function of Saturation Nonlinearity **93**

B Magnetic Force for Bearings **99**

C Open-loop Matrices: Numerical Results **104**

List of Figures

2-1 Static balancing model 15

2-2 A rotor that is statically out of balance 16

2-3 Correction planes 18

2-4 Balanced disk on a massless, horizontal elastic shaft 21

2-5 Gyroscopic Movement 22

2-6 The Fixed and Rotating Coordinate Systems 23

2-7 Possible configurations for steady motion of a disk 33

2-8 Damper and Spring 34

2-9 Rotating disk with a spring-restrained mass in a radial slot 35

2-10 Disk on flexible mounted bearings 36

2-11 Lissajous figures traced by a point on a shaft at a given longitudinal station undergoing transverse vibratory motions at the same frequency on two planes 41

3-1 The Relationship between the Control u and the Coil Currents I_l and I_u 43

3-2 The control current setup in the radial direction 46

3-3 A Rotor Model 49

4-1 The open-loop roots 62

4-2 Linear Quadratic Regulator Design 63

4-3 LQ Loop 65

4-4 LQR Design: Closed-loop Poles 66

4-5 LQR Design: Frequency Domains, $\rho = 10^{-3}$ 68

4-6 LQR Design: Frequency Domains, $\rho = 10^{-3}$ 68

4-7 LQR Design: Initial Value, $\rho = 10^{-3}$ 69
4-8 LQR Design: Disturbance Rejection Test, $\rho = 10^{-3}$ 69
4-9 LQR-design Roots 72
4-10 LQR Design: Frequency Domains, $\rho = 10^{-3}, b = 100$ 73
4-11 LQR Design: Frequency Domains, $\rho = 10^{-3}, b = 100$ 74
4-12 LQR Design: Initial Value, $\rho = 10^{-3}, b = 100$ 75
4-13 LQR Design: Disturbance Rejection Test, $\rho = 10^{-3}, b = 100$ 75
4-14 LQR Design with Saturation Limit 76
4-15 Closed-loop System 78
4-16 A saturation nonlinearity 79
4-17 Closed-loop transfer function, r = 0.5, k = 1, tol = 0.006 80
4-18 Closed-loop transfer function, r = 0.5, k = 2, tol = 0.03 80
4-19 Closed-loop transfer function, r = 0.3, k = 1, tol = 0.01 81
4-20 Closed-loop transfer function, r = 0.3, k = 2, tol = 0.03 82
4-21 Stability Checking 83
4-22 Minimum stiffness, without any describing function element 84
4-23 Minimum stiffness, r = 0.5, k = 1, tol = 0.006 85
4-24 Minimum stiffness, r = 0.5, k = 2, tol = 0.03 85
4-25 Minimum stiffness, r = 0.3, k = 1, tol = 0.01 86
4-26 Minimum stiffness, r = 0.3, k = 2, tol = 0.03 87
4-27 Disturbance-to-output, r = 0.5, k = 1, tol = 0.006 88
4-28 Disturbance-to-output, r = 0.5, k = 2, tol = 0.03 88
4-29 Disturbance-to-output, r = 0.3, k = 1 89
4-30 Disturbance-to-output, r = 0.3, k = 2 90

A-1 A nonlinear element and its describing function representation 94
A-2 A saturation nonlinearity 95
A-3 Saturation; axis1 = $\frac{x}{\delta}$, axis2 = Magnitude 97

B-1 Coil Windings for an Electromagnet of a Bearing 100
B-2 Coil and Contour for Faraday's Law 100

Chapter 1

Introduction

The magnetic bearing setup consisting of four magnets is widely manufactured in order to apply the non-contacting type control force to a rotor system during operation. A magnetic bearing typically consists of an even number of electromagnetics with alternating north and south poles wrapped around the axis of a rotating shaft. The poles are oriented facing the axis in a journal bearing and parallel to the axis in a thrust bearing [9]. A setup generally consists of two separate systems, which are an axial positioning system (*thrust bearing*), and a pair of radial positioning systems (*journal bearing*). If it is necessary to protect, in event of power failure or loss of critical system, then an auxiliary bearing (*catcher bearing*, or *backup operational bearing*) could be augmented to the system.

Journal and *stator*, like those of an induction motor, are stacks of ferromagnetic lamination so thin that its eddy current effect becomes negligible. A *journal* is a plain disk, while a *stator* is wound with magnetizing coils to form pairs of north-south poles; each is driven by a separate power amplifier, which actively controls the current in the coils. A *rotor* is suspended and stabilized within a stator. Steady state (*bias*) current is induced to the magnetizing coils. The control current is superimposed on the bias current to regulate the attractive force on the journal. The bias current is much larger than the control current, and the total current never changes its polarity

in a power amplifier[1]. If the journal excursion is relatively large in gap, then the linearized controls are essentially uncoupled in two independent directions [3].

1.1 Advantages and Disadvantages

Magnetic bearing systems are indispensable for

1. suspending and spinning the shaft at high speed operation,
2. the ability to utilize thinner and less rigid shafts which results in reduced weight and increased in design flexibility,
3. its frictionless nature resulting in high temperature or vacuum condition operation,
4. lubrication-free operations resulting in the savings in construction time, start-up time (e.g. oil flushing), maintenance time and related maintenance free operations,
5. having the adjustable damping and stiffness which mainly depend upon the frequency,
6. permitting the active control of bearing dynamics characteristics which lead to the foundation of an external control algorithm,
7. having the existing wide range of possible dynamic characteristics enabling the placement of the critical operation speeds of a particular machine,
8. optimization at several different speeds by merely changing the constant system parameters.

[1]Such setup satisfies the control circuitry and provides a base for a linearized control scheme.

On the other hand, the disadvantages include

1. high initial equipment cost,
2. lack of the operating data to confirm the performance expectations,
3. unstable characteristic.

Due to their unstable nature, they require external electrical control to regulate electromagnetic forces acting on bearings[2].

Nowadays, the magnetic bearing applications are found in some industrial, military, and space systems. The advancement in rotor and material technology has resulted in some applications such as turbines and compressors, rotating at the speeds previously unattainable, e.g. *maglev* (magnetically levitated) high-speed train.

1.2 Types of magnetic bearings

Three main types of magnetic bearings [9]:

1. *active* magnetic journal bearings, such in turbo-machinery. Its advantages over fluid film bearings include the low power loss, the elimination of lubrication systems, and the control ability of the bearing forces to minimize vibration.
2. *passive* magnetic bearings.
3. *hybrid* magnetic bearings, i.e. eddy current magnetic bearings.

An active magnetic bearing generally consists of a stationary electromagnet called *stator*, and a rotating ferrous material called *rotor* that are used to allow a shaft to be suspended in a magnetic field. The shaft position is maintained dynamically. Such process is done utilizing sensors that provide continuous feedback through control and amplification system to the electromagnetic poles to suspend the shaft. One example of its applications is a *gas compressor*.

[2] *Earnshaw* theorem states that stable and complete levitation cannot be achieved by solely using permanent magnets [6].

Based on the types of configuration (either of the two force mechanism), in conventional bearing, the attractive force is generated between a magnet and a piece of magnetic material as in fluid film, ball or rolling element devices, where load capacity is determined by wear and heating. Such scheme is highly unstable; it requires feedback control to obtain a desired *stiffness* characteristic[4]. Another scheme is based on the force of repulsion, which is caused by eddy current induced in a conducting but non-magnetic rotor and some stationary magnets driven by a time-varying current. Lately, magnetic bearings were invented where their specific load capacity is only due to the saturation of the magnetic material.

The primary role of any bearing is to restrain the motion of the supporting rotor in response to any applied loads, and also the load response to satisfy a given set of performance constraints[3] However, no explicit load capacity requirement has been established for stability (by the dynamic properties of the bearing itself) on the bearings.

The rotating parts, while having the same characteristics as the stator and rotor of an electric motor, are able to provide a long life without requirement for planned maintenance. The bearing is not sensitive to many process fluids, or within certain limits, to the process fluid temperature or pressure. In a submerged motor concept, the complexity associated with gas/lubricant seals or gas buffering is eliminated. The on-line control of the rotor allows loading, eccentricity, shaft position and vibration to be controlled and remotely monitored for both short and long terms. The machine vibration reduction will extend the operating life significantly and reduce cost of routine maintenance and repair. The system reliability will also be improved, and could be enhanced further with redundant controls and power supplies. Furthermore, the shaft speed rangle will be unlimited by circumferential speed and bearing limitations [12].

This thesis will investigate the feasibility of electromagnet suspension of a rotating shaft without mechanical contact. In such configuration, there are many possibilities to implement a wide variety of modern control strategies under computer control

[3]When it is achieved, the load is said to be *accommodated.*

[7, 11].

Chapter two describes the dynamics analysis of a rotor system. The rotor is assumed to consist of a rigid disk on a flexible shaft (*Jeffcott* model). Taking into account the mass unbalance and shaft flexibility, the general fomulation is then derived for this specific model of rotor. Some important dynamic features of a rotor due to its critical speed, whirling, and asymmetric shaft are also discussed.

Chapter three describes the performance of a magnetic bearing system. The rigid disk model derived on Chapter 2 is extended for the rigid body of a rotor to include the gyroscopic effect motion. The inherently nonlinear system is formulated and linearized at its equilibrium operating point. The system matrices is then set up to analize the nominal performance.

Chapter four presents the numerical and simulation results. The LQ regulator methodology is utilized to stabilize the open-loop system. The describing function element to represent the current limitation at the input is then applied, and the system is analized to determine its overall closed-loop performance.

Chapter five provides the conclusion and recommendation for further research.

Chapter 2

Rotor Dynamics

2.1 Introduction

This chapter covers some fundamental aspects of a rotor from its static and dynamic perspectives. *Sect.2.1.* illustrates the cause of static, dynamic, and flexibility imbalances, while *sect.2.2.* demonstrates how to overcome such imbalance types by the so-called balancing methods. Rotor imbalance can result in a gravity effect (*sect.2.3.*) that will generate a pulsating torque on the shaft. Gyroscopic effect upon the rotor critical speed is also determined in *sect.2.4.* Furthermore, the influence of asymmetry of rotating shaft parts on the critical speeds is remarked in *sect.2.5.* In *sect.2.6.*, the flexibility of the shaft and the mount could be represented as elastic springs, while in *sect.2.7.*, the shaft and mount damping are represented as radial dampers. The dynamic instability is partly determined by the shaft deflection (*sect.2.8.*) which depends upon frequencies. More importantly, the critical speed and the rotor natural lateral frequencies are covered in *sect.2.9.* Shaft whirling is mentioned in the last part (*sect.2.10.*).

2.2 Imbalance

In any real system, when a disk is set on an infinitely rigid shaft, there is always an offset distance of the center of mass from the geometric center of its concentrically

round section due to mass imbalance. Such offset distance is called *eccentricity* (ϵ) [14].

There are three (3) types of imbalance:

1. *Static imbalance*, where the center of gravity is offset from the axis of rotation while the principal axis of inertia is still oriented in the same direction as the axis of rotation.

2. *Dynamic imbalance*, to describe the angular misalignment of the shaft principal axis of inertia with respect to the axis of rotation. Both static and dynamic imbalance are generally present due to manufacturing tolerances.

3. *Flexibility imbalance* due to the shaft flexibility when it is rotating near the vicinity of its critical speeds.

Imbalance will affect the internal friction of most conventional rotors such as the slippage between one set of contact surfaces of such as built-up rotors may not begin at the same operating speed as between another set. Moreover, an increasing imbalance may enact more sources of internal friction for a given operating speed [14].

In a high speed machine, any small geometric imbalance will cause a large oscillatory force to transmit to the supporting structure, while any large imbalance will increase the possibility of fatigue failures in the rotating shaft or premature bearing wear and seizure.

2.3 Balancing

2.3.1 Static Balancing

Static imbalance can be detected without acting the rotor into rotation. If a statically imbalanced shaft with concentrically round surface is set across two perfect level, flat and parallel supports, then the rotor will rotate until its center of the mass is at the lowest point. The method of balancing is then to affix a mass 180 degrees away from

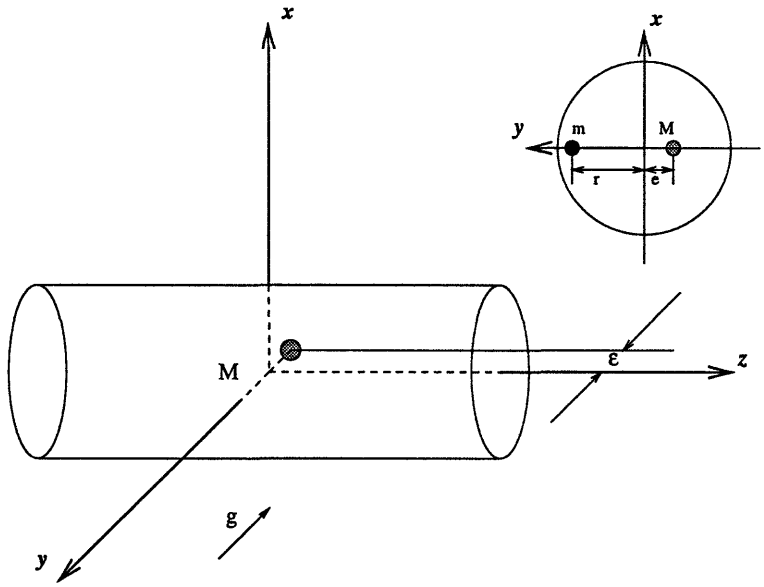

Figure 2-1: Static balancing model

this center of mass. In practice, the rotor is propped on a balance machine and the weights are moved around to the points where the rotor balances on a level.

The imbalanced shaft (Fig. 2-1) has the following values for the center of gravity:

$$x_g = 0,\ y_g = -\varepsilon,\ z_g = 0 \tag{2.1}$$

The center of gravity, with an additional mass affixed on the surface of the shaft 180 degrees away, is given by

$$x_g = z_g = 0,\ y_g = \frac{M\epsilon - mr}{m + M} \tag{2.2}$$

where M is the original rotor mass, and m is the affixed mass. It is the interest here that m is set at a distance equal to $M\epsilon/r$, so that the rotor will be statically balanced $y_g = 0$.

2.3.2 Dynamic Balancing

In order to carry out the method of dynamic balancing [14], the rotor is mounted on the mobile platform of a balancing machine. By a dynamometer or such, the rotor

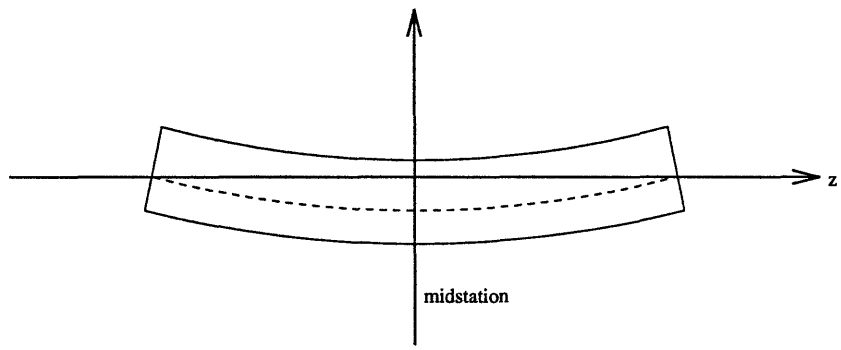

Figure 2-2: A rotor that is statically out of balance

is let spin up to speed and vibrate [1]. The balance points are noted by computer and the proper balance weight spots are then indicated by measuring the amplitude and phase of platform vibration.

The components of the balancing machine include

1. mechanical platform assembly to reflect the necessary degrees of freedom of a rotor,

2. a driving system to set a specific speed of rotation,

3. measuring devices to carefully detect the motion of the platform, and

4. an accurate device for adding and removing material at specific locations on the rotor.

Theoretically, for a rigid rotor, the cross product of inertia must equal to zero, that is

$$I_{xz} = I_{yz} = 0 \tag{2.3}$$

[1]It is an obvious sign of imbalance.

The mass products of inertia, I_{zx} and I_{zy}, are given by

$$I_{xz} = \int_V xzdm \tag{2.4}$$

$$I_{yz} = \int_V yzdm \tag{2.5}$$

where dm is an elemental mass ($dm = \rho dV$) of the body. If the rotor material is made perfectly homogeneous, then ρ will be constant over the volume V. The off-diagonal quantities of I's are then equal to zero, given that the rotor is concentrically round with respect to a normal plane to the axis of rotation.

If this is true and the x and y coordinates of the center of mass are also zero, that is

$$x_g = y_g = 0 \tag{2.6}$$

then the rotor is both statically and dynamically balanced.

If the shaft center line is slightly bowed into an arc symmetrically about the normal to the rotor midstation 2-2, then the rotor will be statically out of balance but not dynamically [2]. Any inhomogeneity would cause dynamic imbalance unless the dynamic distribution is again symmetrical with respect to the midplane.

If a rigid rotor is dynamically out of balance, two correcting weights are affixed in two arbitrarily positioned planes, which are called correction planes (Fig. 2-3), normal to the axis of rotation and located at $z = z_1$ and $z = z_2$. The correction masses are denoted as m_1 and m_2, and located at (x_1, y_1, z_1) and (x_2, y_2, z_2) respectively. If the original imbalanced rotor has mass M and cross products of inertia I_{zx} and I_{zy}, then the balanced cross products of inertia (with the correction mass added), are

$$I_{xz}^{new} = I_{xz} + m_1 x_1 z_1 + m_2 x_2 z_2, \tag{2.7}$$

$$I_{yz}^{new} = I_{yz} + m_1 y_1 z_1 + m_2 y_2 z_2 \tag{2.8}$$

[2]If there is no symmetry then there is dynamic imbalance as well.

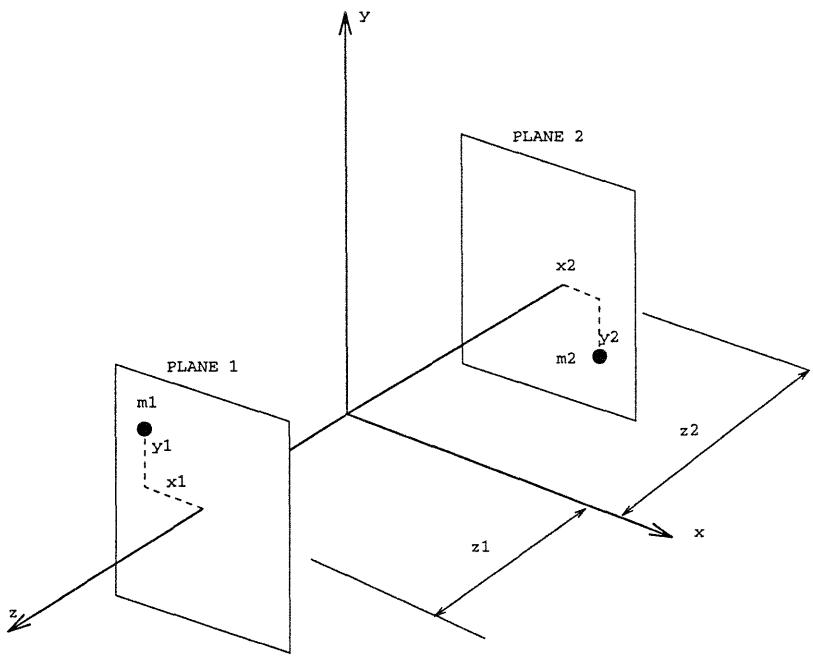

Figure 2-3: Correction planes

The coordinates of the new center of mass are given by

$$x_g^{new} = \frac{Mx_g + m_1x_1 + m_2x_2}{M + m_1 + m_2}, \tag{2.9}$$

$$y_g^{new} = \frac{My_g + m_1y_1 + m_2y_2}{M + m_1 + m_2} \tag{2.10}$$

To have the rotor both statically and dynamically balanced, it is necessary that

$$x_g^{new} = 0 \quad \Rightarrow m_1x_1 + m_2x_2 = -M\bar{x}_c \tag{2.11}$$

$$y_g^{new} = 0 \quad \Rightarrow m_1y_1 + m_2y_2 = -M\bar{y}_c \tag{2.12}$$

$$I_x^{new}z = 0 \quad \Rightarrow z_1(m_1x_1) + z_2(m_2x_2) = -I_{xz} \tag{2.13}$$

$$I_y^{new}z = 0 \quad \Rightarrow z_1(m_1y_1) + z_2(m_2y_2) = -I_{yz} \tag{2.14}$$

As implicitly shown above, the coordinates x_1, x_2, y_1, y_2, z_1, z_2 are determined by the four equations. The implication of a mass negative quantity is that of material

removal. The formula proves that it is possible to balance the rotor by using two masses, given the $\bar{x}_c$, $\bar{y}_c$, I_{xz}, and I_{yz} [3].

2.3.3 Flexible Shaft Balancing

When the rotor is rotating at a speed in excess of the lowest natural frequency, it can no longer be considered rigid, because the true position of the mass center and its instantaneous cross products of inertia will be different for each operating speed. In order to account for this effect, the balancing is determined according to the particular vibration modes, assuming that the rotary inertia effects of the rotor cross sections and the attached disks may be neglected. The drawback of this method is that the natural vibration frequencies and mode shapes of the rotating shaft are the same as those of the standstill shaft. The fundamental aspect of this so-called *modal balancing* is to use the natural vibration modes as generalized coordinates. The modal equations have the inherent orthogonality, making it possible to uncouple equations and determine the necessary correction weights to balance out the reactions of the lower modes.

Modal Balancing

A theoretical modal balancing technique may not always overcome vibration entirely at the required range of operating speeds, even if the gyroscopic moments are completely negligible. The generalized imbalanced force at its source, weighted by each particular modal deflection shape, acts as the only driving function in this normal mode analysis. If the imbalance distribution has sharp variations or if its shape is like the deflection shape of one of the higher modes, the generalized force that excites the higher modes may be large enough. Unless those modes are included in the balancing procedure, the dynamic bearing reactions may still be large. A modal balancing technique using only the lower modes is sufficient only if the harmonic content of the imbalance distribution is not too large [14].

[3] In practice, it is difficult to determine these predetermined constants experimentally without already having balanced the rotor.

Harmonics Balancing

The method of harmonics balancing, as combined methods of balancing states is stated as follows: a massless flexible rotor holding r concentrated masses, supported on b bearings, with an imbalance, can be entirely balanced by weights distributed in $n = r + b$ different planes along the rotor length. This method of complete balancing eliminates any dynamic reaction in any bearing at any rotating speed, given that the imbalanced masses are small compared to the whole mass of the rotor, and that the flexure due to the imbalance is small compared to the eccentricities of the static imbalance. For futher information in this harmonic balancing method, one may refer to [14].

2.4 Gravity Effect

If the axis of rotation were horizontal, and the disk had imbalance, the force of the center of gravity would become a transverse excitation source. Viewed in the stationary frame, the force is directing downward, but in the rotating system, it is sinusoidally varying with frequency of vibration, that is

$$-mg\, sin\omega t, \qquad in\, the\, \mathbf{j}\, direction \tag{2.15}$$

$$-mg\, cos\omega t, \qquad in\, the\, \mathbf{k}\, direction \tag{2.16}$$

A different way of looking into this gravity effect on a rotating horizontal shaft is to consider the frequency of the exciting force is zero in a fixed coordinate system, but once-per-revolution in the rotating system. In other words, the imbalance would initiate a once-per-revolution pulsating torque on a horizontal shaft.

2.5 Gyroscopic Effect

If the disk doesn't remain in one plane when it is rotating (particularly at higher speeds), then the so-called *gyroscopic effect* must be taken into account of the rotor

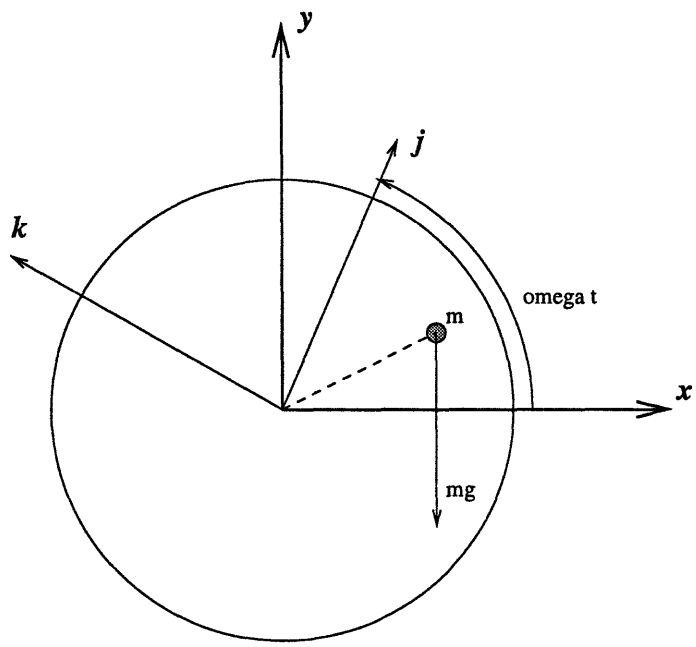

Figure 2-4: Balanced disk on a massless, horizontal elastic shaft

dynamics. *Loewy et al.* states in [14] that gyroscopic effect may increase or decrease the critical speeds of a rotor significantly, depending upon the operating speed, size and geometry of the gyroscopic disks, and disk location on the rotating shaft. The gyroscopic moment is determined as proportional to the time rate of change of the shaft's transverse angular displacement and directed 90 degrees from that of transverse angular velocity. Therefore, it is necessary to consider the simultaneous bending of the shaft in two planes, while the polar mass moment of inertia about the shaft center line is an important parameter also.

According to *Dimentberg* [5], the movement can be in the direction of the rotation of the shaft, which is called *forward precession*, or in the opposite direction, which is called *reverse precession.* If the disk rotates with Ω and deviates about the **z** axis by an angle φ, then the movement tends to displace the positive end of the **z** axis towards the $\mathbf{\Omega}$ axis.

Defining the disc mass as m, the equatorial and polar moments of inertia of the

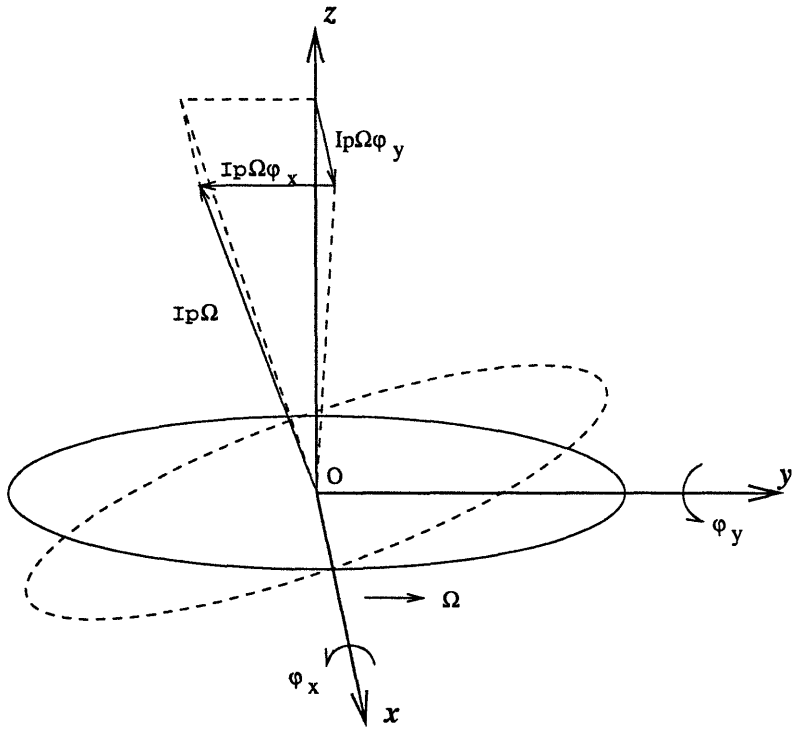

Figure 2-5: Gyroscopic Movement

disc mass as I_e and I_p, the displacements of the disc center along the fixed axes and the angles of rotation as x, y, φ_x, and φ_y, while the angular speed of the disc as Ω, the projection of the force $\mathbf{F}$ and the moment $\mathbf{L}$ of the movement on the axes are then given by Fig. 2-5,

$$F_x = m\ddot{x} \tag{2.17}$$

$$F_y = m\ddot{y} \tag{2.18}$$

$$L_x = I_e\dot{\varphi}_x + I_p\Omega\varphi_y \tag{2.19}$$

$$L_y = I_e\dot{\varphi}_y - I_p\Omega\varphi_x \tag{2.20}$$

$$I_{p\Omega} = 0 \tag{2.21}$$

$$L_\Omega = I_p\Omega \tag{2.22}$$

Equating the time derivatives to the projections and the moments of the external

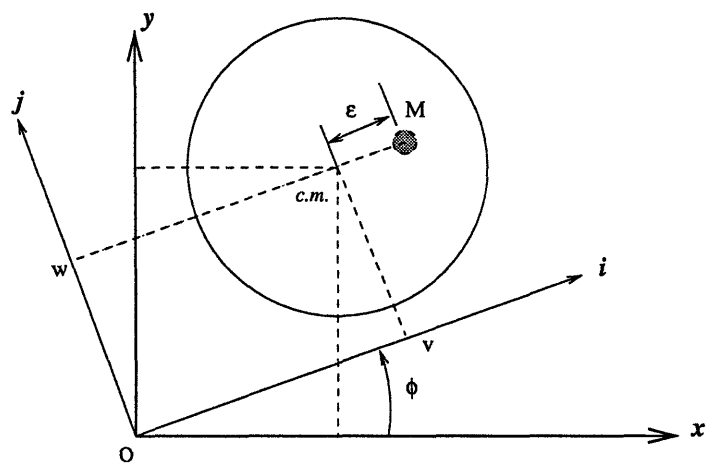

Figure 2-6: The Fixed and Rotating Coordinate Systems

forces respectively, acting on the disc or, which is the same, to the values with the opposite sign of the projections and the moments of the inertial forces, transmitted from the disc to the shaft, the equations for the disc movement are

$$m\ddot{x} = -P_x, \tag{2.23}$$

$$m\ddot{y} = -P_y, \tag{2.24}$$

$$I_e\ddot{\varphi}_y - I_p\Omega\dot{\varphi}_x = -M_y, \tag{2.25}$$

$$I_e\ddot{\varphi}_x + I_p\Omega\dot{\varphi}_y = -M_x \tag{2.26}$$

with $-I_p\Omega\dot{\varphi}_x$ and $I_p\Omega\dot{\varphi}_y$ as the gyroscopic terms.

2.6 System Identification

Following the assumptions made in [14], the static location of the standstill rotor is at O, i.e. $x = y = 0$ or $v = w = 0$. During the rotor movement, the shaft axis is considered deflected from this standstill location. The rotor is running at a constant

angular velocity, i.e. $\phi = \Omega t$.

$$\mathbf{r} = (\varepsilon + v)\mathbf{i} + w\mathbf{j} \tag{2.27}$$

$$= (x + \varepsilon\, cos\Omega t)\mathbf{x} + (z + \varepsilon\, sin\Omega t)\mathbf{y} \tag{2.28}$$

$$\dot{\mathbf{r}} = \dot{v}\mathbf{i} + \dot{w}\mathbf{j} + \Omega\mathbf{k} \times [(\varepsilon + v)\mathbf{i} + w\mathbf{j}]$$

$$= (\dot{v} - \Omega w)\mathbf{i} + (\varepsilon + v)\Omega\dot{w}\mathbf{j} \tag{2.29}$$

Differentiating again, the above equation results in the acceleration of the rotor mass, M. After simplification, the equation is

$$\ddot{\mathbf{r}} = (\ddot{v} - \Omega^2 v - 2\Omega\dot{w} - \Omega^2\varepsilon)\mathbf{i} + (\ddot{w} - \Omega^2 w + 2\Omega\dot{v})\mathbf{j} \tag{2.30}$$

$$= (\ddot{y} - \varepsilon\Omega^2\, cos\Omega t)\mathbf{x} + (\ddot{z} - \varepsilon\Omega^2\, sin\Omega t)\mathbf{y} \tag{2.31}$$

The elastic restoring force acting on the system is provided by the shaft stiffness

$$\mathbf{f}_s = -\kappa(v\mathbf{i} + w\mathbf{j}) \tag{2.32}$$

$$= -\kappa(x\mathbf{x} + y\mathbf{e}_y) \tag{2.33}$$

where κ is the approximated linear spring constant.

The internal friction force, which is viewed as the friction associated with the rotating coordinate system, is given by

$$\mathbf{f}_i = -c_i(\dot{v}\mathbf{i} + \dot{w}\mathbf{j}) \tag{2.34}$$

$$= -c_i[(\dot{x} + \Omega y)\mathbf{x} + (\dot{y} - \Omega x)\mathbf{y}] \tag{2.35}$$

and the external friction force, which is viewed as the friction associated with the fixed coordinate system, is given by

$$\mathbf{f}_e = -c_e[(\dot{v} - \Omega w)\mathbf{i} + (\dot{w} + \Omega v)\mathbf{j}] \tag{2.36}$$

$$= -c_e(\dot{x}\mathbf{x} + \dot{y}\mathbf{y}) \tag{2.37}$$

where c_i and c_e are the approximated internal and external friction constants, respectively. In the case of rotors of magnetic bearing systems, c_i and c_e are zero, due to the frictionless nature of the systems.

The relationship between (x, y) and (i, j) coordinate systems is established via rotational transformation [8] as follows;

$$\begin{bmatrix} x \\ y \end{bmatrix} = \begin{bmatrix} cos\,\phi & -sin\,\phi \\ sin\,\phi & cos\,\phi \end{bmatrix} \begin{bmatrix} v \\ w \end{bmatrix}$$

Since the equation of motion in each frame of reference is

$$m\ddot{\mathbf{r}} = \mathbf{f_s} + \mathbf{f_i} + \mathbf{f}_e, \tag{2.38}$$

then

Fixed coordinate system

$$\ddot{x} + \frac{c_i + c_e}{m}\dot{x} + \frac{\kappa}{m}x + \frac{c_i\Omega}{m}y = \Omega^2\varepsilon\, cos\Omega t, \tag{2.39}$$

$$\ddot{y} + \frac{c_i + c_e}{m}\dot{y} + \frac{\kappa}{m}y - \frac{c_i\Omega}{m}x = \Omega^2\varepsilon\, sin\Omega t, \tag{2.40}$$

or

$$\frac{d}{dt}\begin{bmatrix} x \\ \dot{x} \\ y \\ \dot{y} \end{bmatrix} = \begin{bmatrix} 0 & 1 & 0 & 0 \\ -\frac{\kappa}{m} & -\frac{c_i+c_e}{m} & -\frac{c_i\Omega}{m} & 0 \\ 0 & 0 & 0 & 1 \\ \frac{c_i\Omega}{m} & 0 & -\frac{\kappa}{m} & -\frac{c_i+c_e}{m} \end{bmatrix} \begin{bmatrix} x \\ \dot{x} \\ y \\ \dot{y} \end{bmatrix} + \Omega^2\varepsilon \begin{bmatrix} 0 \\ cos\Omega t \\ 0 \\ sin\Omega t \end{bmatrix}$$

Rotating coordinate system

$$\ddot{v} + \frac{c_i + c_e}{m}\dot{v} + (\frac{\kappa}{m} - \Omega^2)v - 2\Omega\dot{w} - \frac{c_e\Omega}{m}w = \Omega^2\varepsilon, \tag{2.41}$$

$$\ddot{w} + \frac{c_i + c_e}{m}\dot{w} + (\frac{\kappa}{m} - \Omega^2)w + 2\Omega\dot{v} + \frac{c_e\Omega}{m}v = 0, \tag{2.42}$$

or

$$\frac{d}{dt}\begin{bmatrix} v \\ \dot{v} \\ w \\ \dot{w} \end{bmatrix} = \begin{bmatrix} 0 & 1 & 0 & 0 \\ -(\frac{\kappa}{m} - \Omega^2) & -\frac{c_i+c_e}{m} & \frac{c_e\Omega}{m} & 2\Omega \\ 0 & 0 & 0 & 1 \\ -\frac{c_e\Omega}{m} & -2\Omega & -(\frac{\kappa}{m} - \Omega^2) & -\frac{c_i+c_e}{m} \end{bmatrix} \begin{bmatrix} v \\ \dot{v} \\ w \\ \dot{w} \end{bmatrix} + \Omega^2\varepsilon \begin{bmatrix} 0 \\ 1 \\ 0 \\ 0 \end{bmatrix}$$

Using complex representations $\eta = y + \jmath z$ and $u = v + \jmath w$, the equations become

Fixed coordinate system

$$\ddot{\eta} + \frac{c_i + c_e}{m}\dot{\eta} + \frac{\kappa}{m}\eta - \jmath\frac{c_i\Omega}{m}\eta = \Omega^2\varepsilon e^{\jmath\Omega t} \tag{2.43}$$

Rotating coordinate system

$$\ddot{u} + \frac{c_i + c_e}{m}\dot{u} + (\frac{\kappa}{m} - \Omega^2)u + \jmath 2\Omega\dot{u} + \jmath\frac{c_e\Omega}{m}u = \Omega^2\varepsilon \tag{2.44}$$

Then, a particular solution is obtained by setting $\eta = \eta_0 e^{\jmath\Omega t}$ and $u = u_0 e^{\jmath\Omega t}$:

$$\eta_0 = \frac{\Omega^2\varepsilon}{(\frac{\kappa}{m} - \Omega^2 + \jmath\frac{c_e\Omega}{m})} \tag{2.45}$$

and

$$u_0 = \frac{-\Omega^2\varepsilon}{\sqrt{\left(4\Omega^2 - \frac{\kappa}{m}\right)^2 + \left(\frac{c_i+2c_e}{m}\Omega\right)^2}} \tag{2.46}$$

2.7 Asymmetry Of Rotating Shaft Parts

Here is the work of *Ariaratnam* [1]. He analyzed the vibration of unsymmetrical rotating shafts whose flexural rigidities are unequal in the principal directions. The bearings are considered symmetrical in this case.

From Fig.2-6, it is understandable when the shaft is assumed to be unsymmetrical, the equations in (y,z) will contain periodic coefficients, while those in (u,v) will not. Obviously, the latter is easier to handle. The equations are then

$$\ddot{u} - \Omega^2(u + a_1) - 2\Omega\dot{v} = -\frac{EI}{m}\frac{\partial^4}{\partial x^4}(u - u_0) - \alpha(\dot{u} - \Omega v) - \beta\dot{u} - g\, sin\Omega t \quad (2.47)$$

$$\ddot{v} - \Omega^2(v + a_2) + 2\Omega\dot{u} = -\frac{EI}{m}\frac{\partial^4}{\partial x^4}(v - v_0) - \alpha(\dot{v} + \Omega u) - \beta\dot{v} - g\, cos\Omega t \quad (2.48)$$

where m is the constant mass per unit length of the shaft, and $EI_{1,2}$ are the flexural rigidities of the shaft cross section for bending in the planes of OXV, OXW, respectively.

In deriving the above equations, it is assumed that

1. the deflection amount of u, v, u_0, and v_0 are assumed to be small so that the *Euler-Bernoulli* theory of bending may be applicable,

2. the damping forces acting on unit length of the shaft are assumed to be viscous and containing the *external damping* of magnitude $(-m\alpha)$ times the transverse velocity of E relative to the fixed axis, and the *internal damping* of magnitude $(-m\beta)$ times the transverse velocity of the cross section relative to the rotating axis.

By assuming $\Omega = \alpha = \beta = u_0 = v_0 = 0$, the free, undamped, transverse linear vibrations in the principal directions of a perfect standstill shaft of unsymmetrical cross section are given by the equations as follows:

$$\ddot{u} + \frac{EI_1}{m}\frac{\partial^4 u}{\partial x^4} = 0 \quad (2.49)$$

$$\ddot{v} + \frac{EI_2}{m}\frac{\partial^4 v}{\partial x^4} = 0 \quad (2.50)$$

From Eq.2.49, the solutions are of the form

$$u(x,t) = \theta(x)\, cos\,(\omega t + \sigma) \quad (2.51)$$

The spatial function $\theta(x)$ satisfies the equation

$$\frac{d^4\theta}{dx^4} = k^4\theta \tag{2.52}$$

where

$$k^4 = \frac{m\omega^2}{EI_1} \tag{2.53}$$

From Eq.2.52, the general solution is

$$\theta(x) = A\,cos\,kx + B\,sin\,kx + C\,cosh\,kx + D\,sinh\,kx \tag{2.54}$$

where A, B, C, D are constants obtained from the limit conditions at the bearing locations.

Assuming that the mass unbalance is located at (a_1, a_2) in the direction of (**i**,**j**), the functions can be expanded as series in the characteristic functions as follows;

$$a_1(x) = \sum_{r=1}^{\infty} a_{r1}\phi_r(x) \tag{2.55}$$

$$a_2(x) = \sum_{r=1}^{\infty} a_{r2}\phi_r(x) \tag{2.56}$$

$$u_0(x) = \sum_{r=1}^{\infty} e_{r1}\phi_r(x) \tag{2.57}$$

$$v_0(x) = \sum_{r=1}^{\infty} e_{r2}\phi_r(x) \tag{2.58}$$

where the Fourier coefficients a_{r1}, a_{r2}, e_{r1}, and e_{r2} are

$$a_{r1} = \int_0^L a_1(x)\phi_r(x)dx \tag{2.59}$$

$$a_{r2} = \int_0^L a_2(x)\phi_r(x)dx \tag{2.60}$$

$$e_{r1} = \int_0^L e_1(x)\phi_r(x)dx \tag{2.61}$$

$$e_{r2} = \int_0^L e_2(x)\phi_r(x)dx \tag{2.62}$$

The equations of motion are then obtained as follows:

$$\ddot{\xi}_r + (\alpha+\beta)\dot{\xi}_r + (\omega_{r1}^2 - \Omega^2)\xi_r - 2\Omega\dot{\eta}_r - \alpha\Omega\eta_r$$
$$= \Omega^2 a_{r1} + \omega_{r1}^2 e_{r1} - g\Phi_r sin\Omega t \tag{2.63}$$
$$\ddot{\eta}_r + (\alpha+\beta)\dot{\eta}_r + (\omega_{r2}^2 - \Omega^2)\eta_r + 2\Omega\dot{\xi}_r + \alpha\Omega\xi_r$$
$$= \Omega^2 a_{r2} + \omega_{r2}^2 e_{r2} - g\Phi_r cos\Omega t \tag{2.64}$$

or in the matrix equation,

$$\frac{d}{dt}\begin{bmatrix} \xi_r \\ \eta_r \\ \dot{\xi}_r \\ \dot{\eta}_r \end{bmatrix} = \begin{bmatrix} 0 & 0 & 1 & 0 \\ 0 & 0 & 0 & 1 \\ -(\omega_{r1}^2 - \Omega) & \alpha\Omega & -(\alpha+\beta) & 2\Omega \\ -\alpha\Omega & -(\omega_{r2}^2 - \Omega^2) & -2\Omega & -(\alpha+\beta) \end{bmatrix} \begin{bmatrix} \xi_r \\ \eta_r \\ \dot{\xi}_r \\ \dot{\eta}_r \end{bmatrix} +$$

$$\begin{bmatrix} 0 & 0 & 0 & 0 \\ 0 & 0 & 0 & 0 \\ \Omega^2 & 0 & \omega_{r1}^2 & 0 \\ 0 & \Omega^2 & 0 & \omega_{r2}^2 \end{bmatrix} \begin{bmatrix} a_{r1} \\ a_{r2} \\ e_{r1} \\ e_{r2} \end{bmatrix} - g\Phi_r \begin{bmatrix} 0 \\ 0 \\ sin\Omega t \\ cos\Omega t \end{bmatrix}$$

where

α, β=coefficients of the external and internal damping, respectively

ω_r=the natural frequency of transverse vibration

$\Phi_r = \int_0^L \Phi_r(x)dx$, the characteristic mode.

For asymmetrical shaft, $\omega_{r1} \neq \omega_{r2}$, and the equations have to be treated as simultaneous differential equations and solved by elimination of variables.

2.7.1 The Free Vibration

For the free vibration of the rotating shaft, the equations of motion are given by the complementary functions of Eq.2.63- 2.64; the general solutions are

$$\ddot{\xi}_r + (\alpha+\beta)\dot{\xi}_r + (\omega_{r1}^2 - \Omega^2)\xi_r - 2\Omega\dot{\eta}_r - \alpha\Omega\eta_r = 0$$

$$\ddot{\eta}_r + (\alpha+\beta)\dot{\eta}_r + (\omega_{r2}^2 - \Omega^2)\eta_r + 2\Omega\dot{\xi}_r + \alpha\Omega\xi_r = 0$$

A type of possible solutions are of the form

$$\xi_r(t) = Pe^{\lambda t}, \qquad \eta_r(t) = Qe^{\lambda t} \tag{2.65}$$

where λ, P, and Q are constants, providing the characteristic equation

$$\left[\lambda^2 + (\alpha+\beta)\lambda + (\omega_{r1}^2 - \Omega^2)\right]\left[\lambda^2 + (\alpha+\beta)\lambda + (\omega_{r2}^2 - \Omega^2)\right] + (2\Omega\lambda + \alpha\Omega)^2 = 0 \tag{2.66}$$

After simplification,

$$\begin{aligned}\lambda^4 + 2(\alpha+\beta)\lambda^3 + \left[\omega_{r1}^2 + \omega_{r2}^2 + 2\Omega^2 + (\alpha+\beta)^2\right]\lambda^2 \\ + \left[(\alpha+\beta)(\omega_{r1}^2 + \omega_{r2}^2 - 2\Omega^2) + 4\alpha\Omega^2\right]\lambda \\ + (\omega_{r1}^2 - \Omega^2)(\omega_{r2}^2 - \Omega^2) + \alpha^2\Omega^2 = 0\end{aligned} \tag{2.67}$$

According to *Routh's stability criterion*, the solutions will be bounded at all times if all roots of λ have nonpositive real parts:

$$(\alpha+\beta)(\omega_{r1}^2 + \omega_{r2}^2 - 2\Omega^2) + 4\alpha\Omega^2 > 0 \tag{2.68}$$

$$(\omega_{r1}^2 - \Omega^2)(\omega_{r2}^2 - \Omega^2) + \alpha^2\Omega^2 > 0 \tag{2.69}$$

Due to the frictionless nature and vacuum operating condition of magnetic bearing systems, both external and internal damping are absent, i.e. $\alpha = 0$, $\beta = 0$. The characteristic equation (Eq. 2.67) is then reduced to

$$\lambda^4 + (\omega_{r1}^2 + \omega_{r2}^2 + 2\Omega^2)\lambda^2 + (\omega_{r1}^2 - \Omega^2)(\omega_{r2}^2 - \Omega^2) = 0 \tag{2.70}$$

and the corresponding roots are

$$\lambda_{1,2}^2 = -\frac{1}{2}(\omega_{r1}^2 + \omega_{r2}^2) - \Omega^2 \pm \sqrt{\Omega^2(\omega_{r1}^2 + \omega_{r2}^2) + \frac{1}{4}(\omega_{r2}^2 - \omega_{r1}^2)^2} \tag{2.71}$$

If $\Omega = 0$, then $\lambda_{1,2}^2$ are real and unequal. If $\omega_{r1}^2 \neq \Omega \neq \omega_{r2}^2$, then Eq.2.67 gives four fundamental solutions. When Ω is outside the finite intervals $\omega_{r1} \leq \Omega \leq \omega_{r2}, (r = 1, 2, ...)$, $\lambda_{1,2}^2$ are both negative (all values of λ are purely imaginary), and the solutions will be bounded.

If $\Omega = \omega_{r1}, \omega_{r2}$, $(r = 1, 2, ...)$, $\lambda = 0$ is a double root of Eq.2.70, and the solutions are of the form

$$\xi_r(t) = P_1 + P_2 t, \qquad \eta_r(t) = Q_1 + Q_2 t \tag{2.72}$$

which are clearly unbounded due to the factor of t.

The particular solution is then obtained from [1] as follows:

$$\xi_r(t) = \frac{\Omega^2 a_{r1} + \omega_{r1}^2 e_{r1}}{\omega_{r1}^2 - \Omega^2} - \frac{\omega_{r2}^2 - 4\Omega^2}{\omega_{r1}^2\omega_{r2}^2 - 2\Omega^2(\omega_{r1}^2 + \omega_{r2}^2)} g\Phi_r \, sin\Omega t, \tag{2.73}$$

$$\eta_r(t) = \frac{\Omega^2 a_{r2} + \omega_{r2}^2 e_{r2}}{\omega_{r2}^2 - \Omega^2} - \frac{\omega_{r1}^2 - 4\Omega^2}{\omega_{r1}^2\omega_{r2}^2 - 2\Omega^2(\omega_{r1}^2 + \omega_{r2}^2)} g\Phi_r \, cos\Omega t, \tag{2.74}$$

$$r = 1, 2, ...$$

2.7.2 The Forced Vibration

Recalling Eq.2.63 and Eq.2.64, i.e. the particular equations representing the forced vibration due to unbalance, initial lack of straightness, and gravity. This forced motion will be unbounded for some causes as follows:

1. shaft imperfections, i.e. unbalance, initial lack of straightness.

$$\Omega = \omega_{r1}, \qquad \Omega = \omega_{r2}, \qquad r = 1, 2, ...$$

are considered the *critical speeds*,

2. effect of gravity

$$\Omega = \frac{\omega_{r1}\omega_{r2}}{2(\omega_{r1}^2 + \omega_{r2}^2)}, \qquad r = 1, 2, ...$$

is considered the *secondary critical speed.*

2.8 Shaft and Mount

2.8.1 Flexibility

Consider a shaft configuration which consists of a disk, a massless elastic shaft constrained to stationary (x,y) or rotating plane motion (i,j). The bearings are placed at the origin, and the shaft is infinitely stiff in torsion. The shaft transverse (*bending*) flexibility allows translational motion of the disk in the plane of rotation, which may lag (Fig. 2-7a), lead (Fig. 2-7b) by angle ϕ, or be coincident with the shaft rotation (Fig. 2-7c,d). Here, the effect of shaft bending flexibility could be represented as a linear spring. If the shaft bending rigidities are not polar symmetric, then there would be different elastic restoring forces, although the magnitude of the displacements in the direction of the linear springs were all equal. A shaft with significant difference in stiffness in any two directions would be subject to instabilities.

The flexibility effects due to shaft elastic properties and in the shaft bearings are quite similar. If the shaft has polar- symmetric stiffness and the bearing spring rates are isotropic, these two dimensional descriptions become interchangeble. The shaft stiffness would provide a steady radial force, and the bearing springs $k_x = k_y$ would provide the same steady resultant radial force.

2.8.2 Damping

The structural damping of the shaft is represented as a radial damper (Fig.2-8) which is parallel with the springs, acting as a powerful dissipative medium. These damping forces, whether isotropic or not, act very differently from friction in the rotating shaft.

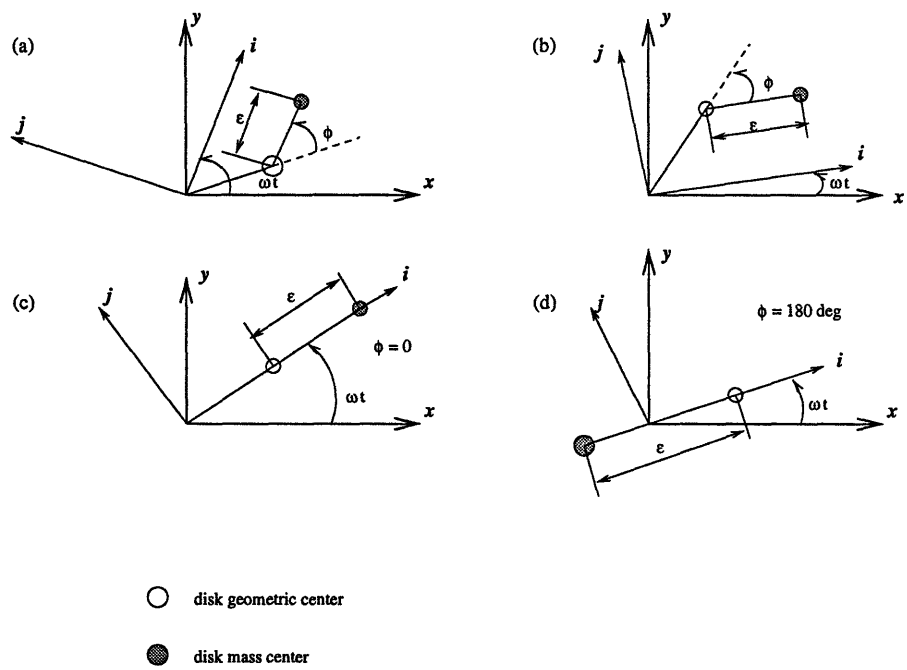

Figure 2-7: Possible configurations for steady motion of a disk

As in the case of the shaft and mount flexibility, any constant amplitude circular whirl would not cause oscillation in the shaft spring, but continuously cycle the springs.

2.9 Instability

A system is considered unstable, when it is not subjected to external forces and has only free motion due to its initial conditions, but its motion develops indefinitely with time. Consider a disk that is perfectly balanced but contains a frictionless, radial slot, in which there is a mass m, restrained by the spring k, as shown in Fig. 2-9. The radial equilibrium of forces on the mass could result from a balance of centrifugal and elastic forces.

$$m\Omega^2(e+v) = kv \tag{2.75}$$

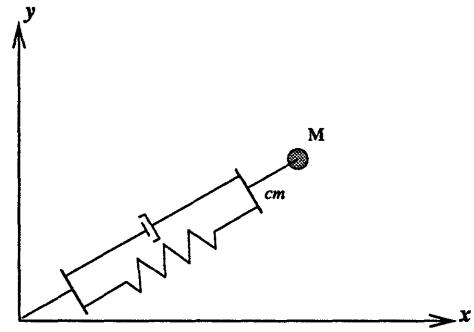

Figure 2-8: Damper and Spring

or

$$v = \frac{m\Omega^2 e}{k - m\Omega^2} = \frac{e}{\frac{k}{m\Omega^2} - 1} \tag{2.76}$$

The elastic deflection v will be unbounded for any initial deflection e if the rotational speed $\Omega_d = \sqrt{\frac{k}{m}}$, which can be considered as *critical.* If the mass is rotating about a mean position $e = 0$ without vibration, then the Newton's second law yields

$$m\ddot{v} = -kv + m\Omega^2 v \tag{2.77}$$

or

$$\ddot{v} + (\frac{k}{m} - \Omega^2)v = 0 \tag{2.78}$$

Viewed in the rotating system, the rotating natural frequency is

$$\omega_{n_R} = \sqrt{\frac{k}{m} - \Omega^2} = \Omega\sqrt{\frac{\omega_n}{\Omega}^2 - 1} \tag{2.79}$$

It is obvious that the divergence speed Ω_d occurs when the rotating natural fre-

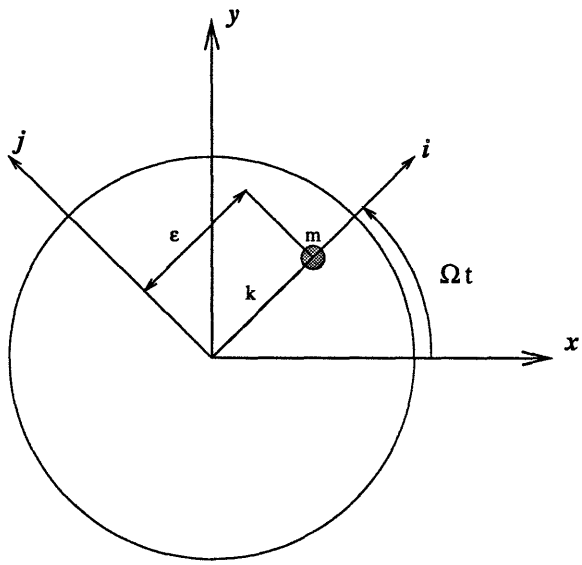

Figure 2-9: Rotating disk with a spring-restrained mass in a radial slot

quency is zero, when viewed in the rotating system. The solution of v is

$$v = v_{0_1} e^{i\omega_{n_R} t} + v_{0_2} e^{-i\omega_{n_R} t} \tag{2.80}$$

which shows that if $\Omega > \Omega_d = \sqrt{\frac{k}{m}}$, one of the two terms will diverge. Thus, Ω_d represents the limit of a semi-infinite region from $\Omega = \Omega_d$ to $\Omega = \infty$.

2.10 Critical Speed

Rotor has certain speed ranges in which vibrations of large amplitude could occur, causing to operate harshly, transmitting large forces to the bearings and exhibiting considerable deflections of the rotor. The critical speed vibration requires external excitation such as provided by rotor unbalance. If the operating speed coincides with the rotor critical speed, then the large forces on the bearings may possibly cause bearing failure, or the resulting excessive rotor deflection may wipe out the internal labyrinth seals causing rotor failure and affecting unit efficiency. *Dunkerley* theorizes that if the rotor had any unbalance (which is generally unavoidable), then it would excite the natural lateral frequencies, generating high vibrational amplitudes if the

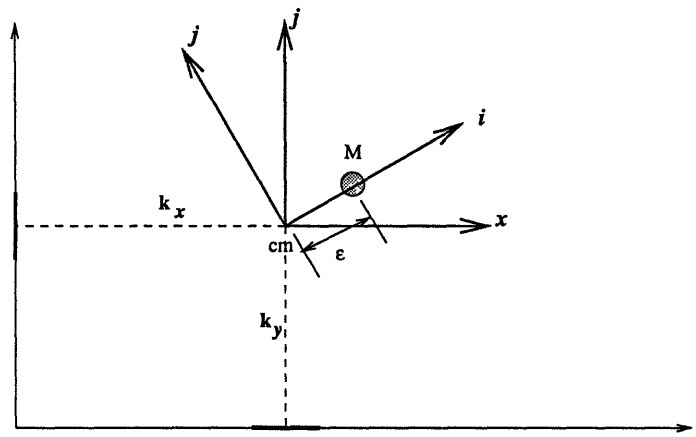

Figure 2-10: Disk on flexible mounted bearings

operating range should coincide to any of these values [13].

Fig. 2-10 above approximates a magnetically levitated horizontal shaft with mass unbalance, where linear springs k_x and k_y represent the magnetic bearing supports in the direction of **x** and **y** axes, respectively. Assumably, each pair of supports for each axis could be represented by only one linear spring. The **x**, **y** axes are fixed at the undeflected bearing location. Letting $k_x = k_y = k$, and $\Omega = \Omega_c = \sqrt{k/m}$ (the undamped natural frequency as viewed in the fixed system), then, the amplitudes will grow unbounded in the absence of damping, and the solutions will be [14]

$$x = \frac{\Omega_c e}{2}(A + t)\, sin\, \Omega_c t + B\, cos\, \Omega_c t, \tag{2.81}$$

$$y = \frac{-\Omega_c e}{2}(A' + t)\, cos\, \Omega_c t + B'\, sin\, \Omega_c t, \tag{2.82}$$

where A, A', B, and B' depend upon the displacements and velocities of x and y at time $t = 0$. The sum resulted of the two motions is a diverging spiral, so Ω_c is also considered as a critical speed, and numerically equal to an undamped natural frequency. However, if $\Omega > \Omega_c$, then the motion will be bounded, and the corresponding ranges will be where the instabilities predictably will occur. Thus, only at the speed Ω_c will result in a whirling divergence linearly with time, as viewed

in the rotating system. In case of the slotted mass, whirling divergence will result exponentially with time beyond the speed of Ω_d, and its rapidness will be determined by how far the unstable range of $\Omega \geq \Omega_d$ is entered.

2.10.1 Coupled Critical Speed

To investigate the rotor response during transition, the rotor angular displacement of the rotating coordinate system is considered to include a specified angular acceleration as [14]

$$\phi = \Omega_0 t + \alpha t^2. \tag{2.83}$$

Hence,

$$\frac{d}{dt}[\phi] = \Omega = \Omega_0 + 2\alpha t, \tag{2.84}$$

$$\frac{d^2}{dt^2}[\phi] = \dot{\Omega} = 2\alpha. \tag{2.85}$$

The angular momentum of the disk about its center of mass is equal to its polar moment of inertia times the angular velocity of the disk. The total moment of force acting about the center of mass is

$$T\mathbf{k} - \varepsilon\mathbf{i} \times \mathbf{f_e} = (T + \varepsilon\kappa w)\mathbf{k}. \tag{2.86}$$

The total moment must equal to the rate of change of the angular momentum, which is $\frac{d}{dt}[\mathbf{L}_{cm} + I_p\Omega]$;

$$T = -\kappa\varepsilon w + I_p\dot{\Omega} \tag{2.87}$$

$$= \kappa\varepsilon(x\, sin\phi - y\, cos\phi) + I_p\dot{\Omega} \tag{2.88}$$

Now, the coupled equations of motion lateral bending-torsion for an unbalanced disk at the center of a flexible shaft is considered, where the shaft is not rotating at a

constant speed. If the instantaneous angular rotation rate Ω is provided by a steady state Ω_0 added by a small perturbation $\dot{\phi}$, then the linearized equations of motion in the coordinate system affixed to the shaft will be as follow (after dropping the multiplication terms of the first derivatives)

from Eq. 2.41 and Eq. 2.42

$$\ddot{v} + \frac{c_i + c_e}{m}\dot{v} + (\frac{\kappa}{m} - \Omega_0^2 - 2\dot{\phi}\Omega_0)v - \frac{c_e}{m}(\Omega_0 + \dot{\phi})w - 2\Omega_0\dot{w} = (\Omega_0^2 + 2\dot{\phi}\Omega_0)\varepsilon, \tag{2.89}$$

$$\ddot{w} + \frac{c_i + c_e}{m}\dot{w} + (\frac{\kappa}{m} - \Omega_0^2 - 2\dot{\phi}\Omega_0)w + \frac{c_e}{m}(\Omega_0 + \dot{\phi})v + 2\Omega_0\dot{v} = 0, \tag{2.90}$$

and from Eq. 2.87

$$I_p\ddot{\phi} - \kappa\varepsilon w + \kappa_\phi\phi = T = 0, \tag{2.91}$$

where the applied torque is assumed to be zero in generating these equations.

Assuming that a particular solution for the unbalance force consists of constants for v, w, and ϕ. Substituting into the equations after dropping the first and second derivatives, yields

$$(\frac{\kappa}{m} - \Omega_0^2)v_0 - \frac{c_e}{m}\Omega_0 w_0 = \Omega_0^2\varepsilon, \tag{2.92}$$

$$(\frac{\kappa}{m} - \Omega_0^2)w_0 + \frac{c_e}{m}\Omega_0 v_0 = 0, \tag{2.93}$$

$$-\kappa\varepsilon w_0 + \kappa_\phi\phi = 0 \tag{2.94}$$

and then

$$v_0 = \frac{\Omega_0^2\varepsilon(\frac{\kappa}{m} - \Omega_0^2)}{(\frac{\kappa}{m} - \Omega_0^2)^2 + (\frac{c_e}{m}\Omega_0)^2}, \tag{2.95}$$

$$w_0 = \frac{-\Omega_0^3\varepsilon\frac{c_e}{m}}{(\frac{\kappa}{m} - \Omega_0^2)^2 + (\frac{c_e}{m}\Omega_0)^2}, \tag{2.96}$$

$$\phi_0 = \frac{\kappa\varepsilon}{\kappa_\phi}w_0. \tag{2.97}$$

Assuming that $|c_e| << 1$, then w_0, and consequently ϕ_0 will become very large

if $\Omega_0 = \sqrt{\frac{\kappa}{m}}$, which is the undamped natural frequency of a critical speed. It shows that the classical critical speed is unaffected by the addition of torsional stiffness. Morever, the presence of external damping c_e will avoid the occurence of such critical speed.

The secondary critical speed due to gravity is unimportant, because there is no resonance phenomenon at an operating speed near half the critical. If these conditions are affected by the coupling of bending and torsion, then the equations of motion of the centrally located disk on a horizontal shaft are

$$m\ddot{x} = -\kappa x, \tag{2.98}$$

$$m\ddot{y} = -\kappa y - mg, \tag{2.99}$$

and

$$I_p\ddot{\phi} + \kappa_\phi \phi + \kappa\varepsilon(x\, sin\phi - y\, cos\phi) = 0 \tag{2.100}$$

Adding the terms of $-mgsin(\phi+\Omega_0 t)$ and $-mgcos(\phi+\Omega_0 t)$ on the right-hand sides of the rotating frame equations respectively, and introducing the complex notations $u = v + \jmath w$, and $\bar{u} = v - \jmath w$, the equations of motion become

$$\ddot{u} + \frac{c_i + c_e}{m}\dot{u} + (\frac{\kappa}{m} - \Omega_0^2 - 2\dot{\phi}\Omega_0)u + \jmath 2\Omega_0\dot{u} + \jmath\frac{c_e}{m}(\Omega_0 + \dot{\phi})u$$
$$= (\Omega_0^2 + 2\dot{\phi}\Omega_0)\varepsilon - \jmath g e^{-\jmath(\phi+\Omega_0 t)}, \tag{2.101}$$

$$I_p\ddot{\phi} + \jmath\frac{\kappa\varepsilon}{2}(u - \bar{u}) + \kappa_\phi\phi = 0. \tag{2.102}$$

2.11 Whirling

Whirling is defined as the angular velocity of the rotor mass center. It is considered as a self-excited phenomenon. The exciting force for the case of shaft whirling, is provided by the frictional force, referred to as rotating or rotary damping, generated

between two contacting surfaces when undergoing relative sliding. When the precession rate is smaller than the rotational speed, the rotary damping force becomes a source of excitation, causing the whirl amplitudes to increase. If the rotor centerline is moving with the same angular velocity as the mass center, then it is considered as *synchronous* precession; otherwise, it is *nonsynchronous* precession. It is generally noted that whirling always occurs above the first critical speed [14].

Observing transverse shaft vibration in two mutually perpendicular planes (Fig. 2-11), the frequency and phasing at a given point along the shaft length determine a closed curve, called *Lissajous figure.* It occurs both in the fixed and rotating frame. If it happens in a rotating system and with non-zero phase, then the shaft center will appear to rotate. Viewed from the rotating system, if the rotation is in the same direction as that of the true rotational velocity of shaft, then it will be called a *forward*, *advancing*, or *progressive* mode. Otherwise, it will be called a *reverse*, *backward*, or *retrogressive* mode.

Describing the classical shaft critical speed phenomenon, forward whirl is a limiting case of zero apparent rotation of the shaft center in the rotating system. *Loewy et al.* in [14] states that in a more complex phenomena, the forward or backward precession, viewed from the rotating system, may occur at *integer* multiples of rotational speeds.

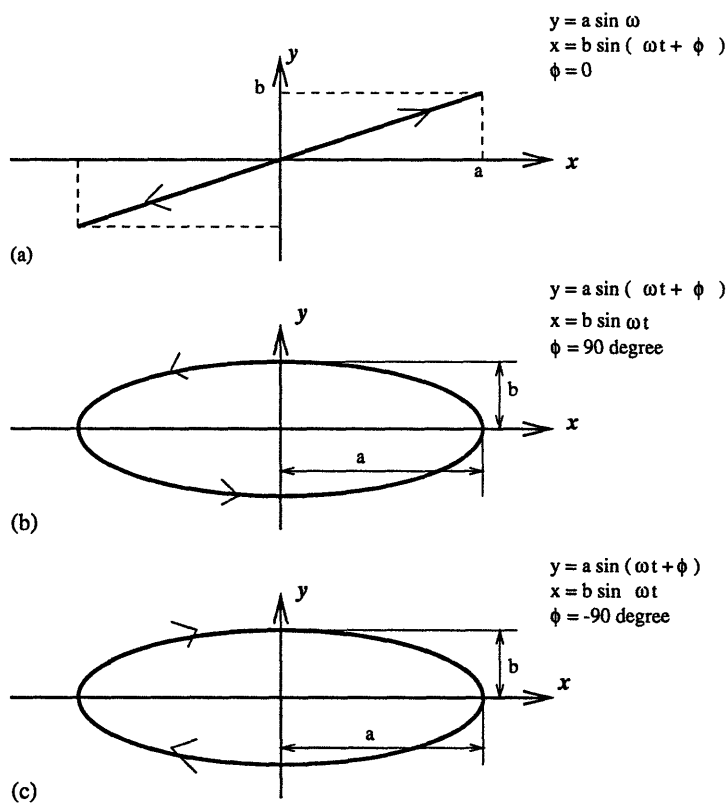

Figure 2-11: Lissajous figures traced by a point on a shaft at a given longitudinal station undergoing transverse vibratory motions at the same frequency on two planes

Chapter 3

Performance Analysis

3.1 Nonlinear System

3.1.1 Current Limitation

To eliminate the complexity by multi control inputs of I_{left} and I_{right}, and to ensure that power is not wasted due to unnecessary work done by the bearing, the following relationship described in [10] between the control u_y and the coil currents I_{left} and I_{right} is used,

Case 1. When control u_y is between $-u_0$ and u_0, i.e. $-u_0 < u_y < u_0$

$$I_{left} = I_0 - 0.5u_y, \qquad I_{right} = I_0 + 0.5u_y \tag{3.1}$$

Case 2. When control u_y is below $-u_0$, i.e. $u_y < -u_0$

$$I_{left} = -u_y, \qquad I_{right} = 0 \tag{3.2}$$

Case 3. When control u_y is above u_0, i.e. $u_y > u_0$

$$I_{left} = 0, \qquad I_{right} = u_y \tag{3.3}$$

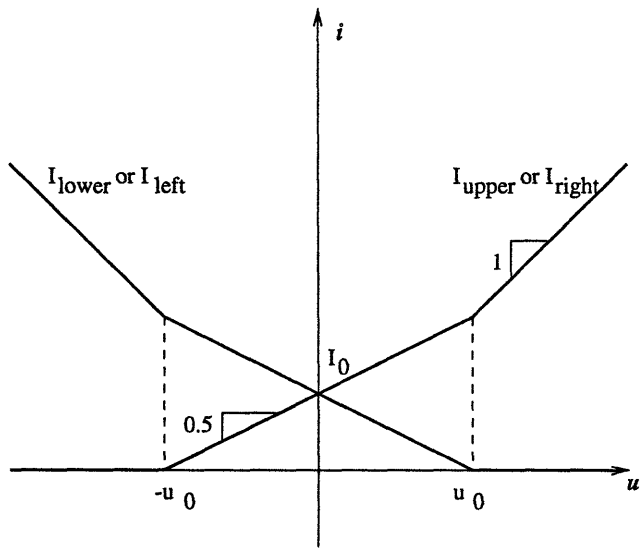

Figure 3-1: The Relationship between the Control u and the Coil Currents I_l and I_u

and similarly for u_z with its corresponding I_{lower} and I_{upper}:

Case 1. When control u_z is between $-u_0$ and u_0, i.e. $-u_0 < u_z < u_0$

$$I_{left} = I_0 - 0.5u_z, \qquad I_{right} = I_0 + 0.5u_z \tag{3.4}$$

Case 2. When control u_z is below $-u_0$, i.e. $u_z < -u_0$

$$I_{left} = -u_z, \qquad I_{right} = 0 \tag{3.5}$$

Case 3. When control u_z is above u_0, i.e. $u_z > u_0$

$$I_{left} = 0, \qquad I_{right} = u_z \tag{3.6}$$

Both relationships $u_y = I_{right} - I_{left}$ and $u_z = I_{upper} - I_{lower}$ always hold among the three cases. The consequences of the three equations relating control u_z to amplifier current is that the lower bearing does not produce unnecessary forces when the absolute value of the control u is above u_0. If the rotor moves down from its equilibrium value (towards the direction of gravity) then the attraction force created by the lower magnets will pull the rotor down even further. Therefore, by making the current to

the lower magnets go to zero, when the rotor deviates from its equilibrium value (in the direction of gravity), the lower magnets are prevented from creating any forces to further increase this deviation. The control current in the upper magnets will create the necessary upward force to bring the rotor back to its equilibrium value (*case 2*). The equation in *case 3* will assure the same type of force creation if the rotor moves up (against the direction of gravity) from its equilibrium value. Therefore, the three equations will prevent the system from wasting any power. The above relationship is graphically shown in Fig.3-1.

To consider also the effect of the permanent magnet, then the equivalent bias current can be defined as $i_0 = I_0 + \frac{M_p}{n}$ and the equivalent nominal air gap distance can be defined as $x_0 = h_0 + \frac{R_p \mu_0 A}{2}$.

3.1.2 Magnetic Saturation

The force generated by the magnetic bearings is calculated as:

$$F = \frac{\phi_1^2}{\mu_0 A} - \frac{\phi_2^2}{\mu_0 A} \tag{3.7}$$

where ϕ_1 and ϕ_2 are the magnetic fluxes in bearing 1 and 2, respectively.

To make the analysis and synthesis general and independent of units, [20] defined the dimensionless variables as follows:

$$F^* = \frac{F\mu_0}{B_{sat}^2 A} \qquad \textit{Normalized Magnetic Force} \tag{3.8}$$

$$i^* = \frac{i}{i_0} \qquad \textit{Normalized Control Current} \tag{3.9}$$

$$x^* = \frac{x}{x_0} \qquad \textit{Normalized Displacement} \tag{3.10}$$

$$B^* = \frac{2x_0 B_{sat}}{n\mu_0 i_0} \qquad \textit{Normalized Bias Flux Density} \tag{3.11}$$

Then, F^* can be written as follows:

$$F^* = \frac{(1+i^*)^2}{B^{*2}(1-x^*)^2} - \frac{(1-i^*)^2}{B^{*2}(1+x^*)^2}, \qquad when \left|\frac{1+i^*}{1-x^*}\right| \leq B^* \; and \; \left|\frac{1-i^*}{1+x^*}\right| \leq B^*$$

$$\text{or neither bearing is saturated,} \tag{3.12}$$

$$F^* = \frac{(1+i^*)^2}{B^{*2}(1-x^*)^2} - 1, \quad \text{when } \left|\frac{1+i^*}{1-x^*}\right| \leq B^* \text{ and } \left|\frac{1-i^*}{1+x^*}\right| > B^*$$

$$\text{or lower bearing is saturated,} \tag{3.13}$$

$$F^* = 1 - \frac{(1-i^*)^2}{B^{*2}(1+x^*)^2}, \quad \text{when } \left|\frac{1+i^*}{1-x^*}\right| > B^* \text{ and } \left|\frac{1-i^*}{1+x^*}\right| \leq B^*$$

$$\text{or upper bearing is saturated,} \tag{3.14}$$

$$F^* = 0, \quad \text{when } \left|\frac{1+i^*}{1-x^*}\right| > B^* \text{ and } \left|\frac{1-i^*}{1+x^*}\right| > B^*$$

$$\text{or both bearings are saturated.} \tag{3.15}$$

For the control input gain not to change its sign during the control action, $\frac{dF^*}{di^*} > 0$ should always be imposed as follows

$$1 + x^{*2} + 2x^*i^* > 0, \quad \textit{if neither bearing is saturated} \tag{3.16}$$

$$i^* > -1, \quad \textit{if lower bearing is saturated} \tag{3.17}$$

$$i^* < 1, \quad \textit{if upper bearing is saturated.} \tag{3.18}$$

When both magnetic bearings are not saturated, utilizing the Taylor's expansion with respect to x^* and i^*, the second order terms are cancelled out due to the symmetry of the magnetic bearings. The linear first order term is given by

$$F_l^* = \frac{4}{B^{*2}}(x^* + i^*) \tag{3.19}$$

where i^* is constrained by Eqn.3.12-3.15 and can be written as

$$-B^*x^* - B^* + 1 \leq i^* \leq B^*x^* + B^* + 1, \quad \textit{if} \quad -1 \leq x^* < \frac{-1}{B^*} \tag{3.20}$$

$$-B^*x^* - B^* + 1 \leq i^* \leq -B^*x^* + B^* - 1, \quad \textit{if} \quad \frac{-1}{B^*} \leq x^* \leq \frac{1}{B^*} \tag{3.21}$$

$$B^*x^* - B^* - 1 \leq i^* \leq -B^*x^* + B^* - 1, \quad \textit{if} \quad \frac{1}{B^*} < x^* \leq 1 \tag{3.22}$$

The range of allowable current is approximated by limiting $|i^*|$ to within 1 so that the saturation and force degradation would not occur and to provide a good control

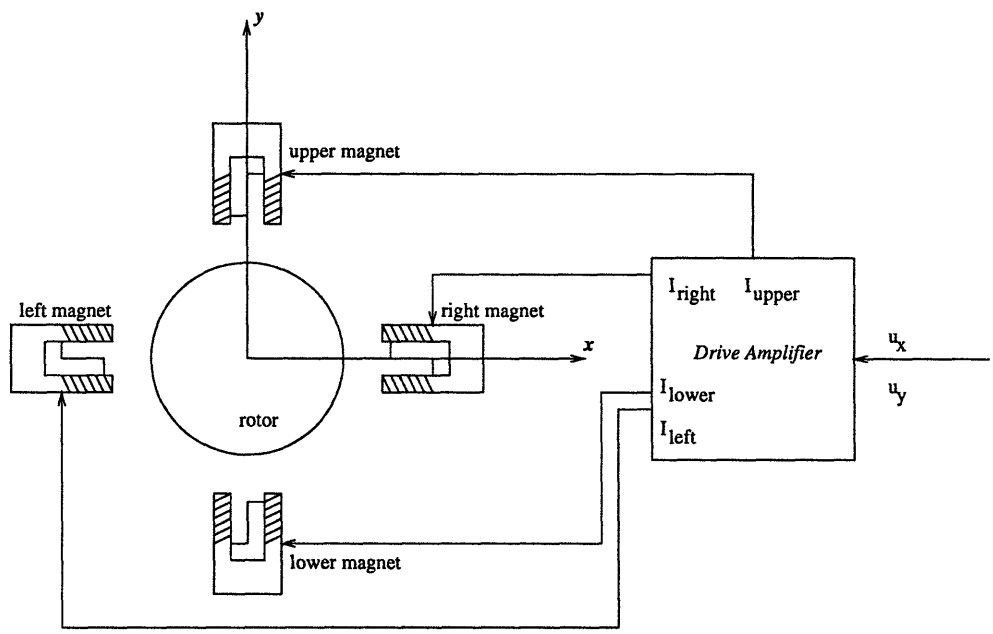

Figure 3-2: The control current setup in the radial direction

characteristic:

$$|i| \leq I_0, \tag{3.23}$$

3.2 System Identification

In this section, the rotor model equation derived from *Chapter 2* is extended. The 2-dimensional disk on flexible shaft is now a massive cylindrical rotor (infinite number of disks) which retains the inherent flexibility of a shaft. Using Eq.2.39, and [20], the equation of motion for one bearing in the x and y direction are given by:

$$m\frac{d^2x}{dt^2} = -F_{left} + F_{right} + \Sigma F_{dx} \tag{3.24}$$

$$m\frac{d^2y}{dt^2} = -F_{lower} + F_{upper} + \Sigma F_{dy} - mg \tag{3.25}$$

Here, F_{dx} and F_{dy} are assumed to consist of the projected radial force (due to the eccentricity ϵ) and the exogenous disturbance force, F_{ext}. Considering that $F_{x_i} = -F_{i_{left}} + F_{i_{right}}$, and $F_{y_i} = -F_{i_{lower}} + F_{i_{upper}}$, (where $i = 1, 2$), the Newton equations

for this two bearing setup becomes

$$m\ddot{x} = m\varepsilon\Omega^2 \, cos\Omega t + F_{x_1} + F_{x_2} + F_{dx} \tag{3.26}$$

$$m\ddot{y} = m\varepsilon\Omega^2 \, sin\Omega t + F_{y_1} + F_{y_2} + F_{dy} - mg \tag{3.27}$$

where

F_{left}=magnetic force by the left magnet,

F_{right}=magnetic force by the right magnet,

h_0=nominal bearing radial clearance,

x =deviation of the shaft from the bearing center, (x component),

y =deviation of the shaft from the bearing center, (y component),

m=rotor mass,

F_{dx}=disturbance force (x component),

F_{dy}=disturbance force (y component),

g =gravity.

The torque equations are obtained from [16] as

$$I_t\ddot{\varphi} - I_a\Omega\dot{\theta} = (I_t - I_a)\tau\Omega^2 sin\Omega t - aF_{x_1} + aF_{x_2} + lF_{dx} \tag{3.28}$$

$$I_t\ddot{\theta} + I_a\Omega\dot{\varphi} = (I_t - I_a)\tau\Omega^2 cos\Omega t - aF_{y_1} + aF_{y_2} - lF_{dy} \tag{3.29}$$

where

I_a=axial mass moment of inertia,

I_t=transverse mass moment of inertia,

φ =roll angle,

θ =yaw angle,

Ω=spinning speed,

ε =static unbalance,

τ =dynamic unbalance,

a =bearing set location from $X'Y'$ plane,

l =exogenous disturbance force location from $X'Y'$ plane.

Defining a new set of coordinates x_i, y_i, $i = 1, 2$ which represent the displacement of the rotor relative to the x and y bearings in each radial bearing set, respectively, and using the following transformations:

$$x = \frac{x_1 + x_2}{2}, \qquad y = \frac{y_1 + y_2}{2} \tag{3.30}$$

$$\varphi = \frac{x_1 - x_2}{2a}, \qquad \theta = \frac{y_1 - y_2}{2a} \tag{3.31}$$

the equations of motion in terms of the magnetic bearing local coordinates x_1, y_1, x_2, and y_2 can be obtained as follows;

$$\begin{aligned} \ddot{x_1} = \quad & \frac{\Omega I_a}{2I_t}(\dot{y_1} - \dot{y_2}) + (\frac{1}{m} + \frac{a^2}{I_t})F_{x_1} + (\frac{1}{m} - \frac{a^2}{I_t})F_{x_2} + (\frac{1}{m} + \frac{al}{I_t})F_{dx} \\ & +\varepsilon\Omega^2 cos\Omega t + (1 - \frac{I_a}{I_t})a\tau\Omega^2 sin\Omega t \end{aligned} \tag{3.32}$$

$$\begin{aligned} \ddot{x_2} = \quad & -\frac{\Omega I_a}{2I_t}(\dot{y_1} - \dot{y_2}) + (\frac{1}{m} - \frac{a^2}{I_t})F_{x_1} + (\frac{1}{m} + \frac{a^2}{I_t})F_{x_2} + (\frac{1}{m} - \frac{al}{I_t})F_{dx} \\ & +\varepsilon\Omega^2 cos\Omega t - (1 - \frac{I_a}{I_t})a\tau\Omega^2 sin\Omega t \end{aligned} \tag{3.33}$$

$$\begin{aligned} \ddot{y_1} = \quad & -\frac{\Omega I_a}{2I_t}(\dot{x_1} - \dot{x_2}) + (\frac{1}{m} - \frac{a^2}{I_t})F_{y_1} + (\frac{1}{m} + \frac{a^2}{I_t})F_{y_2} + (\frac{1}{m} - \frac{al}{I_t})F_{dy} \\ & +\varepsilon\Omega^2 sin\Omega t + (1 - \frac{I_a}{I_t})a\tau\Omega^2 cos\Omega t - g \end{aligned} \tag{3.34}$$

$$\begin{aligned} \ddot{y_2} = \quad & \frac{\Omega I_a}{2I_t}(\dot{x_1} - \dot{x_2}) + (\frac{1}{m} + \frac{a^2}{I_t})F_{y_1} + (\frac{1}{m} - \frac{a^2}{I_t})F_{y_2} + (\frac{1}{m} + \frac{al}{I_t})F_{dy} \\ & +\varepsilon\Omega^2 sin\Omega t - (1 - \frac{I_a}{I_t})a\tau\Omega^2 cos\Omega t - g \end{aligned} \tag{3.35}$$

Using the input relationship of Fig.3-1, the magnetic forces are obtained as

Case 1. When control u is between $-u_0$ and u_0, i.e. $-u_0 < u < u_0$

$$\begin{aligned} F_{x_i} \quad & = -F_{i_{left}} + F_{i_{right}} \\ & = -\frac{\mu_0 A_g N^2 (I_0 - 0.5u_{x_i})^2}{(h_0 + x_i)^2} + \frac{\mu_0 A_g N^2 (I_0 + 0.5u_{x_i})^2}{(h_0 - x_i)^2} \end{aligned} \tag{3.36}$$

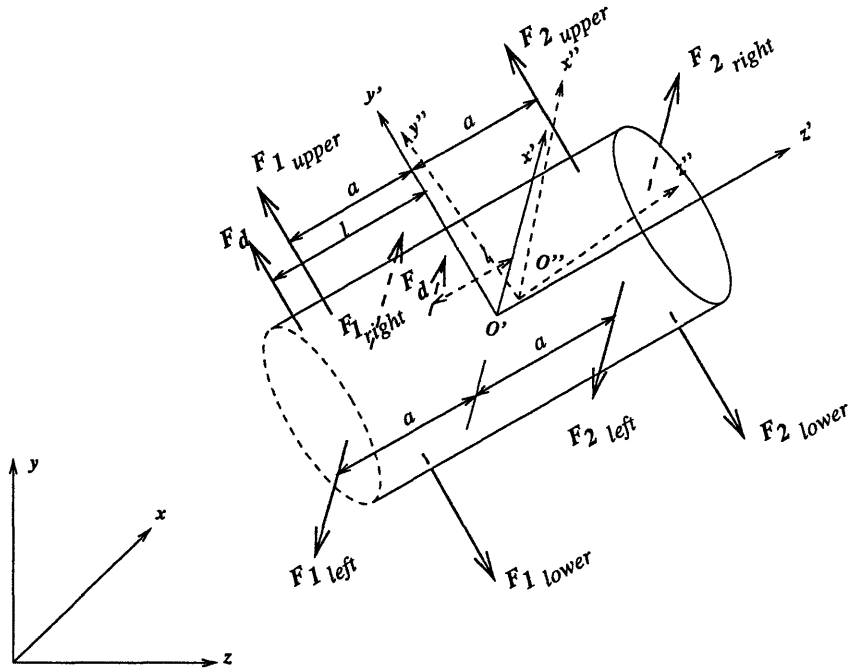

Figure 3-3: A Rotor Model

$$
\begin{aligned}
F_{y_i} &= -F_{i_{lower}} + F_{i_{upper}} \\
&= -\frac{\mu_0 A_g N^2 (I_0 - 0.5u_{y_i})^2}{(h_0 + y_i)^2} + \frac{\mu_0 A_g N^2 (I_0 + 0.5u_{y_i})^2}{(h_0 - y_i)^2}
\end{aligned} \tag{3.37}
$$

Case 2. When control u is below $-u_0$, i.e. $u < -u_0$

$$
\begin{aligned}
F_{x_i} &= -F_{i_{left}} \\
&= -\frac{\mu_0 A_g N^2 (I_0 - 0.5u_{x_i})^2}{(h_0 + x_i)^2}
\end{aligned} \tag{3.38}
$$

$$
\begin{aligned}
F_{y_i} &= -F_{i_{lower}} \\
&= -\frac{\mu_0 A_g N^2 (I_0 - 0.5u_{y_i})^2}{(h_0 + y_i)^2}
\end{aligned} \tag{3.39}
$$

Case 3. When control u is above u_0, i.e. $u > u_0$

$$
\begin{aligned}
F_{x_i} &= F_{i_{right}} \\
&= \frac{\mu_0 A_g N^2 (I_0 + 0.5u_{x_i})^2}{(h_0 - x_i)^2}
\end{aligned} \tag{3.40}
$$

$$
\begin{aligned}
F_{y_i} &= F_{i_{upper}} \\
&= \frac{\mu_0 A_g N^2 (I_0 + 0.5u_{y_i})^2}{(h_0 - y_i)^2}
\end{aligned} \tag{3.41}
$$

where $i = 1, 2$.

At steady state, the current in the upper magnets are positive and the current in the lower magnets are zero, which pertains to Eq.3.36 for the x direction, and Eq.3.41 for the y direction.

Substituting the F_{x_i} and F_{y_i} into the equations of motion and defining the functions $\mathbf{f}(.)$ for the right hand side of Eq.3.32-3.35, the equations of interest are then given as follows:

$$f_{x_1}(x_1, x_2, y_1, y_2, u_{x_1}, u_{x_2}) = \ddot{x_1} \tag{3.42}$$

$$f_{x_2}(x_1, x_2, y_1, y_2, u_{x_1}, u_{x_2}) = \ddot{x_2} \tag{3.43}$$

$$f_{y_1}(x_1, x_2, y_1, y_2, u_{y_1}, u_{y_2}) = \ddot{y_1} \tag{3.44}$$

$$f_{y_2}(x_1, x_2, y_1, y_2, u_{y_1}, u_{y_2}) = \ddot{y_2} \tag{3.45}$$

where the equilibrium values of the current and states are

$$I_{left} = I_{right} = I_{x_0} \tag{3.46}$$

$$I_{upper} = I_{y_0}, I_{lower} = 0 \tag{3.47}$$

$$x = y = 0 \tag{3.48}$$

The linearized model of the state equations are obtained by

$$\begin{aligned} f_{x_1} = \quad & \left.\frac{\partial f_{x_1}}{\partial x_1}\right|_0 \delta x_1 + \left.\frac{\partial f_{x_1}}{\partial \dot{x_1}}\right|_0 \delta \dot{x_1} + \left.\frac{\partial f_{x_1}}{\partial x_2}\right|_0 \delta x_2 + \left.\frac{\partial f_{x_1}}{\partial \dot{x_2}}\right|_0 \delta \dot{x_2} + \left.\frac{\partial f_{x_1}}{\partial y_1}\right|_0 \delta y_1 + \left.\frac{\partial f_{x_1}}{\partial \dot{y_1}}\right|_0 \delta \dot{y_1} \\ & + \left.\frac{\partial f_{x_1}}{\partial y_2}\right|_0 \delta y_2 + \left.\frac{\partial f_{x_1}}{\partial \dot{y_2}}\right|_0 \delta \dot{y_2} + \left.\frac{\partial f_{x_1}}{\partial u_{x_1}}\right|_0 \delta u_{x_1} + \left.\frac{\partial f_{x_1}}{\partial u_{x_2}}\right|_0 \delta u_{x_2} \end{aligned} \tag{3.49}$$

$$\begin{aligned} f_{x_2} = \quad & \left.\frac{\partial f_{x_2}}{\partial x_1}\right|_0 \delta x_1 + \left.\frac{\partial f_{x_2}}{\partial \dot{x_1}}\right|_0 \delta \dot{x_1} + \left.\frac{\partial f_{x_2}}{\partial x_2}\right|_0 \delta x_2 + \left.\frac{\partial f_{x_2}}{\partial \dot{x_2}}\right|_0 \delta \dot{x_2} + \left.\frac{\partial f_{x_2}}{\partial y_1}\right|_0 \delta y_1 + \left.\frac{\partial f_{x_2}}{\partial \dot{y_1}}\right|_0 \delta \dot{y_1} \\ & + \left.\frac{\partial f_{x_2}}{\partial y_2}\right|_0 \delta y_2 + \left.\frac{\partial f_{x_2}}{\partial \dot{y_2}}\right|_0 \delta \dot{y_2} + \left.\frac{\partial f_{x_2}}{\partial u_{x_1}}\right|_0 \delta u_{x_1} + \left.\frac{\partial f_{x_2}}{\partial u_{x_2}}\right|_0 \delta u_{x_2} \end{aligned} \tag{3.50}$$

$$\begin{aligned} f_{y_1} = \quad & \left.\frac{\partial f_{y_1}}{\partial x_1}\right|_0 \delta x_1 + \left.\frac{\partial f_{y_1}}{\partial \dot{x_1}}\right|_0 \delta \dot{x_1} + \left.\frac{\partial f_{y_1}}{\partial x_2}\right|_0 \delta x_2 + \left.\frac{\partial f_{y_1}}{\partial \dot{x_2}}\right|_0 \delta \dot{x_2} + \left.\frac{\partial f_{y_1}}{\partial y_1}\right|_0 \delta y_1 + \left.\frac{\partial f_{y_1}}{\partial \dot{y_1}}\right|_0 \delta \dot{y_1} \\ & + \left.\frac{\partial f_{y_1}}{\partial y_2}\right|_0 \delta y_2 + \left.\frac{\partial f_{y_1}}{\partial \dot{y_2}}\right|_0 \delta \dot{y_2} + \left.\frac{\partial f_{y_1}}{\partial u_{y_1}}\right|_0 \delta u_{y_1} + \left.\frac{\partial f_{y_1}}{\partial u_{y_2}}\right|_0 \delta u_{y_2} \end{aligned} \tag{3.51}$$

$$
\begin{aligned}
f_{y_2} = \quad & \left.\frac{\partial f_{y_2}}{\partial x_1}\right|_0 \delta x_1 + \left.\frac{\partial f_{y_2}}{\partial \dot{x_1}}\right|_0 \delta \dot{x_1} + \left.\frac{\partial f_{y_2}}{\partial x_2}\right|_0 \delta x_2 + \left.\frac{\partial f_{y_2}}{\partial \dot{x_2}}\right|_0 \delta \dot{x_2} + \left.\frac{\partial f_{y_2}}{\partial y_1}\right|_0 \delta y_1 + \left.\frac{\partial f_{y_2}}{\partial \dot{y_1}}\right|_0 \delta \dot{y_1} \\
& + \left.\frac{\partial f_{y_2}}{\partial y_2}\right|_0 \delta y_2 + \left.\frac{\partial f_{y_2}}{\partial \dot{y_2}}\right|_0 \delta \dot{y_2} + \left.\frac{\partial f_{y_2}}{\partial u_{y_1}}\right|_0 \delta u_{y_1} + \left.\frac{\partial f_{y_2}}{\partial u_{y_2}}\right|_0 \delta u_{y_2} \qquad (3.52)
\end{aligned}
$$

Defining

$$
\begin{aligned}
c_1 &= \frac{1}{m} + \frac{a^2}{I_t}, \quad c_2 = \frac{1}{m} - \frac{a^2}{I_t}, \\
c_3 &= \frac{1}{m} + \frac{al}{I_t}, \quad c_4 = \frac{1}{m} - \frac{al}{I_t}, \\
c_5 &= \frac{\Omega I_a}{2I_t}, \\
c_6 &= 1 - \frac{I_a}{I_t},
\end{aligned}
$$

each term of the f_{x_1} becomes

$$
\begin{aligned}
\left.\frac{\partial}{\partial x_1} f_{x_1}\right|_0 &= c_1 \left(\frac{2K(I_0 - 0.5u_{x_1})^2}{m(h_0 + x_1)^3} + \frac{2K(I_0 + 0.5u_{x_1})^2}{m(h_0 - x_1)^3} \right) \\
&= c_1 \frac{4KI_{0_x}^2}{mh_0^3} \qquad (3.53) \\
\left.\frac{\partial}{\partial \dot{x_1}} f_{x_1}\right|_0 &= 0 \qquad (3.54) \\
\left.\frac{\partial}{\partial x_2} f_{x_1}\right|_0 &= c_2 \left(\frac{2K(I_0 - 0.5u_{x_2})^2}{m(h_0 + x_2)^3} + \frac{2K(I_0 + 0.5u_{x_2})^2}{m(h_0 - x_2)^3} \right) \\
&= c_2 \frac{4KI_{0_x}^2}{mh_0^3} \qquad (3.55) \\
\left.\frac{\partial}{\partial \dot{x_2}} f_{x_1}\right|_0 &= 0 \qquad (3.56) \\
\left.\frac{\partial}{\partial y_1} f_{x_1}\right|_0 &= 0 \qquad (3.57) \\
\left.\frac{\partial}{\partial \dot{y_1}} f_{x_1}\right|_0 &= c_5 \qquad (3.58) \\
\left.\frac{\partial}{\partial y_2} f_{x_1}\right|_0 &= 0 \qquad (3.59) \\
\left.\frac{\partial}{\partial \dot{y_2}} f_{x_1}\right|_0 &= -c_5 \qquad (3.60)
\end{aligned}
$$

$$\left.\frac{\partial}{\partial u_{x_1}} f_{x_1}\right|_0 = c_1 \left(\frac{K(I_0 - 0.5u_{x_1})}{m(h_0 + x_1)^2} + \frac{K(I_0 + 0.5u_{x_1})}{m(h_0 - x_1)^2}\right)$$

$$= c_1 \frac{2KI_{0_x}}{mh_0^2} \tag{3.61}$$

$$\left.\frac{\partial}{\partial u_{x_2}} f_{x_1}\right|_0 = c_2 \left(\frac{K(I_0 - 0.5u_{x_2})}{m(h_0 + x_2)^2} + \frac{K(I_0 + 0.5u_{x_2})}{m(h_0 - x_2)^2}\right)$$

$$= c_2 \frac{2KI_{0_x}}{mh_0^2} \tag{3.62}$$

f_{x_2} becomes

$$\left.\frac{\partial}{\partial x_1} f_{x_1}\right|_0 = c_2 \left(\frac{2K(I_0 - 0.5u_{x_1})^2}{m(h_0 + x_1)^3} + \frac{2K(I_0 + 0.5u_{x_1})^2}{m(h_0 - x_1)^3}\right)$$

$$= c_2 \frac{4KI_{0_x}^2}{mh_0^3} \tag{3.63}$$

$$\left.\frac{\partial}{\partial \dot{x_1}} f_{x_1}\right|_0 = 0 \tag{3.64}$$

$$\left.\frac{\partial}{\partial x_2} f_{x_1}\right|_0 = c_1 \left(\frac{2K(I_0 - 0.5u_{x_2})^2}{m(h_0 + x_2)^3} + \frac{2K(I_0 + 0.5u_{x_2})^2}{m(h_0 - x_2)^3}\right)$$

$$= c_1 \frac{4KI_{0_x}^2}{mh_0^3} \tag{3.65}$$

$$\left.\frac{\partial}{\partial \dot{x_2}} f_{x_1}\right|_0 = 0 \tag{3.66}$$

$$\left.\frac{\partial}{\partial y_1} f_{x_1}\right|_0 = 0 \tag{3.67}$$

$$\left.\frac{\partial}{\partial \dot{y_1}} f_{x_1}\right|_0 = -c_5 \tag{3.68}$$

$$\left.\frac{\partial}{\partial y_2} f_{x_1}\right|_0 = 0 \tag{3.69}$$

$$\left.\frac{\partial}{\partial \dot{y_2}} f_{x_1}\right|_0 = c_5 \tag{3.70}$$

$$\left.\frac{\partial}{\partial u_{x_1}} f_{x_1}\right|_0 = c_2 \left(\frac{K(I_0 - 0.5u_{x_1})}{m(h_0 + x_1)^2} + \frac{K(I_0 + 0.5u_{x_1})}{m(h_0 - x_1)^2}\right)$$

$$= c_2 \frac{2KI_{0_x}}{mh_0^2} \tag{3.71}$$

$$\left.\frac{\partial}{\partial u_{x_2}} f_{x_1}\right|_0 = c_1 \left(\frac{K(I_0 - 0.5u_{x_2})}{m(h_0 + x_2)^2} + \frac{K(I_0 + 0.5u_{x_2})}{m(h_0 - x_2)^2}\right)$$

$$= c_1 \frac{2KI_{0_x}}{mh_0^2} \tag{3.72}$$

f_{y_1} becomes

$$\left.\frac{\partial}{\partial x_1} f_{y_1}\right|_0 = 0 \tag{3.73}$$

$$\left.\frac{\partial}{\partial \dot{x_1}} f_{y_1}\right|_0 = -c_5 \tag{3.74}$$

$$\left.\frac{\partial}{\partial x_2} f_{y_1}\right|_0 = 0 \tag{3.75}$$

$$\left.\frac{\partial}{\partial \dot{x_2}} f_{y_1}\right|_0 = c_5 \tag{3.76}$$

$$\left.\frac{\partial}{\partial y_1} f_{y_1}\right|_0 = c_2 \frac{2K(I_0 + 0.5u_{y_1})^2}{m(h_0 - y_1)^3}$$

$$= c_2 \frac{2KI_{0_y}^2}{mh_0^3} \tag{3.77}$$

$$\left.\frac{\partial}{\partial \dot{y_1}} f_{y_1}\right|_0 = 0 \tag{3.78}$$

$$\left.\frac{\partial}{\partial y_2} f_{y_1}\right|_0 = c_1 \frac{2K(I_0 + 0.5u_{y_2})^2}{m(h_0 - x_2)^3}$$

$$= c_1 \frac{2KI_{0_y}^2}{mh_0^3} \tag{3.79}$$

$$\left.\frac{\partial}{\partial \dot{y_2}} f_{y_1}\right|_0 = 0 \tag{3.80}$$

$$\left.\frac{\partial}{\partial u_{y_1}} f_{y_1}\right|_0 = c_2 \frac{K(I_0 + 0.5u_{y_1})}{m(h_0 - y_1)^2}$$

$$= c_2 \frac{KI_{0_y}}{mh_0^2} \tag{3.81}$$

$$\left.\frac{\partial}{\partial u_{y_2}} f_{y_1}\right|_0 = c_1 \frac{K(I_0 + 0.5u_{y_2})}{m(h_0 - y_2)^2}$$

$$= c_1 \frac{KI_{0_y}}{mh_0^2} \tag{3.82}$$

and, f_{y_2} becomes

$$\left.\frac{\partial}{\partial x_1} f_{y_2}\right|_0 = 0 \tag{3.83}$$

$$\left.\frac{\partial}{\partial \dot{x_1}} f_{y_1}\right|_0 = c_5 \tag{3.84}$$

$$\left.\frac{\partial}{\partial x_2} f_{y_2}\right|_0 = 0 \tag{3.85}$$

$$\left.\frac{\partial}{\partial \dot{x_2}} f_{y_1}\right|_0 = -c_5 \tag{3.86}$$

$$\left.\frac{\partial}{\partial y_1} f_{y_2}\right|_0 = c_1 \frac{2K(I_0 + 0.5u_{y_1})^2}{m(h_0 - y_1)^3}$$

$$= c_1 \frac{2KI_{0_y}^2}{mh_0^3} \tag{3.87}$$

$$\left.\frac{\partial}{\partial \dot{y_1}} f_{y_2}\right|_0 = 0 \tag{3.88}$$

$$\left.\frac{\partial}{\partial y_2} f_{y_2}\right|_0 = c_2 \frac{2K(I_0 + 0.5u_{y_2})^2}{m(h_0 - x_2)^3}$$

$$= c_2 \frac{2KI_{0_y}^2}{mh_0^3} \tag{3.89}$$

$$\left.\frac{\partial}{\partial \dot{y_2}} f_{y_1}\right|_0 = 0 \tag{3.90}$$

$$\left.\frac{\partial}{\partial u_{y_1}} f_{y_2}\right|_0 = c_1 \frac{K(I_0 + 0.5u_{y_1})}{m(h_0 - y_1)^2}$$

$$= c_1 \frac{KI_{0_y}}{mh_0^2} \tag{3.91}$$

$$\left.\frac{\partial}{\partial u_{y_2}} f_{y_2}\right|_0 = c_2 \frac{K(I_0 + 0.5u_{y_2})}{m(h_0 - y_2)^2}$$

$$= c_2 \frac{KI_{0_y}}{mh_0^2} \tag{3.92}$$

Setting

$$k_1 = \frac{4KI_{0_x}^2}{mh_0^3}, \qquad k_2 = \frac{2KI_{0_x}}{mh_0^2}, \qquad k_3 = \frac{2KI_{0_y}^2}{mh_0^3}, \qquad k_4 = \frac{KI_{0_y}}{mh_0^2}$$

the state equation form of the linearized equation can then be obtained as follows:

$$\frac{d}{dt}\underbrace{\begin{bmatrix} x_1 \\ x_2 \\ y_1 \\ y_2 \\ \dot{x_1} \\ \dot{x_2} \\ \dot{y_1} \\ \dot{y_2} \end{bmatrix}}_{\mathbf{x}} = \underbrace{\begin{bmatrix} 0 & 0 & 0 & 0 & 1 & 0 & 0 & 0 \\ 0 & 0 & 0 & 0 & 0 & 1 & 0 & 0 \\ 0 & 0 & 0 & 0 & 0 & 0 & 1 & 0 \\ 0 & 0 & 0 & 0 & 0 & 0 & 0 & 1 \\ c_1k_1 & c_2k_1 & 0 & 0 & 0 & 0 & c_5 & -c_5 \\ c_2k_1 & c_1k_1 & 0 & 0 & 0 & 0 & -c_5 & c_5 \\ 0 & 0 & c_2k_3 & c_1k_3 & -c_5 & c_5 & 0 & 0 \\ 0 & 0 & c_1k_3 & c_2k_3 & c_5 & -c_5 & 0 & 0 \end{bmatrix}}_{\mathbf{A}} \begin{bmatrix} x_1 \\ x_2 \\ y_1 \\ y_2 \\ \dot{x_1} \\ \dot{x_2} \\ \dot{y_1} \\ \dot{y_2} \end{bmatrix} +$$

$$\underbrace{\begin{bmatrix} 0 & 0 & 0 & 0 \\ 0 & 0 & 0 & 0 \\ 0 & 0 & 0 & 0 \\ 0 & 0 & 0 & 0 \\ c_1k_2 & c_2k_2 & 0 & 0 \\ c_2k_2 & c_1k_2 & 0 & 0 \\ 0 & 0 & c_2k_4 & c_1k_4 \\ 0 & 0 & c_1k_4 & c_2k_4 \end{bmatrix}}_{\mathbf{B}} \underbrace{\begin{bmatrix} u_{x_1} \\ u_{x_2} \\ u_{y_1} \\ u_{y_2} \end{bmatrix}}_{\mathbf{u}} + \underbrace{\begin{bmatrix} 0 & 0 \\ 0 & 0 \\ 0 & 0 \\ 0 & 0 \\ c_3 & 0 \\ c_4 & 0 \\ 0 & c_4 \\ 0 & c_3 \end{bmatrix}}_{\mathbf{L}} \underbrace{\begin{bmatrix} F_{dx} \\ F_{dy} \end{bmatrix}}_{\mathbf{F}_d} +$$

$$\underbrace{\begin{bmatrix} 0 \\ 0 \\ 0 \\ 0 \\ \varepsilon\Omega^2 cos\Omega t + c_6 a\tau\Omega^2 sin\Omega t \\ \varepsilon\Omega^2 cos\Omega t - c_6 a\tau\Omega^2 sin\Omega t \\ \varepsilon\Omega^2 sin\Omega t + c_6 a\tau\Omega^2 cos\Omega t - g \\ \varepsilon\Omega^2 sin\Omega t - c_6 a\tau\Omega^2 cos\Omega t - g \end{bmatrix}}_{\mathbf{d}}$$

or in the compact form as

$$\dot{\mathbf{x}} = \mathbf{A}\mathbf{x} + \mathbf{B}\mathbf{u} + \mathbf{L}\mathbf{F}_d + \mathbf{d} \tag{3.93}$$

The matrix $\mathbf{A}$ can be segmentized as follows

$$\mathbf{A} = \begin{bmatrix} \mathbf{A}_{11} & \mathbf{A}_{12} \\ \mathbf{A}_{21} & \mathbf{A}_{22} \end{bmatrix}$$

where

$$\begin{aligned}
\mathbf{A}_{11} &= \mathbf{0}, \\
\mathbf{A}_{12} &= \mathbf{I}, \\
\mathbf{A}_{21} &= \begin{bmatrix} c_1k_1 & c_2k_1 & 0 & 0 \\ c_2k_1 & c_1k_1 & 0 & 0 \\ 0 & 0 & c_2k_3 & c_1k_3 \\ 0 & 0 & c_1k_3 & c_2k_3 \end{bmatrix}, \\
\mathbf{A}_{22} &= \begin{bmatrix} 0 & 0 & c_5 & -c_5 \\ 0 & 0 & -c_5 & c_5 \\ -c_5 & c_5 & 0 & 0 \\ c_5 & -c_5 & 0 & 0 \end{bmatrix}
\end{aligned}$$

The matrix $\mathbf{A}_{21}$ and the matrix $\mathbf{A}_{22}$ represent the *stiffness* and the *gyroscopic effect* of the system, respectively. They show that the total force in one axis direction is only affected by the spring-effect forces in its own axis and the damping forces in the other axis. The gyroscopic coupling effect appears as the constant $c_5 = \frac{\Omega I_a}{2I_t}$'s in the matrix $\mathbf{A}_{22}$, due to the rotation speed Ω.

The transfer function matrix from input to output is obtained by performing *Laplace transform* as follows:

$$[s\mathbf{I} - \mathbf{A}]\mathbf{x} \quad = \mathbf{B}\mathbf{u} + \mathbf{L}\mathbf{F}_d + \mathbf{d}$$

$$\Rightarrow \mathbf{x} \quad = [s\mathbf{I} - \mathbf{A}]^{-1}\mathbf{B}\mathbf{u} + [s\mathbf{I} - \mathbf{A}]^{-1}\mathbf{L}\mathbf{F}_d + [s\mathbf{I} - \mathbf{A}]^{-1}\mathbf{d}$$

and in the final form,

$$\mathbf{x} = \mathbf{G}(s)\mathbf{u} + \mathbf{G}(s)\mathbf{B}^{-1}\mathbf{L}\mathbf{F}_d + \mathbf{G}(s)\mathbf{B}^{-1}\mathbf{d} \tag{3.94}$$

where $\mathbf{G}(s) = [s\mathbf{I} - \mathbf{A}]^{-1}\mathbf{B}$.

The disturbance rejection transfer function is

$$\mathbf{T}_d(s) = [s\mathbf{I} - \mathbf{A}]^{-1}\mathbf{L} \tag{3.95}$$

having the same characteristic roots as the open-loop transfer function, but the different transmission zeros as depending upon the matrix $\mathbf{L}$.

The characteristic equation is

$$\left(s^2 - k_1(c_1 + c_2)\right)\left(s^2 - k_3(c_1 + c_2)\right)\left[\left(s^2 - k_1(c_1 - c_2)\right)\left(s^2 + k_3(c_1 + c_2)\right) - (2sc_5)^2\right] = 0 \tag{3.96}$$

First criterion of *Routh-Hourwitz* to determine the system stability is the requirement that all coefficient be positive. Here, the system is proven to be unstable, because of the violation to

$$k_1(c_1 + c_2) + k_3(c_1 + c_2) < 0 \tag{3.97}$$

$$c_1 < c_2 \Rightarrow \frac{1}{m} + \frac{a^2}{I_t} < \frac{1}{m} - \frac{a^2}{I_t} \tag{3.98}$$

3.3 Summary

The rotor model has been extended from its simple *Jeffcott* assumption to take into account its massive body dynamics. Each of the magnetic bearing attracts the body to provide support in the $\mathbf{x}$ and $\mathbf{y}$ direction, one pair for each end. Their locations are equidistant from the rotor geometrical center. The rotor static unbalance, and

dynamic unbalance are also accounted into the system equation. Moreover, some exogenous disturbance force are anticipated by also including the forces into the formulation; their locations are assumed to be known in advance.

In order to analize the performance, the system nonlinear equation is linearized at its equilibrium point. The system matrices are then developed for some known constants corresponding to this equilibrium point. From the system equation, open-loop transfer functions from every specific input type to the system can be obtained.

Due to the current saturation in each bearing, the performance is limited. This limitation will be modeled as nonlinearity elements, and included in the system to study how the overall system performance will deviate from the desired shape. This subject is covered in the next section of this thesis.

Chapter 4

Simulation and Results

4.1 Introduction

The formulation in *Chap.3* is exercised using the provided physical constants of the system at the *MIT* lab. The open-loop transfer function is closed utilizing LQ regulator algorithm, whose performance is nominally satisfied. The describing function (*quasi- linearization*) is applied to approximate the current input limitation and the overall performance of the closed-loop system is then analized.

4.2 System Parameters

The paramaters used in this study are found in reference [10]:

Input current in horizontal axis,	I_{0_x}	$= 0.36$ A
Input current in vertical axis,	I_{0_y}	$= 1.25$ A
Mass,	m	$= 2.2$ kg
Air gap,	h_0	$= 2.5 \cdot 10^{-4}$ m
Gap surface,	Ag	$= 9.75 \cdot 10^{-5}\ m^2$
Coil turns,	N	$= 100$ turns
Permeability,	μ_0	$= 1.26 \cdot 10^{-6} N/A^2$

$$
\begin{aligned}
\mathrm{K} &= \mu_0 A_g N^2 = 1.23 \cdot 10^{-6} Nm^2/A^2 \\
\text{Transversal mass of inertia,} \quad I_t &= 8.285 \cdot 10^{-3}\ kg.m^2 \\
\text{Axial mass of inertia,} \quad I_a &= 1.555 \cdot 10^{-3} kg.m^2
\end{aligned}
$$

Applying the provided constants into the system equation, the plant matrices are then obtained as follows:

$$
\mathbf{A} = \begin{bmatrix}
0 & 0 & 0 & 0 & 1 & 0 & 0 & 0 \\
0 & 0 & 0 & 0 & 0 & 1 & 0 & 0 \\
0 & 0 & 0 & 0 & 0 & 0 & 1 & 0 \\
0 & 0 & 0 & 0 & 0 & 0 & 0 & 1 \\
19099 & -2256.1 & 0 & 0 & 0 & 0 & 70.383 & -70.383 \\
-2256.1 & 19099 & 0 & 0 & 0 & 0 & -70.383 & 70.383 \\
0 & 0 & -13600 & 115130 & -70.383 & 70.383 & 0 & 0 \\
0 & 0 & 115130 & -13600 & 70.383 & -70.383 & 0 & 0
\end{bmatrix},
$$

$$
\mathbf{B} = \begin{bmatrix}
0 & 0 & 0 & 0 \\
0 & 0 & 0 & 0 \\
0 & 0 & 0 & 0 \\
0 & 0 & 0 & 0 \\
2.3873 & -0.28201 & 0 & 0 \\
-0.28201 & 2.3873 & 0 & 0 \\
0 & 0 & -1.3600 & 11.513 \\
0 & 0 & 11.513 & -1.3600
\end{bmatrix},
$$

$$\mathbf{L} = \begin{bmatrix} 0 & 0 \\ 0 & 0 \\ 0 & 0 \\ 0 & 0 \\ 0.65305 & 0 \\ 0.25604 & 0 \\ 0 & 0.25604 \\ 0 & 0.65305 \end{bmatrix}, \mathbf{d} = \begin{bmatrix} 0 \\ 0 \\ 0 \\ 0 \\ \varepsilon\Omega^2 cos\Omega t + 0.056\tau\Omega^2 sin\Omega t \\ \varepsilon\Omega^2 cos\Omega t - 0.056\tau\Omega^2 sin\Omega t \\ \varepsilon\Omega^2 sin\Omega t + 0.056\tau\Omega^2 cos\Omega t - 9.8 \\ \varepsilon\Omega^2 sin\Omega t - 0.056\tau\Omega^2 cos\Omega t - 9.8 \end{bmatrix}.$$

The corresponding state variable of the plant equation is

$$\mathbf{x} = \begin{bmatrix} x_1 & x_2 & y_1 & y_2 & \dot{x_1} & \dot{x_2} & \dot{y_1} & \dot{y_2} \end{bmatrix}'$$

where $x_{1,2}$, $y_{1,2}$ are the rotor position in **x** and **y** axis coordinate, respectively, and $\dot{x_{1,2}}$, $\dot{y_{1,2}}$ are the rotor's velocity viewed from the **x** and **y** axis, respectively.

The corresponding input variable of the plant equation is

$$\mathbf{u} = \begin{bmatrix} u_{x_1} & u_{x_2} & u_{y_1} & u_{y_2} \end{bmatrix}'$$

where $u_{(.)}$ is the input current corresponding to the axis designated by (.).

The disturbance input variable is

$$\mathbf{F}_d = \begin{bmatrix} F_{dx} & F_{dy} \end{bmatrix}'$$

where $F_{d(.)}$ is the disturbance input parallel to axis $d(.)$.

The open-loop poles of the plant equation, as shown in Fig.4-1, are

$$8.1411 \cdot 10^{-15} \pm \jmath 382.12, \pm 129.78, \pm 137.21, \pm 318.64$$

Obviously, the plant is unstable due to some of the open-loop poles at the right

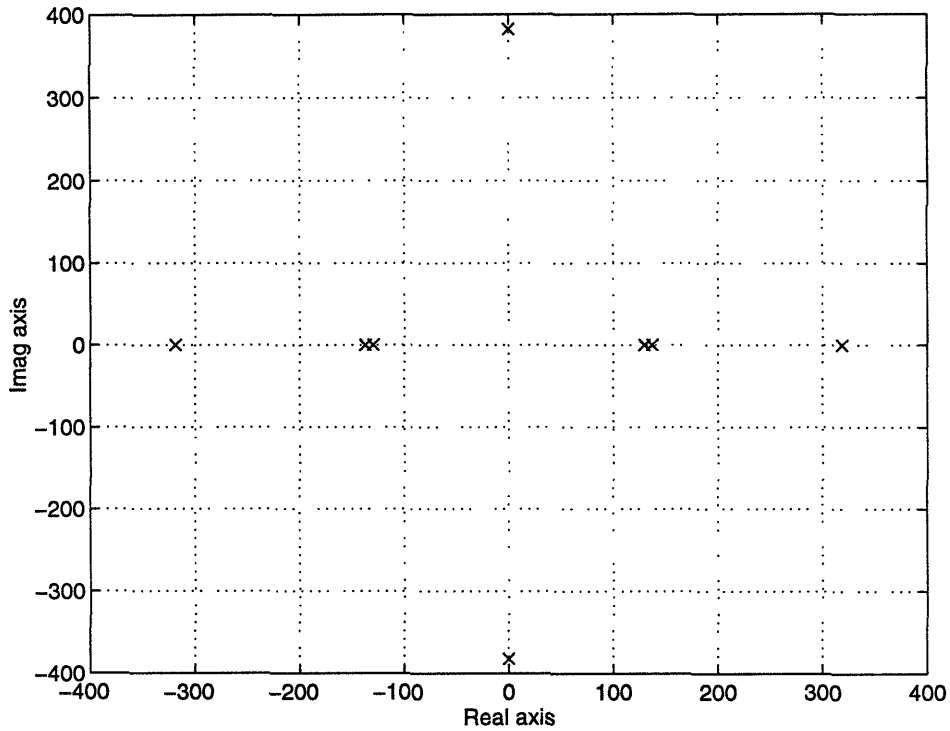

Figure 4-1: The open-loop roots

half plane, i.e. s = 129.78, 137.21 and 318.64. There are also two unstable complex poles, i.e. $8.1411 \cdot 10^{-15} \pm j382.12$, due to the gyroscopic effect.

4.3 LQ Regulator

The special properties of ferromagnetic materials used and the unstable nature of magnetic bearings will result in several performance limitations. Therefore, to satisfy certain performance specifications including the system stiffness, bandwidth, and rejectable disturbance, an integrated consideration on the system dynamics, control algorithm, and hardware design is absolutely necessary.

Recalling from Eq.3.93, the plant model in state space form is

$$\dot{\mathbf{x}} = \mathbf{A}\mathbf{x} + \mathbf{B}\mathbf{u} + \mathbf{L}\mathbf{F}_d + \mathbf{d} \tag{4.1}$$

$$\mathbf{y} = \mathbf{C}\mathbf{x} \tag{4.2}$$

The purpose here is to devise an LQ feed-back controller that minimizes the

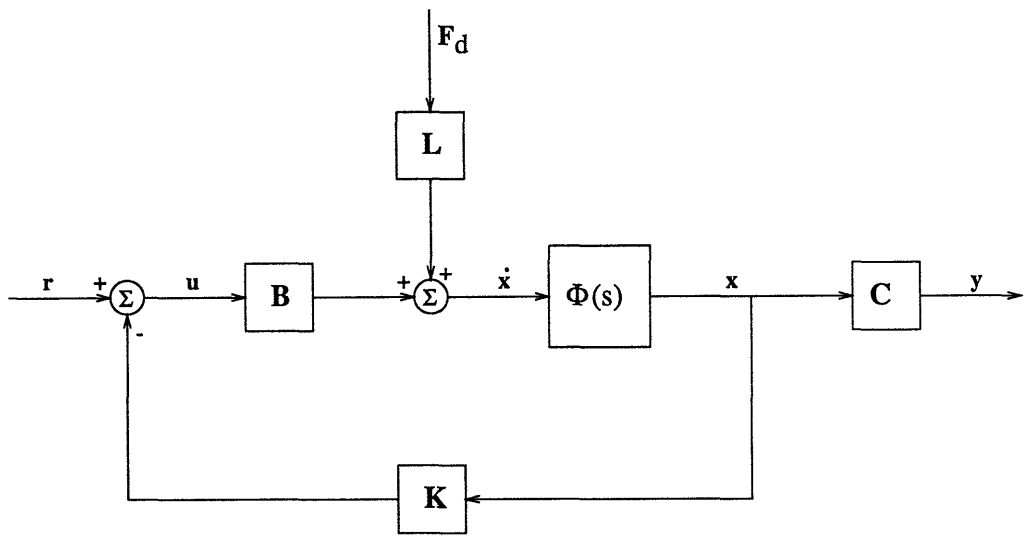

Figure 4-2: Linear Quadratic Regulator Design

quadratic cost function

$$J = \lim_{T \to \infty} \int_0^T [\mathbf{x}'(t)\mathbf{Q}\mathbf{x}(t) + \mathbf{u}'(t)\mathbf{R}\mathbf{u}(t)]\, dt \tag{4.3}$$

where

$$\mathbf{Q} = \mathbf{Q}' \geq 0, \qquad \mathbf{R} = \mathbf{R}' > 0 \tag{4.4}$$

under the assumption that $[\mathbf{A}, \mathbf{B}]$ is *controllable.*

There are model uncertainties, non-linearities, various kinds of disturbances and possibly many constraints on realistic solutions; none of which can easily be given a mathematical representation. Here, it is of interest in using the LQ theory as a method for synthesizing a controller for the magnetic bearing system, with the state weighting matrix $\mathbf{Q}$ and the input weighting matrix $\mathbf{R}$ which appear in the problem formulation considered as *tuning parameters* which are to be adjusted until a satisfactory design is considered.

For most physical devices, there is a maximum limit at which the input level cannot increase. Hence, some large control gains may not be realizable if applied for

the systems utilizing such devices. Therefore, the control input has to be limited, and this is imposed by the matrix $\mathbf{R}$, which is generally calculated as $\frac{1}{\rho}\mathbf{I}$, where ρ is an arbitrary constant. In order to avoid such saturation to occur, ρ can be set to be really small ($\rho \to 0$) i.e. the solution of a *cheap* control.

The solution of minimizing the cost function J is to let the control signal $\mathbf{u}$ be a linear function of the state:

$$\mathbf{u}(s) = -\mathbf{K}\mathbf{x}(s) \tag{4.5}$$

where the state-feedback matrix $\mathbf{K}$ is given by

$$\mathbf{K} = \mathbf{R}^{-1}\mathbf{B}'\mathbf{P} \tag{4.6}$$

while $\mathbf{P}$ satisfies the *algebraic Riccati equation*

$$\mathbf{A}'\mathbf{P} + \mathbf{P}\mathbf{A} - \mathbf{P}\mathbf{B}\mathbf{R}^{-1}\mathbf{B}'\mathbf{P} + \mathbf{Q} = 0 \tag{4.7}$$

and under the condition that $\mathbf{P} = \mathbf{P}' \geq 0$.

The matrix $\mathbf{K}$ exists, and the closed-loop system is internally stable, provided the state-space $[\mathbf{A}, \mathbf{B}]$ is *controllable.* Of the plant of interest,

$$rank \begin{bmatrix} \mathbf{B} & \mathbf{AB} & \mathbf{A}^2\mathbf{B} & \dots & \mathbf{A}^6\mathbf{B} & \mathbf{A}^7\mathbf{B} \end{bmatrix} = 8 \tag{4.8}$$

so the assumption of controllability is satisfied here.

From Fig.4-3, defining $\mathbf{G}_{LQ}(s)$ as the LQ loop transfer function, $\mathbf{S}_{LQ}(s)$ as the LQ sensitivity, and $\mathbf{C}_{LQ}(s)$ as the LQ complementary sensitivity transfer function, the LQ-based design system has the following asymptotic behavior:

$$\lim_{\rho\to 0} \mathbf{K}_{LQ}(s)\mathbf{G}(s) = \mathbf{G}_{LQ} = \mathbf{K}\mathbf{\Phi}(s)\mathbf{B} \tag{4.9}$$

$$\lim_{\rho\to 0} \mathbf{S}(s) = \mathbf{S}_{LQ} = (\mathbf{I} + \mathbf{G}_{LQ})^{-1} \tag{4.10}$$

$$\lim_{\rho\to 0} \mathbf{C}(s) = \mathbf{C}_{LQ} = (\mathbf{I} + \mathbf{G}_{LQ})^{-1}\mathbf{G}_{LQ} \tag{4.11}$$

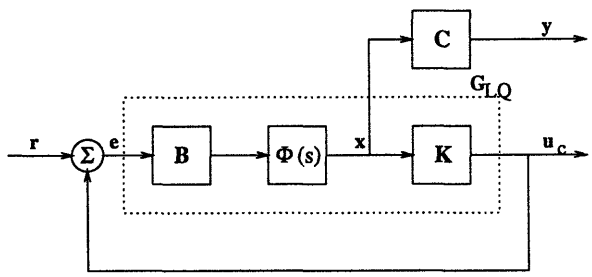

Figure 4-3: LQ Loop

As will be shown later, the singular values of the complementary sensitivity $\mathbf{C}_{LQ}$, and the sensitivity $\mathbf{S}_{LQ}$, are useful in the evaluation of the robustness, tracking ability, and disturbance attenuation of the system.

The LQR designs have built-in performance and robustness guarantees independent of the plant and design parameters. The designed controller is similar to a *regulator* where the system output follows a desired position indicated by the reference input. The procedure allows one to choose the design parameters and improve the closed-loop dynamics to achieve the desirable performance.

For this particular LQR design, the matrix $\mathbf{Q}$ provides equal weight for the position

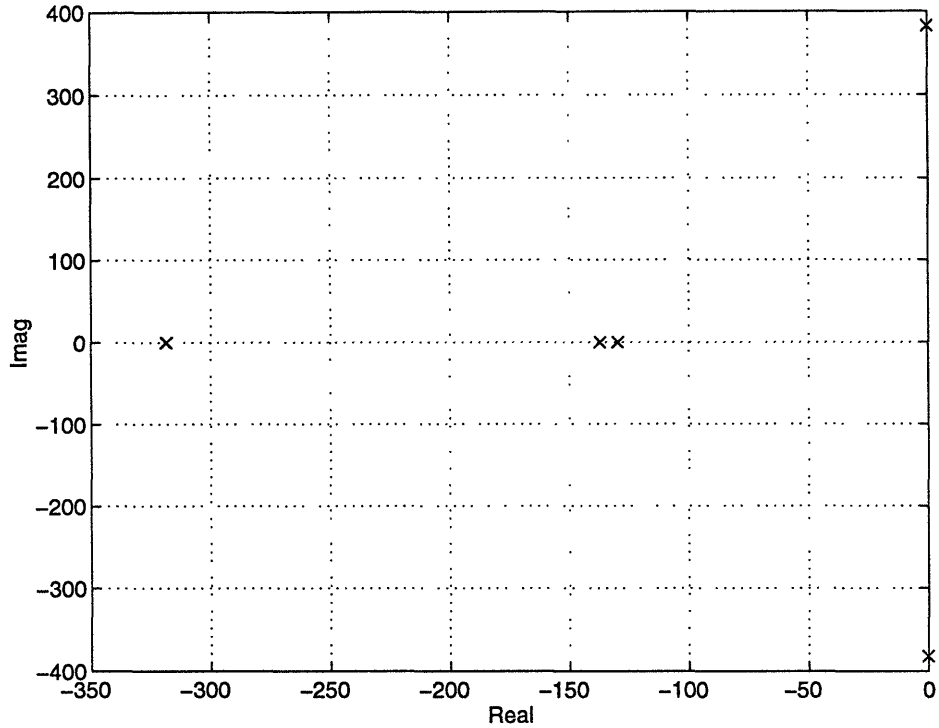

Figure 4-4: LQR Design: Closed-loop Poles

states and the velocity states, i.e.

$$\mathbf{Q} = \begin{bmatrix} 1 & 0 & 0 & 0 & 0 & 0 & 0 & 0 \\ 0 & 1 & 0 & 0 & 0 & 0 & 0 & 0 \\ 0 & 0 & 1 & 0 & 0 & 0 & 0 & 0 \\ 0 & 0 & 0 & 1 & 0 & 0 & 0 & 0 \\ 0 & 0 & 0 & 0 & 1 & 0 & 0 & 0 \\ 0 & 0 & 0 & 0 & 0 & 1 & 0 & 0 \\ 0 & 0 & 0 & 0 & 0 & 0 & 1 & 0 \\ 0 & 0 & 0 & 0 & 0 & 0 & 0 & 1 \end{bmatrix} \tag{4.12}$$

and ρ is arbitrarily chosen to be 10^{-3}, i.e.

$$\mathbf{R} = \frac{1}{\rho}\mathbf{I} = \begin{bmatrix} 1000 & 0 & 0 & 0 \\ 0 & 1000 & 0 & 0 \\ 0 & 0 & 1000 & 0 \\ 0 & 0 & 0 & 1000 \end{bmatrix} \tag{4.13}$$

The designed system is stable since all of the LQ closed-loop poles are in the

left-half plane, as shown in Fig.4-4, which are

$$-0.21755 \pm j382.12,\ -129.75,\ -129.81,\ -137.18,\ -137.24,\ -318.48,\ -318.80$$

The closed-loop dynamics with disturbances (Fig.4-2) is defined as

$$\begin{aligned} \dot{\mathbf{x}}(t) &= [\mathbf{A} - \mathbf{BK}]\mathbf{x}(t) + \mathbf{LF}_d(t) \\ \mathbf{y}(t) &= \mathbf{Cx}(t) \end{aligned}$$

Solving the algebraic Riccati equation, the optimal control matrix is obtain as follows:

$$\mathbf{K} = \begin{bmatrix} 13722 & 2278.1 & -4513.0 & 4513.0 & 98.410 & 24.877 & 4.8102 & -4.8102 \\ 2278.1 & 13722 & 4513.0 & -4513.0 & 24.877 & 98.410 & -4.8102 & 4.8102 \\ -3610.4 & 3610.4 & 12848 & 7152.3 & -23.197 & 23.197 & 28.332 & 34.435 \\ 3610.4 & -3610.4 & 7152.3 & 12848 & 23.197 & -23.197 & 34.435 & 28.332 \end{bmatrix},$$

and then

$$\mathbf{A}-\mathbf{BK} = \begin{bmatrix} 0 & 0 & 0 & 0 & 1 & 0 & 0 & 0 \\ 0 & 0 & 0 & 0 & 0 & 1 & 0 & 0 \\ 0 & 0 & 0 & 0 & 0 & 0 & 1 & 0 \\ 0 & 0 & 0 & 0 & 0 & 0 & 0 & 1 \\ -13017 & -3825.0 & 12047 & -12047 & -227.92 & -31.636 & 57.543 & -57.543 \\ -3825.0 & -13017 & -12047 & 12047 & -31.636 & -227.92 & -57.543 & 57.543 \\ -46477 & 46477 & -78471 & -23058 & -369.00 & 369.00 & -35.792 & -279.35 \\ 46477 & -46477 & -23058 & -78471 & 369.00 & -369.00 & -279.35 & -357.92 \end{bmatrix}.$$

A plot of the singular values are shown in Fig.4-5 - 4-6. Recalling that the LQR design controller is similar to a regulator where the system output follows a desired position indicated by the reference input, the output of the system is able to perform well as shown in the complementary sensitivity $\mathbf{C}_{LQ}$ in Fig.4-6. The magnitude of

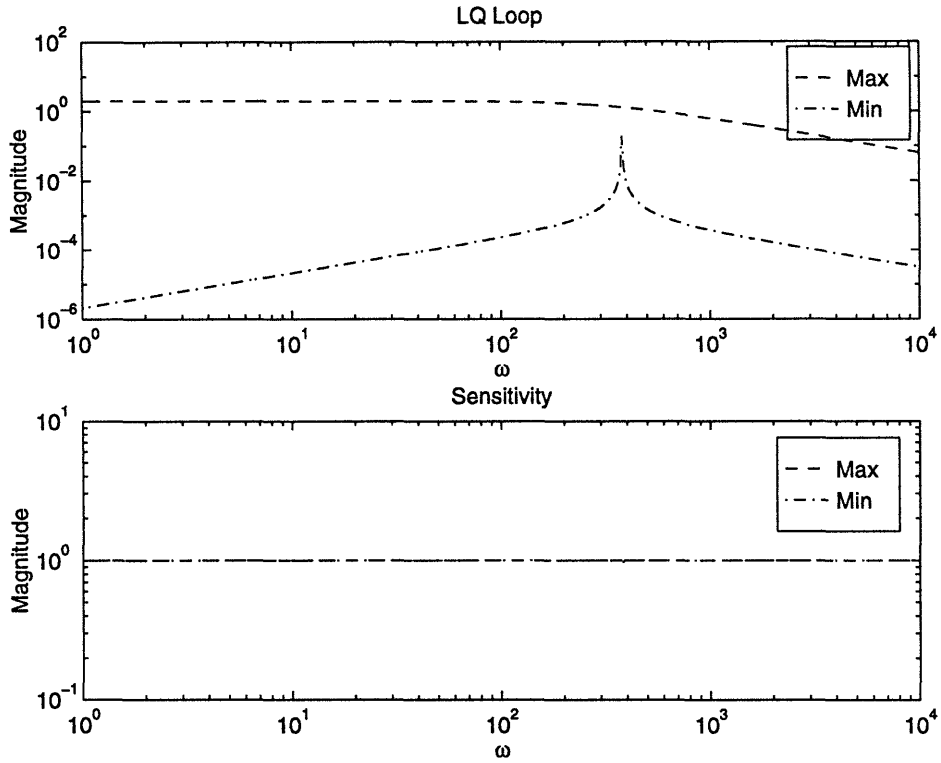

Figure 4-5: LQR Design: Frequency Domains, $\rho = 10^{-3}$

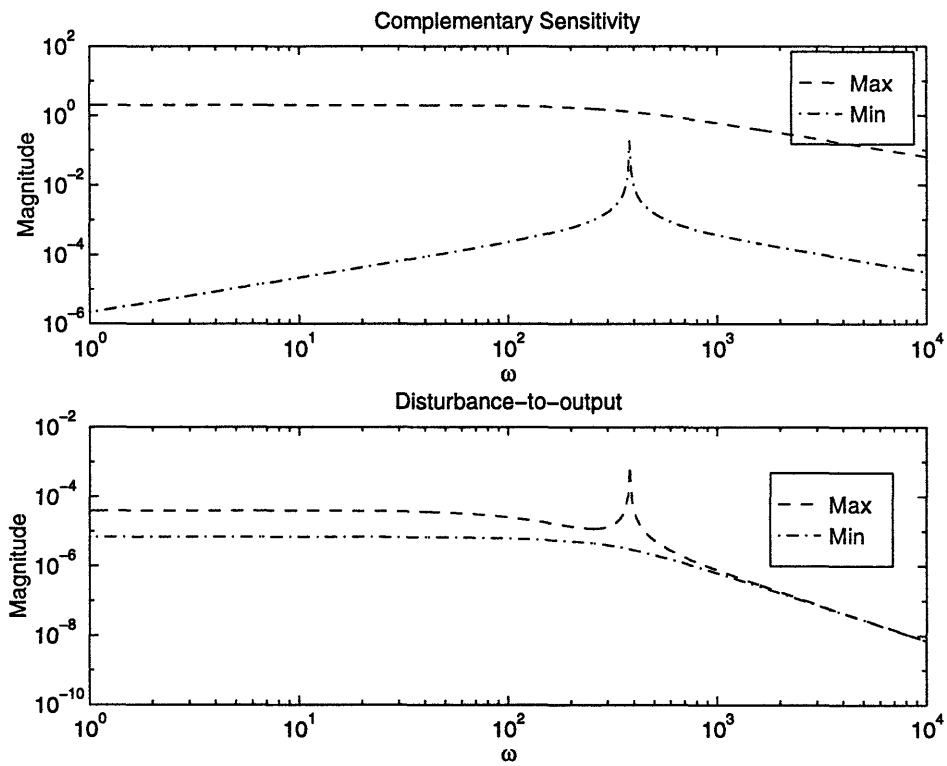

Figure 4-6: LQR Design: Frequency Domains, $\rho = 10^{-3}$

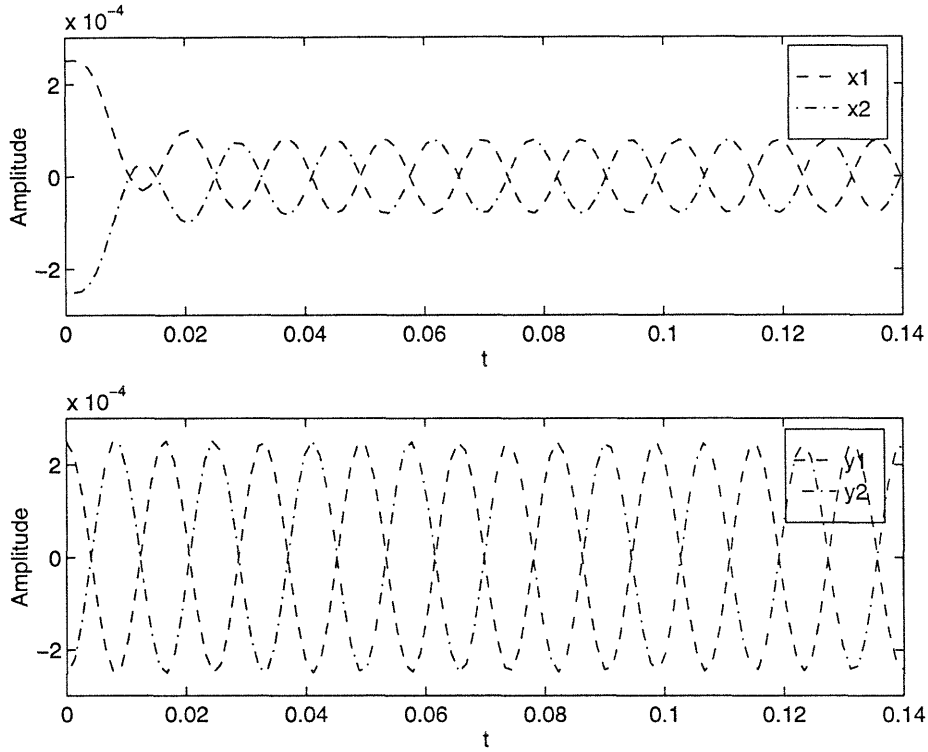

Figure 4-7: LQR Design: Initial Value, $\rho = 10^{-3}$

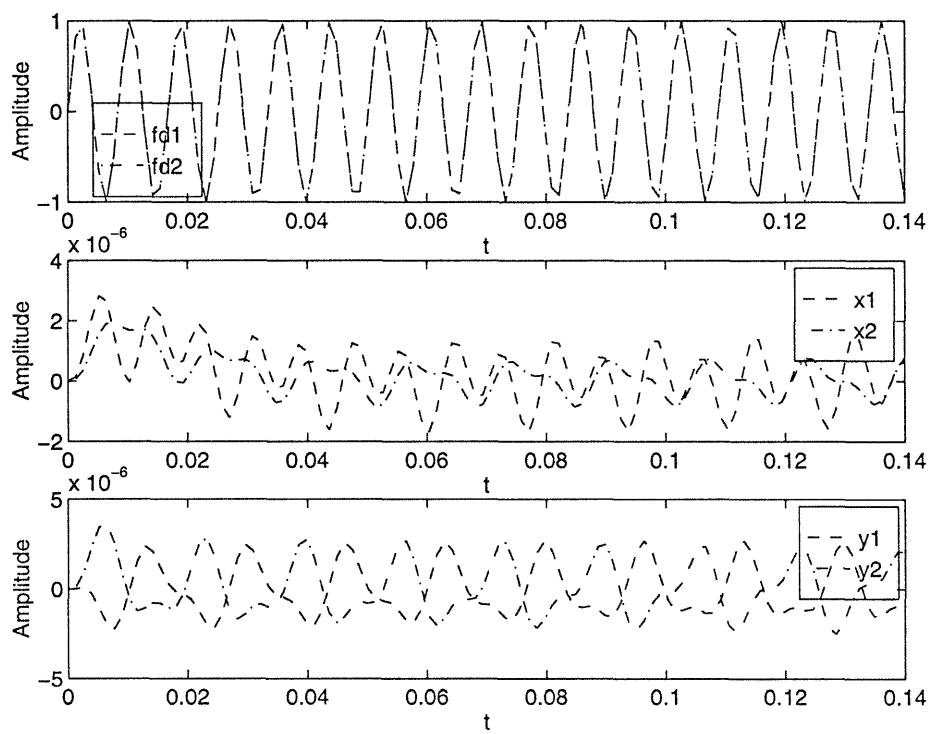

Figure 4-8: LQR Design: Disturbance Rejection Test, $\rho = 10^{-3}$

$\mathbf{C}_{LQ}$ equals approximately one, which shows that the closed-loop system is able to follow the desired trajectory. The roll-off rate is -20 dB/decade, which indicates good robustness to unmodelled high frequency dynamics. The sensitivity $\mathbf{S}_{LQ}$ equals one for all frequencies, meaning that fairly good disturbance rejection is achieved for the class of step disturbances (but not as yet desired, as shown in another LQR design in the next subsection). As the overall design, both of the sensitivity $\mathbf{S}_{LQ}$ and $\mathbf{C}_{LQ}$ satisfy the LQ-designed system performance and robustness requirements as described in [2]. [1] The LQ-design disturbance-to-output frequency response has small gains of $3.9733 \cdot 10^{-5}$ and $6.8560 \cdot 10^{-6}$ at low frequency and attenuates the disturbance input at high frequency. The peak occurs the critical frequency of 382.12 Hz.

In order to investigate robust stability and robust performance of the proposed control method, the simulation results for $\rho = 10^{-3}$ are obtained using the designed controller matrix. In order to test the LQR-design system for any initial condition, the rotor is brought to the farthest possible position; that is, the rotor is almost touching the sensor, and with no initial velocity, i.e.

$$\mathbf{x}_0 = \begin{bmatrix} h_0 & -h_0 & h_0 & -h_0 & \mathbf{0}_{1\times 4} \end{bmatrix}'$$

where h_0 is the maximum bearing clearance, i.e. 0.25 mm. From Fig.4-7, it shows that the LQR-design system is somewhat able to bring the rotor into its stable position in the $\mathbf{x}$ axis with a relatively smaller amplitude of continuing oscillation.

[1] Under the condition that the matrix $\mathbf{R} = \mathbf{R}' > 0$, diagonal, the LQR design closed-loop system guarantees

1. *system performance*

$$\sigma_{min}\left[\mathbf{I} + \mathbf{G}_{LQ}(s)\right] \geq 1 \Rightarrow \sigma_{max}\left[\mathbf{S}_{LQ}(s)\right] \leq 1\,(= 0\,dB) \tag{4.14}$$

2. *system robustness*

$$\sigma_{min}\left[\mathbf{I} + \mathbf{G}_{LQ}^{-1}(s)\right] \geq \frac{1}{2} \Rightarrow \sigma_{max}\left[\mathbf{C}_{LQ}(s)\right] \leq 2\,(= 6\,dB) \tag{4.15}$$

Thus, it deduces from the above that the system is characterized by scalar gain margin in the range of $\frac{1}{2}$ to ∞, and phase margin in the range of -60 to 60 degree.

4.3.1 LQR Design with Relative Stability

For the main purpose of reducing further the continuing oscillation from an initial rotor condition, i.e. start-up process, the quadratic cost function is modified as

$$J = \lim_{T\to\infty} \int_0^T e^{2bt} \left[\mathbf{x}'(t)\mathbf{Q}\mathbf{x}(t) + \mathbf{u}'(t)\mathbf{R}\mathbf{u}(t)\right] dt, \qquad b \geq 0 \tag{4.16}$$

Here, $-b$ is the right end limit of the real axis, meaning that all of the resulting closed-loop poles will reside on the left-side area of this limit, i.e. $\Re(s) < -b$.

In order that the cost is kept minimum, J has to remain finite. Since $b \geq 0$, the quadratic integrand has to decrease faster than e^{-2bt}, i.e.

$$\mathbf{x}'(t)\mathbf{Q}\mathbf{x}(t) + \mathbf{u}'(t)\mathbf{R}\mathbf{u}(t) \leq Me^{-2bt} \tag{4.17}$$

where M is a positive constant.

Then, it is true that

$$\Re\left(\lambda_i\left[\mathbf{A} - \mathbf{B}\mathbf{K}\right]\right) < -b \tag{4.18}$$

where λ_i, i=1,2,... are the characteristic roots. Thus, both the closed-loop state, $\mathbf{x}$(t), and the closed-loop control, $\mathbf{u}$(t) decay faster than e^{-bt}.

The *modified algebraic Riccati equation* is then

$$[\mathbf{A} + b\mathbf{I}]'\mathbf{P} + \mathbf{P}[\mathbf{A} + b\mathbf{I}] - \mathbf{P}\mathbf{B}\mathbf{R}^{-1}\mathbf{B}'\mathbf{P} + \mathbf{Q} = 0 \tag{4.19}$$

The similar assumption as the pervious section still applies here. For $\rho = 10^{-3}$, and $b = 100$, the $\mathbf{A}$ matrix is now $[\mathbf{A}_{plant} + 100\mathbf{I}]$ and

$$rank\begin{bmatrix} \mathbf{B} & \mathbf{AB} & \mathbf{A}^2\mathbf{B} & \ldots & \mathbf{A}^6\mathbf{B} & \mathbf{A}^7\mathbf{B} \end{bmatrix} = 8 \tag{4.20}$$

so the assumption of controllability is satisfied.

With the similar matrix $\mathbf{Q}$ and matrix $\mathbf{R}$ as those in the previous section (Eq.4.12

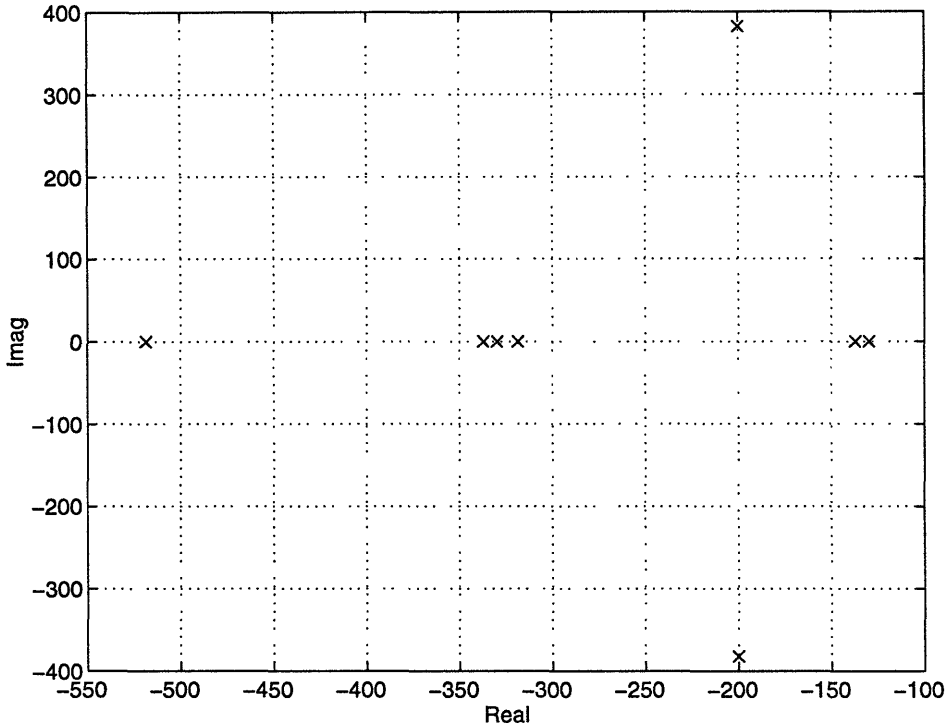

Figure 4-9: LQR-design Roots

and Eq.4.13), the resulting closed-loop poles, as shown in Fig.4-9, are

$$-129.78,\ -137.21,\ -200.00 \pm j382.12,\ -318.64,\ -329.78,\ -337.21,\ -518.64$$

Solving the modified algebraic Riccati equation, the optimal control matrix is obtained as follows:

$$\mathbf{K} = \begin{bmatrix} 26207 & 2122.0 & -7612.4 & 7612.4 & 188.87 & 29.419 & 5.9655 & -5.9655 \\ 2122.0 & 26207 & 7612.4 & -7612.4 & 29.419 & 188.87 & -5.9655 & 5.9655 \\ -4446.7 & 4446.7 & 14561 & 11715 & -28.769 & 28.769 & 23.801 & 58.665 \\ 4446.7 & -4446.7 & 11715 & 14561 & 28.769 & -28.769 & 58.665 & 23.801 \end{bmatrix},$$

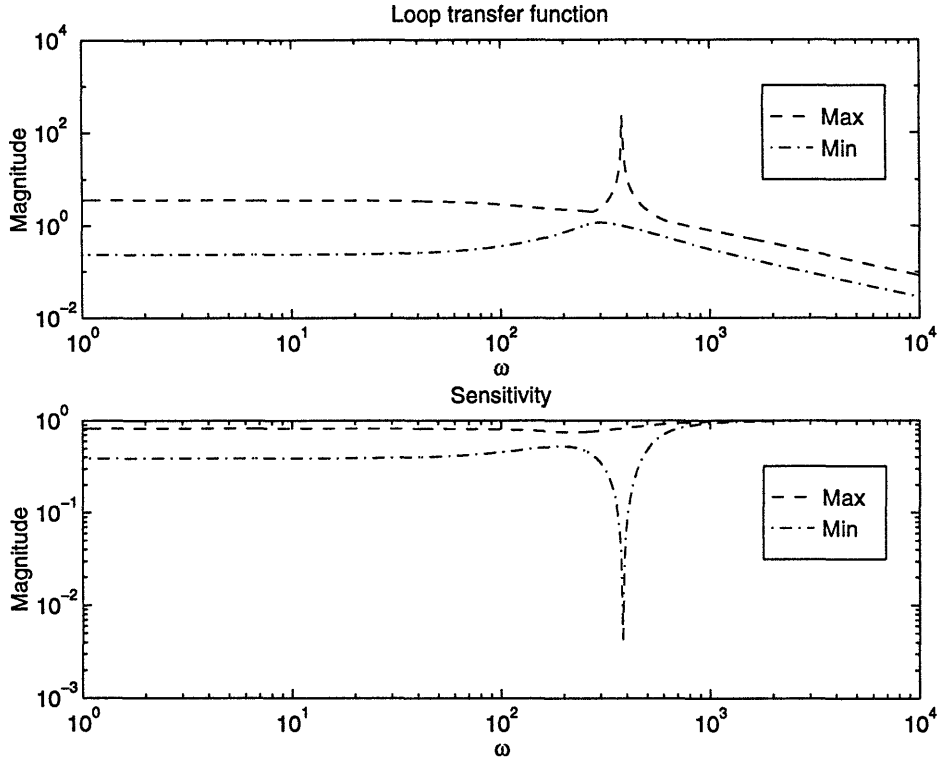

Figure 4-10: LQR Design: Frequency Domains, $\rho = 10^{-3}, b = 100$

and then

$$\mathbf{A}-\mathbf{BK} = \begin{bmatrix} 0 & 0 & 0 & 0 & 1 & 0 & 0 & 0 \\ 0 & 0 & 0 & 0 & 0 & 1 & 0 & 0 \\ 0 & 0 & 0 & 0 & 0 & 0 & 1 & 0 \\ 0 & 0 & 0 & 0 & 0 & 0 & 0 & 1 \\ -42867 & 68.582 & 20320 & -20320 & -442.59 & -16.971 & 54.459 & -54.459 \\ 68.602 & -42867 & -20320 & 20320 & -16.971 & -442.59 & -54.459 & 54.459 \\ -57242 & 57242 & -128670 & -36581 & -440.72 & 440.72 & -643.04 & -194.23 \\ 57242 & -57242 & -36581 & -128670 & 440.72 & -440.72 & -194.23 & -643.04 \end{bmatrix}.$$

A plot of the singular values are shown in Fig.4-10 - 4-11. The loop transfer function $\mathbf{G}_{LQ}$ starts off at DC gain of 3.5556 and 0.23504 at low frequencies, and stays constant until the frequency reaches the root at 382.12 Hz where a peak occurs. The roll-off rate is -20 dB/decade at high frequencies. The sensitivity $\mathbf{S}_{LQ}$ has DC gains at 0.82237 and 0.38839 at low frequencies, a valley at the root frequency of 382.12 Hz. The sensitivity $\mathbf{S}_{LQ}$ and $\mathbf{S}_{dy}$ are small at low frequencies which means good disturbance rejection for the class of step disturbance. The sensitivity $\mathbf{S}_{LQ}$ is also very small at the pole frequency of 382.12 Hz, which means suppresion of the

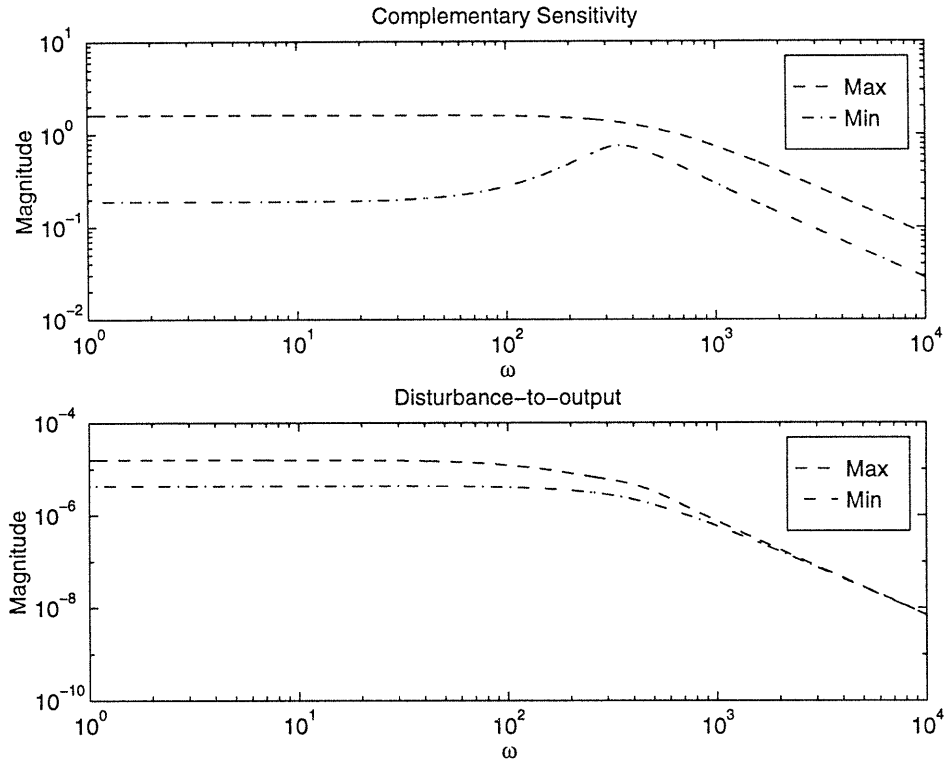

Figure 4-11: LQR Design: Frequency Domains, $\rho = 10^{-3}, b = 100$

imbalance forces. The complementary sensitivity $\mathbf{C}_{LQ}$ has DC gains at 1.6144 and 0.1905 at low frequencies (which indicates good tracking in the frequency range), and elimination of the peak at 382.12 Hz of $\mathbf{G}_{LQ}$. Thus, the closed-loop system has managed to avoid any possible physical damage due to the peak at 382.12 Hz as shown in the previous LQ design closed-loop system. The roll-off rate is -20 dB/decade, which shows good robustness to unmodeled high frequency dynamics. The system performance for disturbance rejection is good, provided that the DC gains are considerably small, i.e. $1.5766 \cdot 10^{-5}$ and $4.3408 \cdot 10^{-6}$, and rolls off at 40 dB/decade at high frequencies.

The simulation result is again obtained for this designed controller as shown in Fig.4-12 with the initial value of

$$\mathbf{x}_0 = \begin{bmatrix} h_0 & -h_0 & h_0 & -h_0 & \mathbf{0}_{1\times 4} \end{bmatrix}'$$

where h_0 is the maximum bearing clearance, i.e. 0.25 mm.

Then, it shows that this particular LQR-designed system is able to bring the rotor into its stable position within a relatively short period of time, i.e. $3T = 0.03$ sec, where T is the designated time constant $\frac{1}{b} = 0.01$ sec. The designed system has also

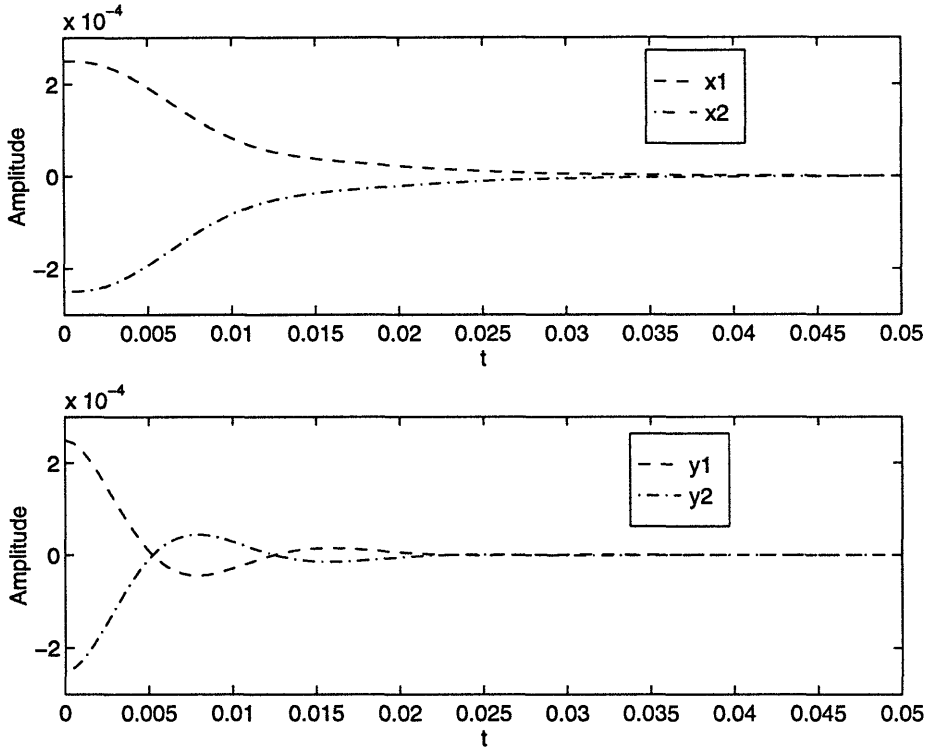

Figure 4-12: LQR Design: Initial Value, $\rho = 10^{-3}, b = 100$

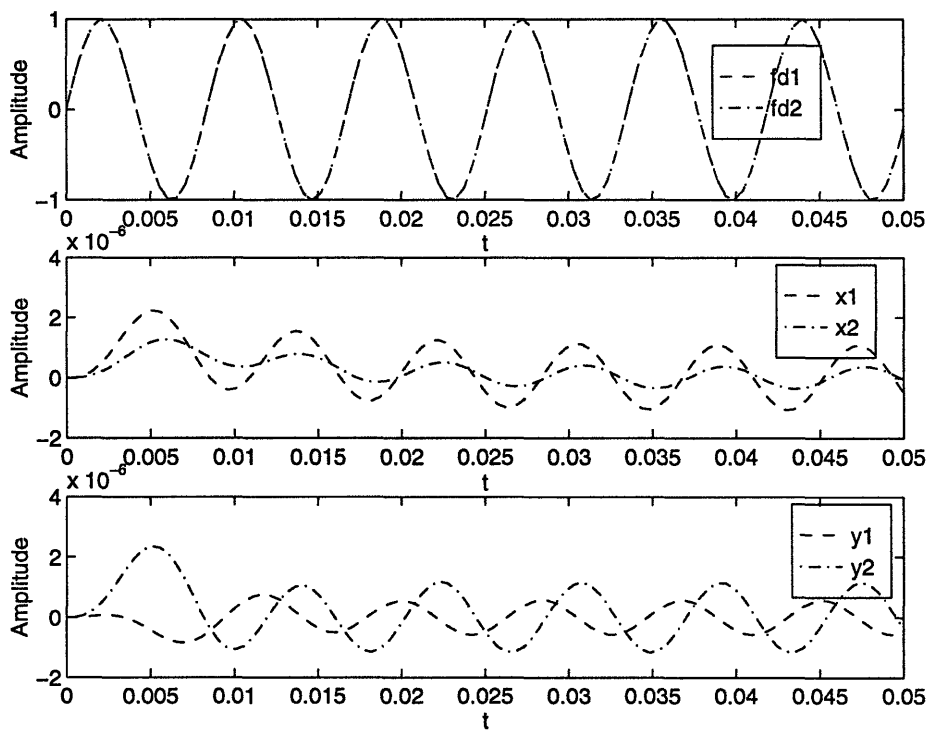

Figure 4-13: LQR Design: Disturbance Rejection Test, $\rho = 10^{-3}, b = 100$

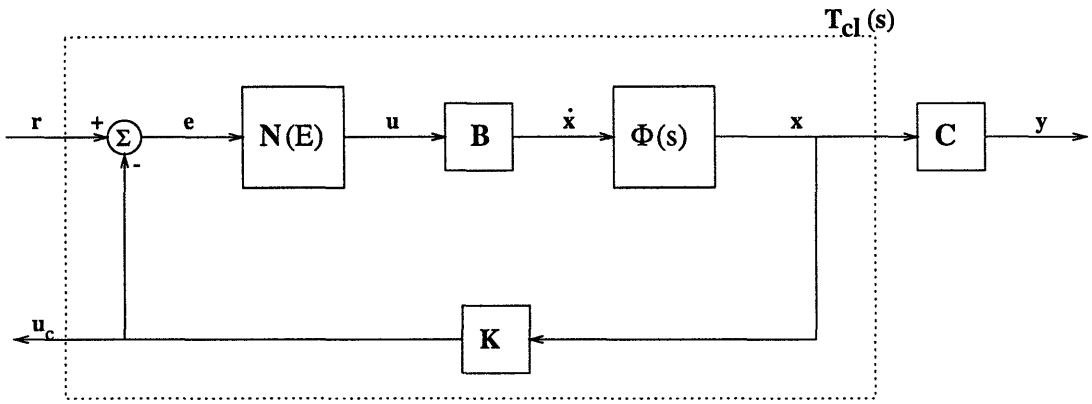

Figure 4-14: LQR Design with Saturation Limit

been tested with several different configurations of initial condition, and the results prove satisfactory.

4.4 Saturation Limit

In order to make the describing function method to work, it is necessary that the input to the describing function be a sinusoidal with no harmonics. This is not the case for the input in general. However, since most of the open-loop transfer functions of any systems could be represented as low-pass filters, the necessary assumption is satisfied.

The method of generating the closed-loop transfer function to include the effect of a describing function is credited to [15]. Referring to Fig.4-15 with a *SISO* perspective, (i.e. observing the input and output as scalar numbers rather than vectors) the method works as follows: for a selected describing function of N, transfer function of $\left|\frac{e}{r}\right|$ is plotted. Due to the interdependency of e and N, once the value of N is known then also the value of e is known and constant along the curve. Since the transfer function $\left|\frac{e}{r}\right|$ is the magnitude ratio of e to r, it means that for a constant e, the value of r is changing according to the change in magnitude ratio. Once, the desired r

with its corresponding ω is located along the curve, the magnitude ratio can then be projected to get the closed-loop curve, i.e. $\left|\frac{u_c}{r}\right|$. This procedure is repeated for many different values of N for greater degree of accuracy.

Although the method was originally derived for $SISO$ cases, it could be extended to $MIMO$ cases as well. The difference is that the use of singular values to generate the frequency response plots for $MIMO$ cases, instead of merely taking the scalar magnitude gain of the desired transfer functions in $SISO$ cases. The transfer function relating $\mathbf{u}_c$ and $\mathbf{r}$ is dependent upon the amplitude of E, the descriptor of an as yet $\mathbf{e}$. In order to overcome this circular difficulty, σ_{max} and σ_{min} of $\mathbf{T}_{re}$ are generated with $\mathbf{e}$ and $\mathbf{N}$ treated as an independent variable state vector due to their interdependency. Since the contour of $\mathbf{T}_{ru_c}$ for constant $\mathbf{r}$ is desired and the interested value of $\mathbf{r}$ is known in advance, the points on the $\sigma_{max}\left[\mathbf{T}_{re}\right]$ and $\sigma_{min}\left[\mathbf{T}_{re}\right]$ curves which correspond to this particular $\mathbf{r}$ could be identified. These points then are transferred to generate $\sigma_{max}\left[\mathbf{T}_{ru_c}\right]$ and $\sigma_{min}\left[\mathbf{T}_{ru_c}\right]$ curves and connected to provide a contour for the given input value of $\mathbf{r}$. Since $\mathbf{N}$ is constant along any of the $\sigma_{max}\left[\mathbf{T}_{re}\right]$ and $\sigma_{min}\left[\mathbf{T}_{re}\right]$ curves, the value of $\mathbf{e}$ at the input of describing function is constant along each curve. By knowing $\mathbf{r}$ and the relationship of $\mathbf{e}(s) = \mathbf{T}_{re}(s)\mathbf{r}(s)$, the desired $\mathbf{e}$, the corresponding $\mathbf{N}$ and the frequency ω can be located from the $\mathbf{T}_{re}$ curves. Those value are then transferred to $\mathbf{T}_{ru_c}$ curve to plot the closed-loop transfer function with constant $\mathbf{r}$.

From Fig.4-14, it is obtained that

$$\mathbf{e}(s) = \left[\mathbf{I} + \mathbf{K}\mathbf{\Phi}(s)\mathbf{B}\mathbf{N}(s)\right]^{-1}\mathbf{r}(s) \tag{4.21}$$

$$\mathbf{u}_c(s) = \left[\mathbf{I} + \mathbf{K}\mathbf{\Phi}(s)\mathbf{B}\mathbf{N}(s)\right]^{-1}\left[\mathbf{K}\mathbf{\Phi}(s)\mathbf{B}\mathbf{N}(s)\right]\mathbf{r}(s) \tag{4.22}$$

Defining $\mathbf{T}_{re}(s)$ as the closed-loop transfer function from input reference $\mathbf{r}$ to tracking error $\mathbf{e}$, and $\mathbf{T}_{ru_c}(s)$ as the closed-loop transfer function from input reference $\mathbf{r}$ to $\mathbf{u}_c$, the two transfer function of interest can now be written as

$$\mathbf{T}_{re}(s) = \left[\mathbf{I} + \mathbf{K}\mathbf{\Phi}(s)\mathbf{B}\mathbf{N}(s)\right]^{-1} \tag{4.23}$$

$$\mathbf{T}_{ru_c}(s) = \left[\mathbf{I} + \mathbf{K}\mathbf{\Phi}(s)\mathbf{B}\mathbf{N}(s)\right]^{-1}\left[\mathbf{K}\mathbf{\Phi}(s)\mathbf{B}\mathbf{N}(s)\right] \tag{4.24}$$

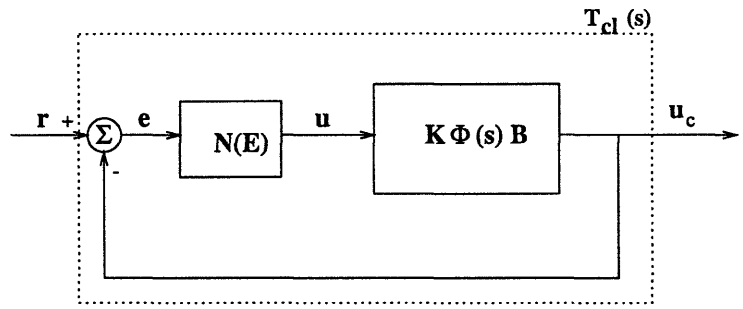

Figure 4-15: Closed-loop System

The describing function, $N(\mathcal{X})$, of a saturation function is defined as follows[2];

$$N(\mathcal{X}) = \frac{2k}{\pi}\left[arcsin\left(\frac{\delta}{\mathcal{X}}\right) + \left(\frac{\delta}{\mathcal{X}}\right)\sqrt{1-\left(\frac{\delta}{\mathcal{X}}\right)^2}\right] \tag{4.25}$$

where

δ = limit,

k = linearity slope,

$\mathcal{X}$= input amplitude.

The saturation value **N** will change depending upon the error **e**, which in turn depending upon the reference input **r**. Therefore, one might expect to have different closed-loop frequency responses for different values of r. In order to observe the difference, plots are generated for $\mathbf{r} = 0.3\mathbf{I}_{4\times1}, 0.5\mathbf{I}_{4\times1}$, and $k = 1, 2$. *Note that because only the frequency response value which is affected by the describing function is desired to know, the plots only show the points where the saturation limit are reached (the nonlinear gain). Some gaps in the plots of the frequency response should not be considered as NaN (not a number)'s nor zeros, but conform to the values as the system*

[2]See App.A

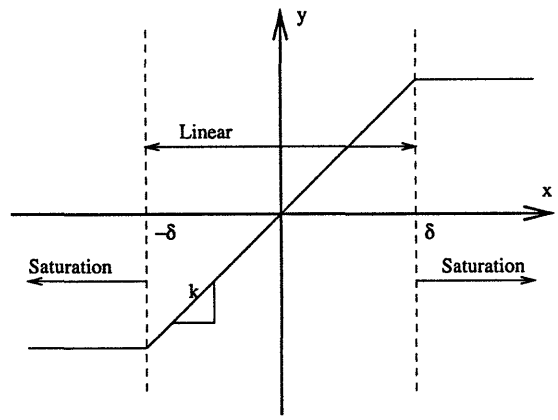

Figure 4-16: A saturation nonlinearity

undergoes in the linear range, i.e. no saturation limit.

4.4.1 Results

1. Fig.4-17: $r = 0.5$, $k = 1$

   The maximum singular value has DC gain of 1.6844 at low frequencies, separating into three different gain branches at the frequency of approximately 4 Hz. The highest jump goes to the gain value of 3.2301; the middle branch increases to the gain value of 2.2844, while the lowest gain stays the same constant value as the DC gain. These three branch then merge at the roll-off rate of 20 dB/decade at high frequencies.

2. Fig.4-18: $r = 0.5$, $k = 2$

   The DC gain of the maximum singular values is 6.4873 at low frequencies. At the frequency of approximately 7.4057 Hz, the gain separates into two, where the low one decreases to the gain value of 4.8240 while the high one stays the same constant value as the DC gain. These two branches merge at the frequency of approximately 24.6 Hz at the gain value of 4.78 and roll-off at the rate of 20 dB/decade at high frequencies.

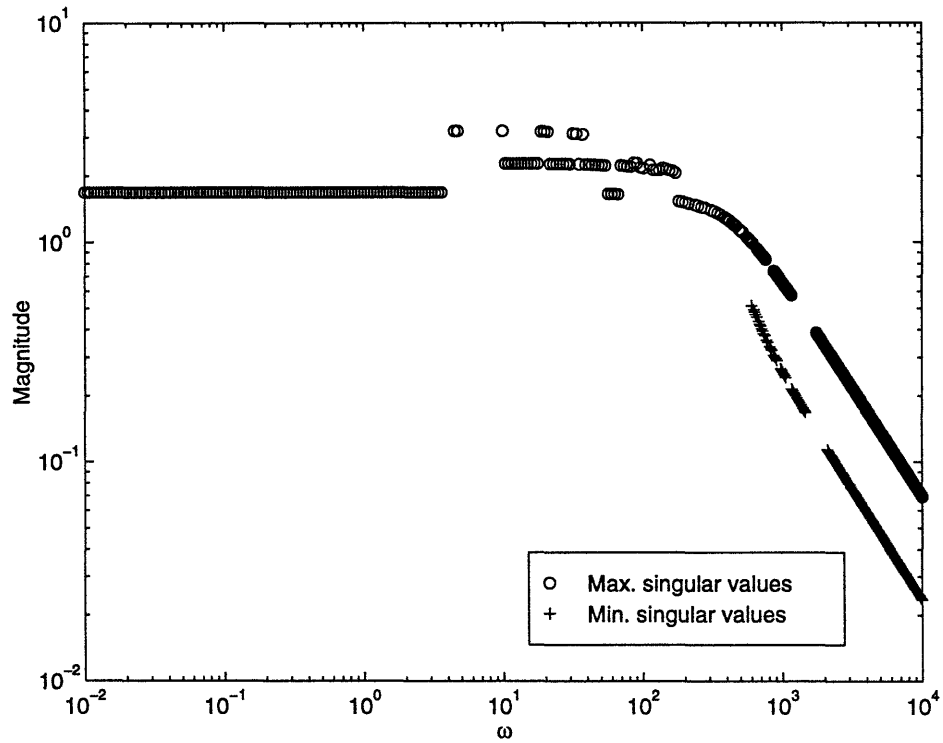

Figure 4-17: Closed-loop transfer function, r = 0.5, k = 1, tol = 0.006

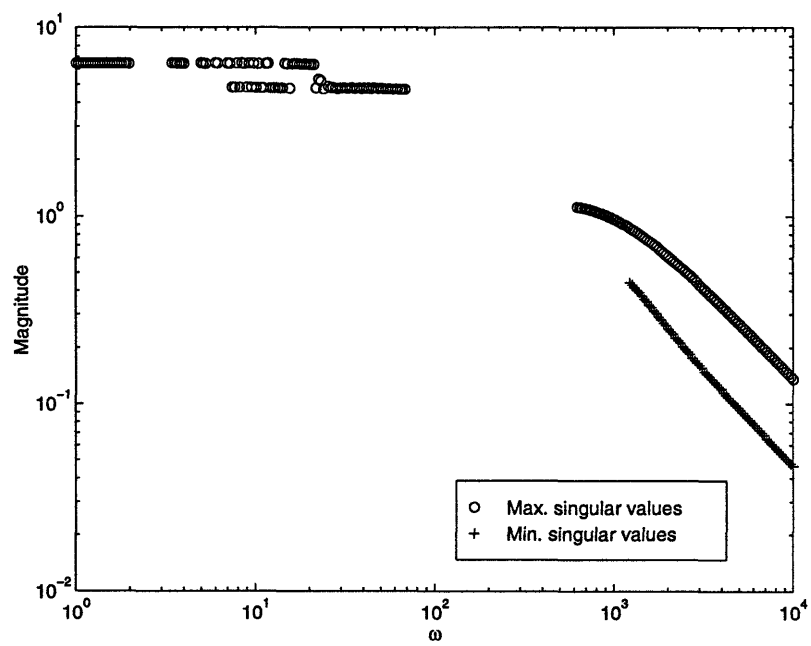

Figure 4-18: Closed-loop transfer function, r = 0.5, k = 2, tol = 0.03

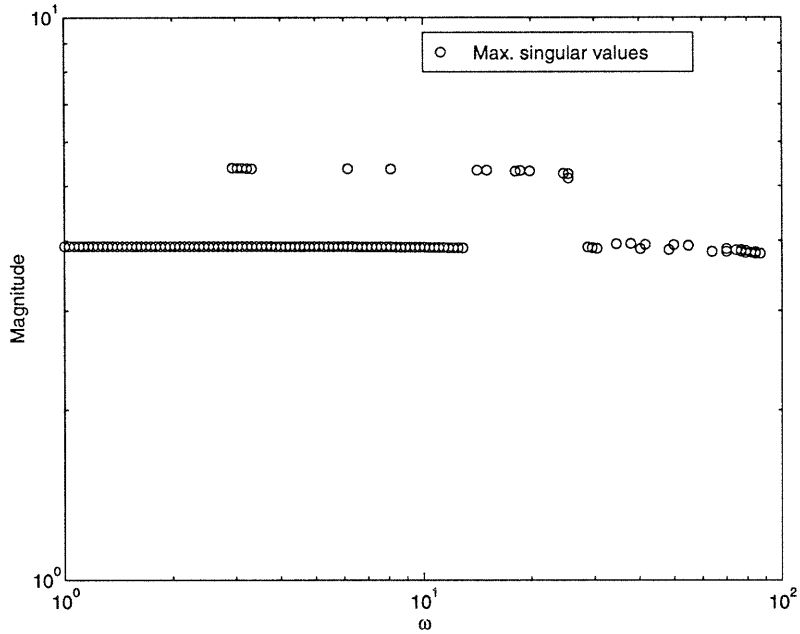

Figure 4-19: Closed-loop transfer function, r = 0.3, k = 1, tol = 0.01

3. Fig.4-19: *r = 0.3, k = 1*

   The frequency response has DC gain of 3.9083 at low frequencies, separating into two gains with the high one jumps to the gain value of 5.3838 at the frequency of 2.9392 Hz. Both gains then merge at the frequency of approximately similar to the low frequency DC gain value of 3.9083.

4. Fig.4-20: *r = 0.3, k = 2*

   The constant DC gain is 10.8243 at low frequencies. Similar to the case of *r = 0.5, k = 2*, the gain divides into two at the frequency of approximately 2.5235 Hz, with the low gain decreases to a gain value of 8.0313. Both gains then merge at this low gain at the frequency of 12.7505 Hz.

4.5 Stability: Popov method

In order to check whether the system will exhibit some self-sustained oscillations called *limit cycles*, the extension of Nyquist criterion called *Popov stability criterion* can be applied. Beforehand, the variables in the loop (Fig.4-15) must satisfy the

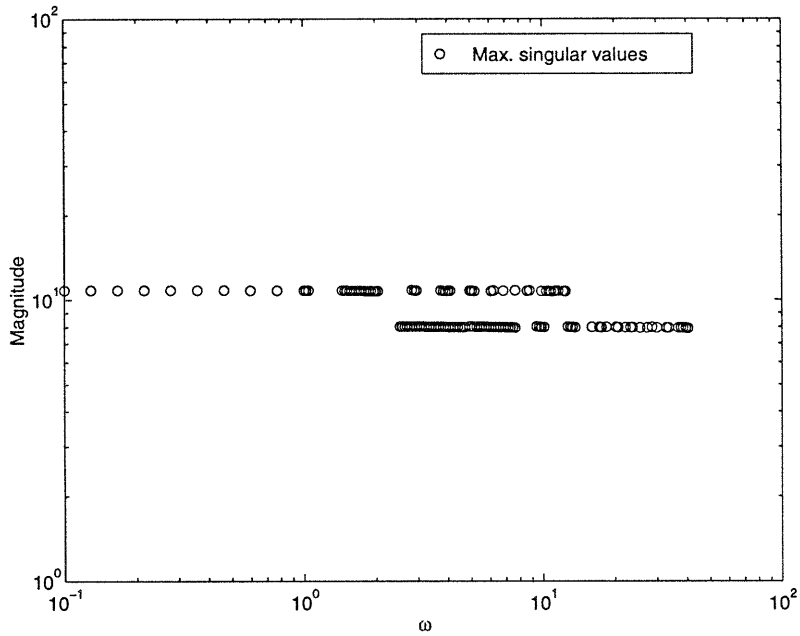

Figure 4-20: Closed-loop transfer function, r = 0.3, k = 2, tol = 0.03

following relations as in [2, 19]

$$\begin{aligned} \Rightarrow \mathbf{e}(\jmath\omega) &= -\mathbf{u}_c(\jmath\omega) \\ \Rightarrow \mathbf{u}(\jmath\omega) &= \mathbf{N}(E)\mathbf{e}(\jmath\omega) \\ \Rightarrow \mathbf{u}_c(\jmath\omega) &= \underbrace{\mathbf{K}\mathbf{\Phi}(\jmath\omega)\mathbf{B}}_{\mathbf{G}_{LQ}(\jmath\omega)}\mathbf{u}(\jmath\omega) \end{aligned}$$

Thus, $\mathbf{u}_c(\jmath\omega) = -\mathbf{G}_{LQ}(\jmath\omega)\mathbf{N}(E)\mathbf{u}_c(\jmath\omega)$. Because $\mathbf{u}_c(\jmath\omega) \neq \mathbf{0}$, this implies

$$\mathbf{G}_{LQ}(\jmath\omega)\mathbf{N}(E) + \mathbf{I} = \mathbf{0} \tag{4.26}$$

For MIMO cases, the stability checking is to satisfy

$$det\left[\mathbf{G}_{LQ}(\jmath\omega)\right] = -det\left[\mathbf{N}^{-1}(E)\right] \tag{4.27}$$

Fig.4-21 shows that for the frequency range of from 10^{-2} to 10^6 Hz, the $\mathbf{G}_{LQ}$ curve *doesn't* intersect the curve of $\mathbf{N}^{-1}$. The beginning tip of the curve $\mathbf{G}_{LQ}$ has

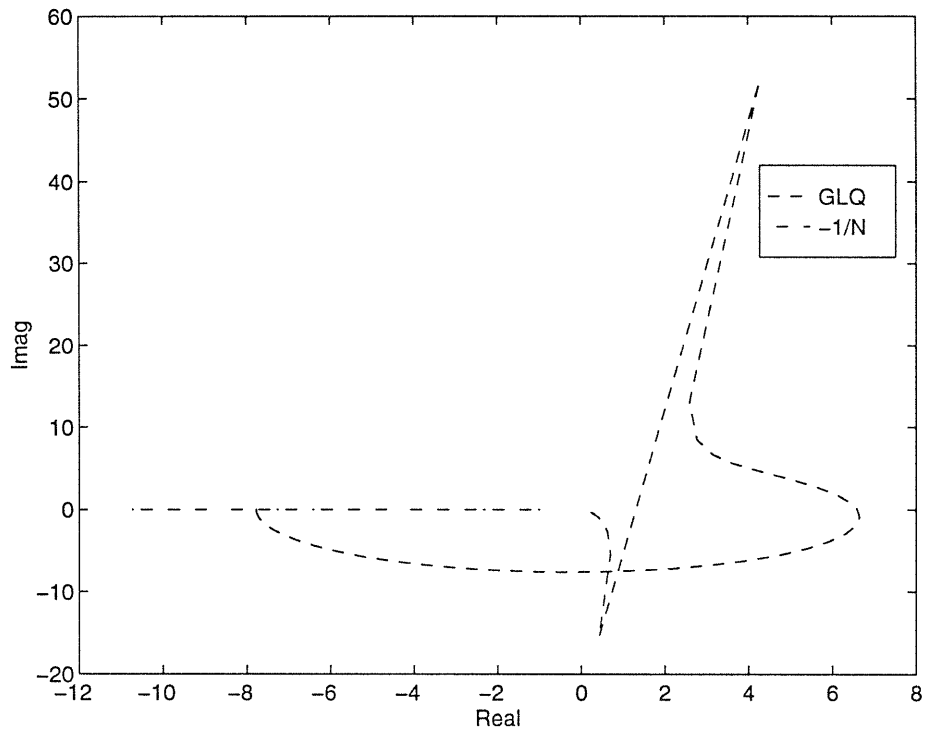

Figure 4-21: Stability Checking

a limit of the negative x axis, and in this particular frequency range it is found to be $-7.7760 - \jmath 2.1875 \cdot 10^{-3}$. Therefore, one may conclude that based upon Popov stability criterion, there is no possibility that any limit cycle will occur in the system.

4.6 Stiffness

In this rotating shaft case, the system stiffness at its rotational speed is of concern. In order to find the system stiffness at the rotor operating frequency range, the LQR methodology is utilized with $\mathbf{F}_d$ synchronized with the *rotor speed* Ω such as follows:

$$\mathbf{H}(\jmath\Omega) = \left[\mathbf{G}(\jmath\Omega)\mathbf{S}(\jmath\Omega)\mathbf{B}^{-1}\mathbf{L}\right]^{-1} \tag{4.28}$$

Fig.4-22 shows the variation of the stiffness with frequency range from 10^{-4} to 10^{4} Hz. Since the frequency of interest is in the range of $0 \leq \Omega \leq 45{,}000$ rpm or $0 \leq \Omega \leq 750$ Hz, a vertical dashed line is added as the upper frequency limit in the graph, to show that only the left-hand side of the dashed line is of interest.

The overall minimum stiffness is 2.2409 N/m. At the highest operating frequency of 750 Hz, the minimum stiffness is found to be 5.5363 N/m.

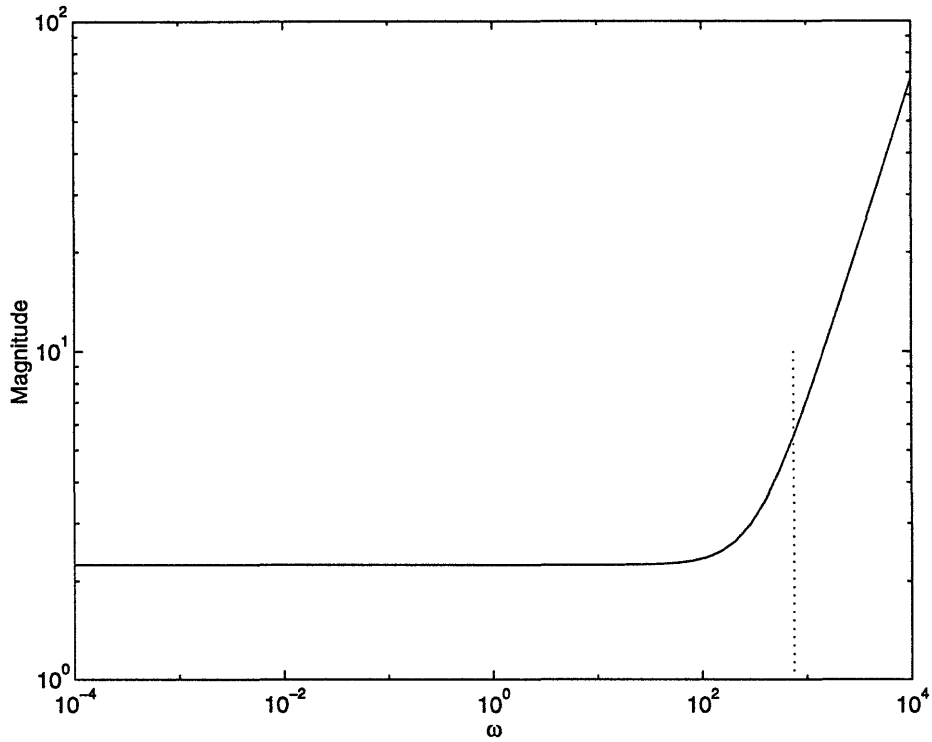

Figure 4-22: Minimum stiffness, without any describing function element

4.6.1 Results

1. Fig.4-23: $r = 0.5,\ k = 1$

   The DC gain starts at the value of 2.0988 at low frequencies. It splits at the frequency of 4.4464 Hz, where the low one decreases to the value of 0.4845 being the minimum stiffness over the whole frequency response, the median one decreases to 1.5165, and the high one stays the same constant value as the low-frequency DC gain. The three gains then emerge and increase at the rate of 20 dB/decade at high frequencies.

2. Fig.4-24: $r = 0.5,\ k = 2$

   The frequency response has DC gain of 0.5484 at low frequencies, being the minimum stiffness over the whole frequency response. It splits into two at the frequency of 1.4584 Hz, where the high one reaches the gain value of 1.0750. The gains then emerge and increase at the rate of 20 dB/decade at high frequencies.

3. Fig.4-25: $r = 0.3,\ k = 1$

   The frequency response DC gain is 1.1460 at low frequencies. The gain splits into two at the frequency of 2.9392 Hz, where the low one decreases to the gain value of 0.5346 being the minimum stiffness over the whole frequency re-

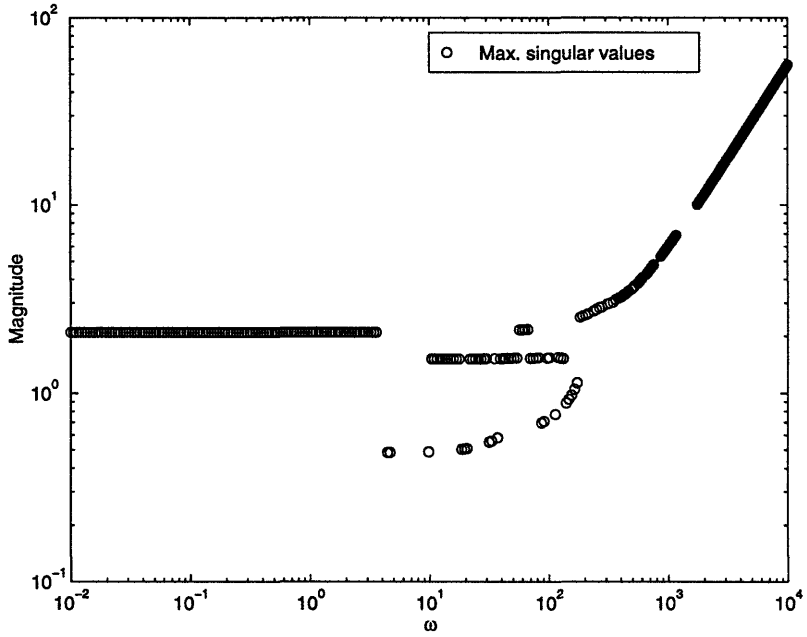

Figure 4-23: Minimum stiffness, r = 0.5, k = 1, tol = 0.006

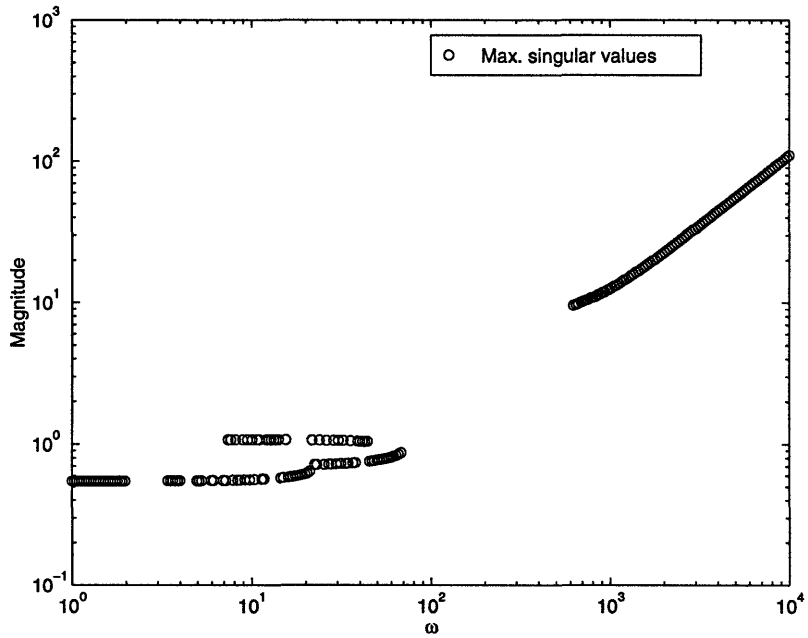

Figure 4-24: Minimum stiffness, r = 0.5, k = 2, tol = 0.03

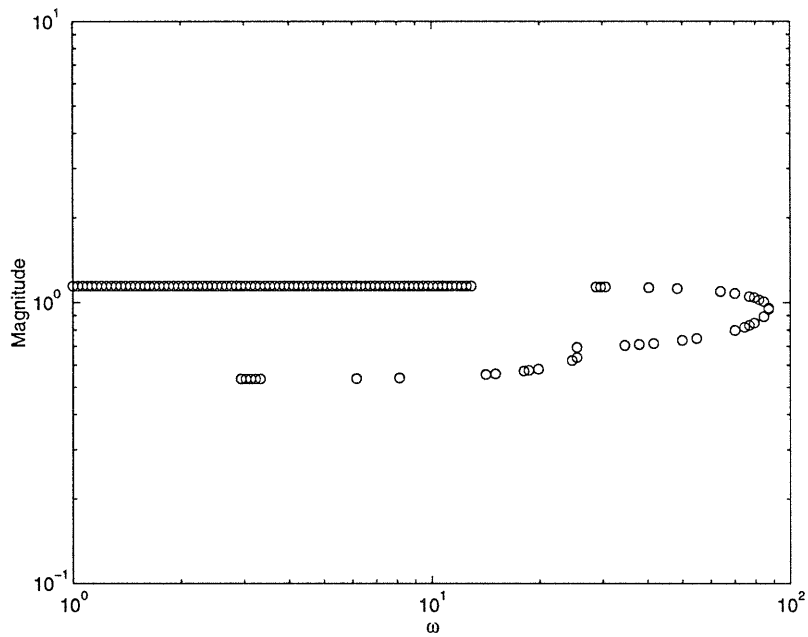

Figure 4-25: Minimum stiffness, r = 0.3, k = 1, tol = 0.01

sponse. The two then merge to the gain value of 0.9483 at the frequency of approximately 87.056 Hz.

4. Fig.4-26: *r = 0.3, k = 2*

   The DC gain at low frequencies is 0.5793, being the minimum stiffness over the whole frequency response. It splits at the frequency of 1.4481, where the high one reaches to the gain value of 0.6994. This high gain splits at the frequency of 2.5235 Hz, where the high one goes to 0.7586, which in turn, splits at the frequency of 5.2920 Hz where the high one reaches 0.9735. The gains then merge to the gain value of 0.8663 at the frequency of 40.555 Hz.

4.7 Disturbance

Disturbance-to-output transfer function matrix, $\mathbf{S}_{dy}(s)$

$$\mathbf{y}(s) = \mathbf{S}_{dy}(s)\mathbf{d}(s) \tag{4.29}$$

$$\mathbf{S}_{dy}(s) = \mathbf{C}\left[s\mathbf{I} - \mathbf{A} + \mathbf{B}\mathbf{N}(E)\mathbf{K}\right]^{-1}\mathbf{L} \tag{4.30}$$

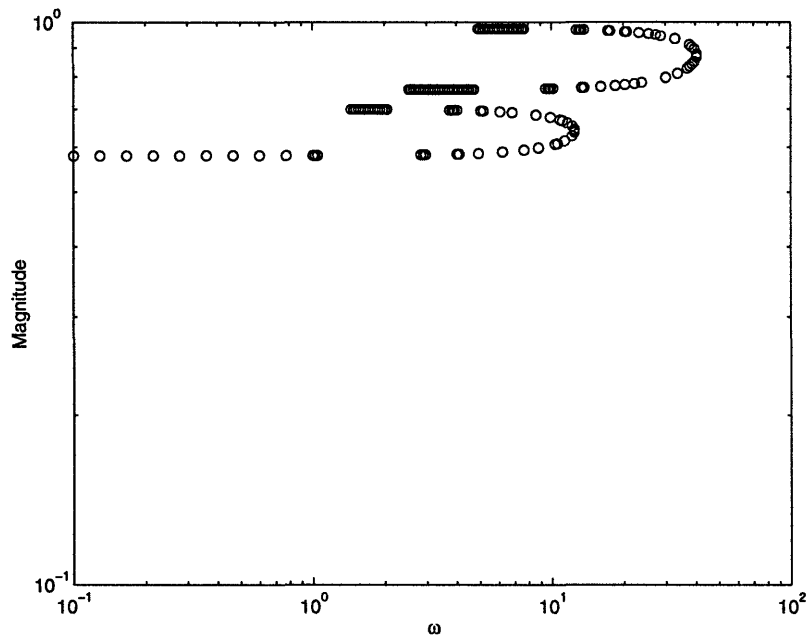

Figure 4-26: Minimum stiffness, r = 0.3, k = 2, tol = 0.03

In the rotating machine, the periodic disturbance comes from the rotor imbalance, which is the **d** term in the equation of motion. This disturbance input is synchronized with the rotational speed, Ω.

4.7.1 Results

1. Fig.4-27: *r = 0.5, k = 1*

   The frequency response has a DC value of $1.73 \cdot 10^{-5}$ at low frequencies, splits into three branches at the frequency of 4 Hz, with the highest gain at the value of $1.686 \cdot 10{-}4$, the median gain at $2.84 \cdot 10^{-3}$, and the lowest gain stays similar as the constant low-frequency DC value. The three gains merge and roll-off at the rate of 20 dB/decade at high frequencies.

2. Fig.4-28: *r = 0.5, k = 2*

   The DC constant gain is $2.988 \cdot 10^{-4}$ at low frequencies. The gain splits into two at the frequency of 7.4057 Hz, where the lowest gain decreases to $5.68 \cdot 10^{-5}$, and the highest gain stays similar with the low-frequency DC gain. The two

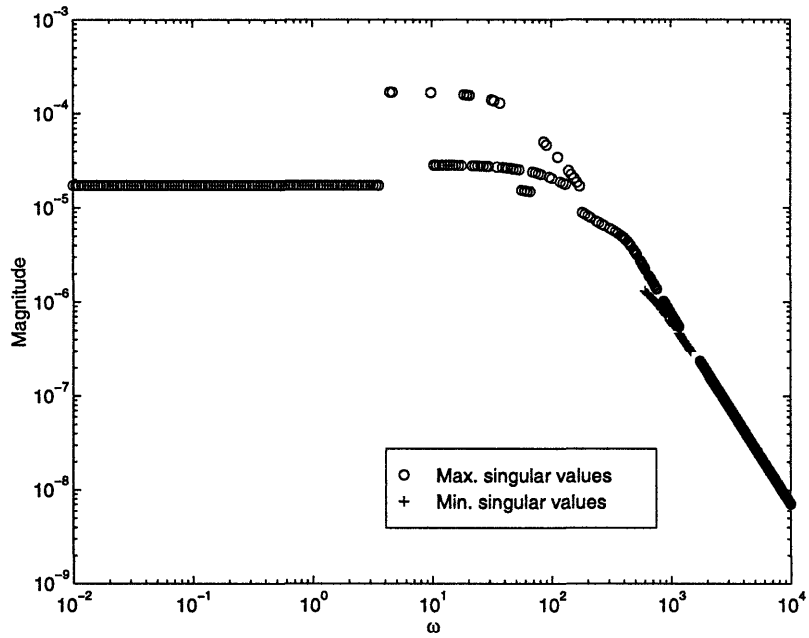

Figure 4-27: Disturbance-to-output, r = 0.5, k = 1, tol = 0.006

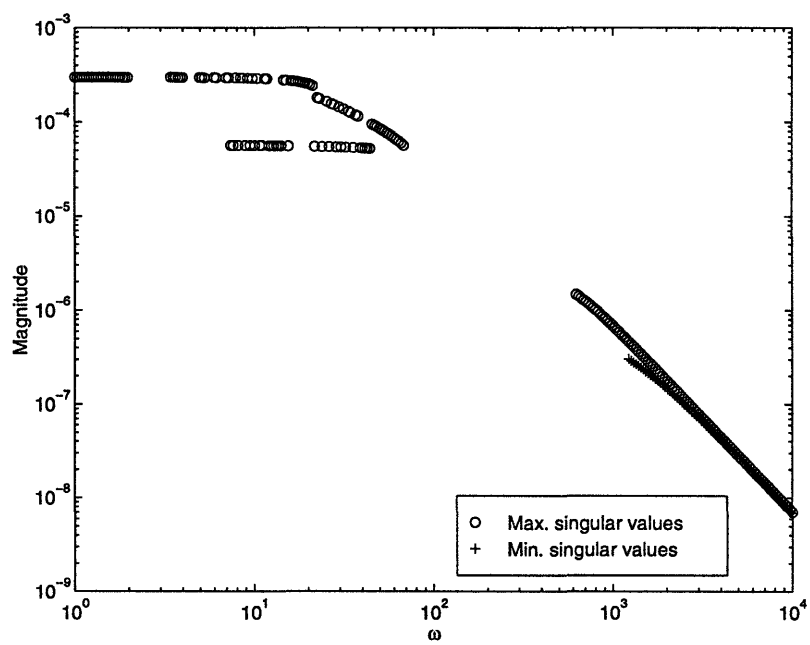

Figure 4-28: Disturbance-to-output, r = 0.5, k = 2, tol = 0.03

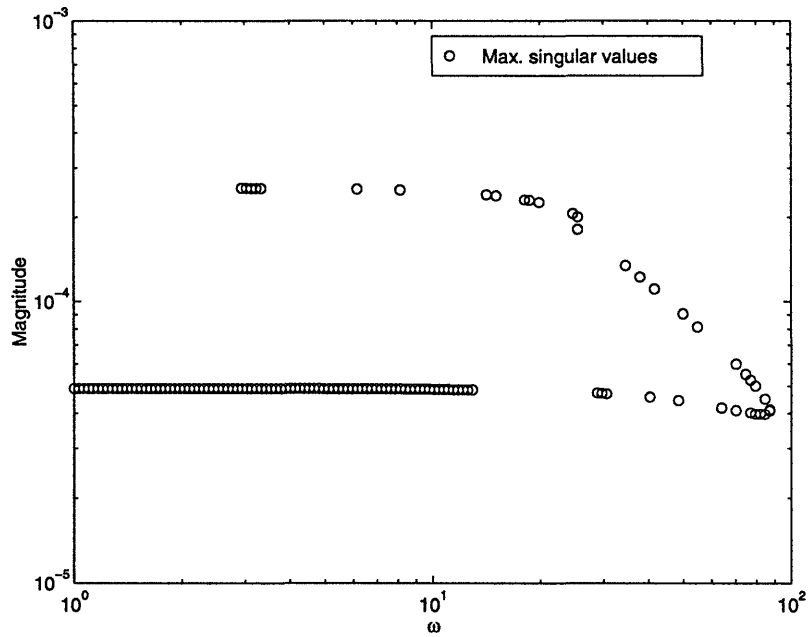

Figure 4-29: Disturbance-to-output, r = 0.3, k = 1

then merge and roll-off at the rate of 20 dB/decade at high frequencies.

3. Fig.4-29: *r = 0.3, k = 1, tol = 0.01*

   With the DC gain at the constant value of $4.91 \cdot 10^{-5}$, the frequency response has high jump to the value of $2.544 \cdot 10^{-4}$ and the low one stays at the same value as the low-frequency DC gain. The two gains then merge at the frequency of approximately 87 Hz.

4. Fig.4-30: *r = 0.3, k = 2, tol = 0.03*

   The frequency response starts with DC gain of $4.713 \cdot 10^{-4}$ at low frequencies. The gain splits into two at the frequency of 1.4481 Hz, with the low gain decreases to $3.784 \cdot 10^{-4}$ and the high gain stays the same as the low-frequency DC gain. The low gain then splits again at the frequency of 2.5235 Hz with the lower value goes to $2 \cdot 10^{-4}$. As the frequency is increased, the latter gain splits at the frequency of 5.2920 Hz, with the lower value goes to $7.38 \cdot 10^{-5}$.

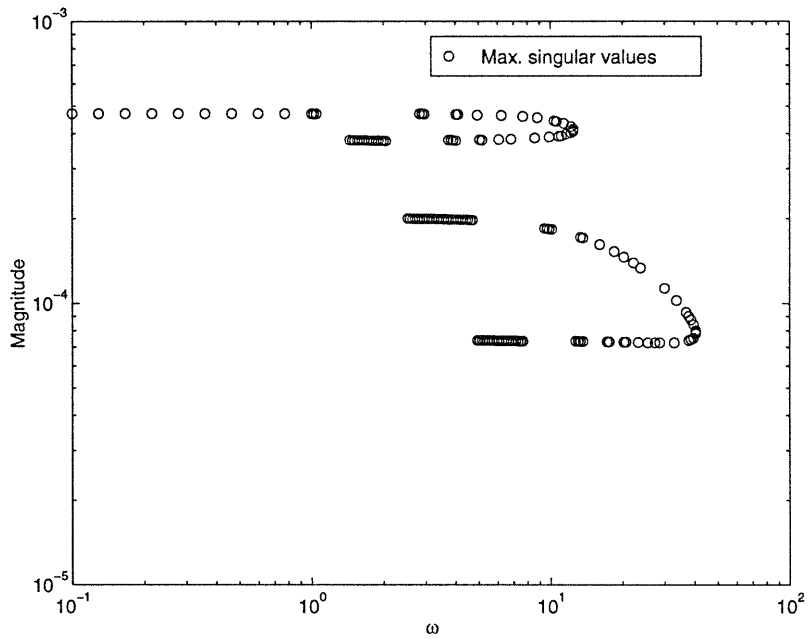

Figure 4-30: Disturbance-to-output, r = 0.3, k = 2

	w/o DF	*r = 0.5*		*r = 0.3*	
		k = 1	*k = 2*	*k = 1*	*k = 2*
σ_{max} [$\mathbf{T}_{ru}$]	1.6144	1.6844	6.4873	3.9083	10.8243
σ_{max} [$\mathbf{S}_{dy}$]	$1.6 \cdot 10^{-5}$	$1.73 \cdot 10^{-5}$	$2.988 \cdot 10^{-4}$	$4.91 \cdot 10^{-5}$	$4.713 \cdot 10^{-4}$
$\mathbf{H}$, N/m	2.2409	2.0988	0.5484	1.1460	0.5793

Table 4.1: DC gains

4.8 Summary

Clearly, increasing the slope k of the saturation limit element will result in higher gain as expected, and smaller stiffness. On the other hand, increasing the reference point r, results in the decreased response amplitude of $\mathbf{T}_{ru}$ and $\mathbf{S}_{dy}$.

For some frequency responses that have multivalued gain, the median gains are considered unstable due to their flexibility to switch rapidly between the high and low gains. Although the median gains are clearly shown in the plots, they cannot be observed experimentally.

Chapter 5

Conclusion and Recommendation

A rotating shaft operating under suspension of magnetic bearing system is taken into consideration. Its open-loop instability is characterized by the occurence of high peak at the frequency of 382.12 Hz. In order to bring the rotating shaft up to the highest attainable operating frequency of 750 Hz, the shaft has to pass the peak at the frequency of 382.12 Hz. Since such peak might cause damage to the system due to the considerably high gain, the frequency is considered *critical.* The situation might be avoided by having a feedback for the open-loop to bring about stability, and eliminate the high gain.

A magnetic bearing system setup by induced current is analized in its linear operating range. The system has performance limitation primarily due to the induced current saturation in the bearings, hence, limiting the amount of eletromagnetic force needed to suspend the rotor. The system is synthesized using the *LQR methodology* to succesfully meet the nominal performance stability. The LQR methodology allows one to choose the bearing design parameters so that the unstable, open-loop system has the capability to achieve performance specifications. The effect of saturation limit is then approximated using *describing function method*, that provides linear scalar values for the nonlinearity element for the purpose of performance analysis.

The existence of a saturation limit element causes the closed- loop system to behave in a nonlinear manner. One of the nonlinear characteristics that can be observed here is *jump resonance.* As discussed in the *Sect.4.4, 4.6*, and *4.7*, the frequency re-

sponse plots show several *multivalued responses* as a result of the saturation limit and may cause instability of the closed-loop system. Such phenomena may be avoided by applying more damping to the system[1].

One of the shortcoming of the method proposed by [15] is that it works nicely in SISO cases, but not quite satisfactory in MIMO cases. The singular values are seemingly obtained only for greater frequency range of either the maximum or minimum values, but not both. The reason is due to the fact that the way the method works is to project the magnitudes of the reference point $\mathbf{r}$ to the tracking error $\mathbf{e}$ in order to obtain the magnitudes of the closed-loop system. i.e. from the reference point $\mathbf{r}$ to the output $\mathbf{u}$. The magnitude ratio of $\left|\frac{e}{r}\right|$ may not cross with one of the singular value curve; hence, no intersection points exist.

The important use of *prefilter* should be considered in the high stiffness system so that the magnetic bearing would not be saturated during the initial startup. In the calculation procedure to determine the system identification, some parameters are ignored such as the possibility of *magnetic flux leakage*, which would make the bearing force capacity less than desired. In order to overcome this, a *compensating* factor can be used in the design parameters.

As mentioned in the issue of balancing, the *flexibility* of rotor would be a problem when the rotor spins in the viscinity of one of its critical speeds. Although the rigid body assumption is no longer valid in this situation, the methodology presented can still be applied. In this case, the problem only needs to be reformulated by considering modal information such as the natural frequency, mode shapes and modal masses of the rotor, as addressed in the method of modal balancing.

[1]See [17].

Appendix A

The Describing Function of Saturation Nonlinearity

As nonlinear systems are different than any linear counterparts, there is no possibility of generalizing from the responses for any classes of inputs to the response of any other input of nonlinear systems. In the absence of input, a nonlinear system has an important variety of response characteristics. The system might respond to small initial conditions by returning in a stable manner to rest, and it might respond to large initial conditions by diverging in an unstable manner, or it might lead to a continuing oscillation which does not depend upon the initial conditions.

For a feedback-system configuration which is of primary interest to study magnetic bearing systems, the signal at the input to the nonlinearity depends both on the input to the system and the signal that is fed back within the system. The forms which may be expected to appear at the nonlinearity input are those which are resulting from the filtering effect of the linear part of the loop. This leads to derive quasi-linear approximators for nonlinear elements, which describe approximately the transfer function characteristics of the nonlinearity, and are termed *describing functions.* This most widely used method makes possible to determine whether or not there is danger of sustained oscillations or destructive instability and how such behavior can be avoided.

The accuracy of this method is primarily determined (Fig.A-1) that

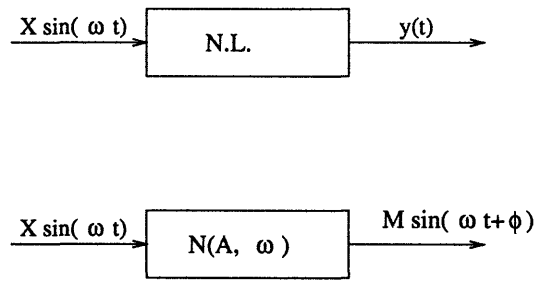

Figure A-1: A nonlinear element and its describing function representation

1. the harmonics at the output can be neglected,
2. the piecewise linear approximation of the nonlinear element is valid for analysis in the range of interest,
3. the input of the nonlinear element can be approximated as a sinusoid.

Assuming that the input to the system is sinusoidal, defined by

$$x(t) = \mathcal{X}\, sin\, \omega t \tag{A.1}$$

the describing function or sinusoidal describing function of the system is defined to be the complex ratio of the fundamental harmonic component of the output to the input. According to [18, 17],

$$N = \frac{\mathcal{Y}_1}{\mathcal{X}} \angle \phi_1 \tag{A.2}$$

where

N=describing function,

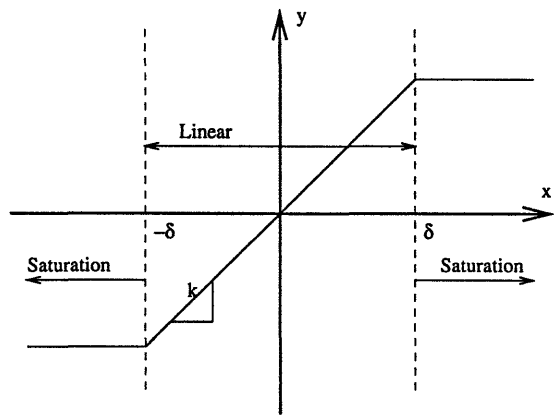

Figure A-2: A saturation nonlinearity

$\mathcal{X}$=amplitude of input sinusoid,

$\mathcal{Y}_1$=amplitude of the fundamental harmonic component of output,

ϕ_1=phase shift between the fundamental harmonic component of the output and the input,

$M_1(\mathcal{X}) = \sqrt{A_1^2 + B_1^2}$,

$\phi_1(\mathcal{X}) = \arctan(\frac{A_1}{B_1})$.

Each component of the output is given by the formula for the Fourier coefficients:

$$y_n(t)$$

$$= A_n \cos n\omega t + B_n \sin n\omega t \tag{A.3}$$

$$= \mathcal{Y}_n \sin(n\omega t + \phi_n) \tag{A.4}$$

where

$$A_n = \frac{1}{\pi}\int_{-\pi}^{\pi} y(t)\cos(nt)\,dt, \tag{A.5}$$

$$B_n = \frac{1}{\pi}\int_{-\pi}^{\pi} y(t)\sin(nt)\,dt. \tag{A.6}$$

Referring to the characteristic curve (Fig. A-2), the gain of the linear region of

the saturation nonlinearity is k. Since the characteristic curve is skew symmetric, the Fourier series expansion of $y(t)$ involves only the odd harmonics, B_n.

Therefore, $y_1(t)$ can be written as

$$y_1(t) = \mathcal{Y}_1 \, sin\, \omega t \tag{A.7}$$

where

$$\mathcal{Y}_1 = B_1 = \frac{2}{\pi}\int_0^{\pi} y(t)\, sin\, t\, dt \tag{A.8}$$

The equations of the output result are

$$y(t) = \begin{cases} k\mathcal{X} sin\omega t, & \text{for } 0 \leq t < t_1 \\ k\delta, & \text{for } t_1 \leq t < \frac{\pi}{2\omega} \end{cases}$$

and

$$\mathcal{X}\, sin\, \omega t_1 = \delta \tag{A.9}$$

Putting into account the symmetry over the four quarter of a period, the output $\mathcal{Y}_1$ can be obtained by integrating the equations as follows:

$$\begin{aligned} \mathcal{Y}_1 &= \frac{4}{\pi}\int_0^{t_1} k\mathcal{X}\, sin^2\, t\, dt + \frac{4}{\pi}\int_{t_1}^{\frac{\pi}{2}} k\delta\, sin\, t\, dt, \\ &= \frac{2\mathcal{X}k}{\pi}\left[sin^{-1}\left(\frac{\delta}{\mathcal{X}}\right) + \frac{\delta}{\mathcal{X}}\sqrt{1-(\frac{\delta}{\mathcal{X}})^2}\right] \end{aligned} \tag{A.10}$$

The relative magnitudes of $\mathcal{Y}_1$ and $\mathcal{Y}_3$ are also of interest:

$$\mathcal{Y}_1 = \frac{2k\mathcal{X}}{\pi}\left(t_2 + \frac{sin\, 4t_2}{2}\right) \tag{A.11}$$

$$\mathcal{Y}_3 = \frac{2k\mathcal{X}}{3\pi}\left(\frac{sin\, 2t_2}{2} + \frac{sin\, 4t_2}{4}\right) \tag{A.12}$$

where $\frac{\mathcal{Y}_1}{\mathcal{X}}$ is the describing function, and $|\frac{\mathcal{Y}_3}{\mathcal{Y}_1}|$ measures the accuracy of the describing-

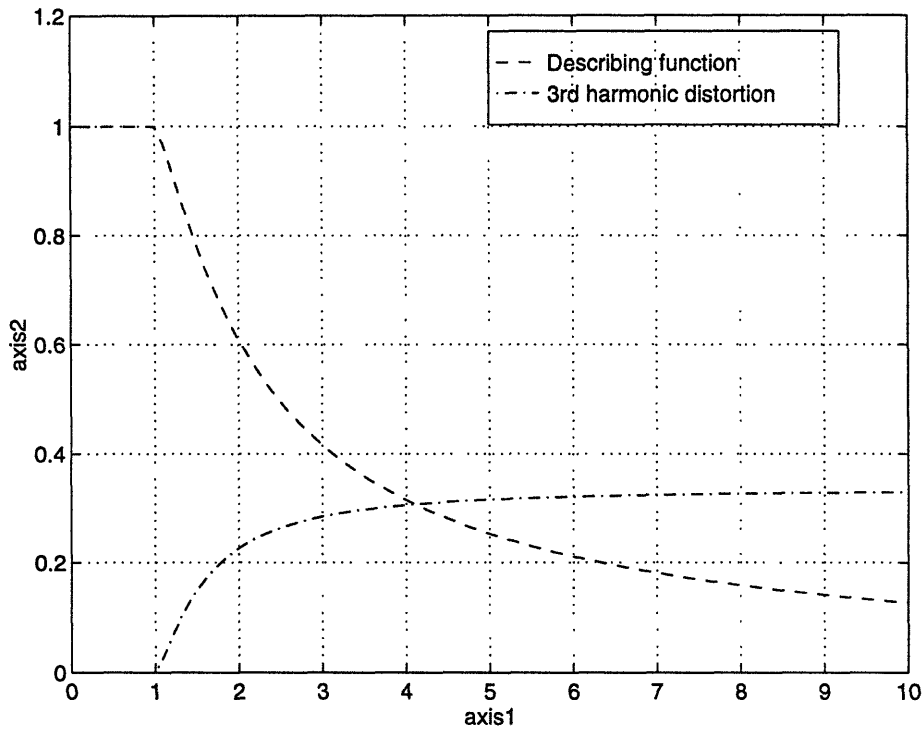

Figure A-3: Saturation; axis1 = $\frac{\mathcal{X}}{\delta}$, axis2 = Magnitude

function analysis.

The describing function N of the saturation nonlinearity and the relative third harmonic may then be given by Fig.A-3;

$$\begin{aligned} N = \frac{\mathcal{Y}_1}{\mathcal{X}} &= \frac{2k}{\pi}\left[arcsin(\frac{\delta}{\mathcal{X}}) + \frac{\delta}{\mathcal{X}}\sqrt{1-(\frac{\delta}{\mathcal{X}})^2}\right] \\ &= \frac{2k}{\pi}\left[t_2 + \frac{sin\,2t_2}{2}\right] \end{aligned} \tag{A.13}$$

and

$$\frac{\mathcal{Y}_3}{\mathcal{Y}_1} = \left(\frac{1}{6}\right)\frac{2\,sin\,2t_2 + sin\,4t_2}{2t_2 + sin\,2t_2} \tag{A.14}$$

where

$$t_2 = arcsin\left(\frac{\delta}{\mathcal{X}}\right) \tag{A.15}$$

Due to the nature of this nonlinearity, the describing function is real, being a function only of the magnitude of the sinusoidal input. Morever, the input sinusoid $x(t) = \mathcal{X}sin\omega t$ and the fundamental harmonic component $y_1(t)$ are in phase, i.e.

$\phi_1 = 0$, because saturation does not cause the delay of the response to input.

As shown in Fig.A-3, N reduces to zero as $\mathcal{X}$ approaches ∞. The relative amplitude of the 3rd harmonic distortion to the fundamental harmonic component increases to a maximum value of $\frac{1}{3}$ for small $arcsin\left(\frac{\delta}{\mathcal{X}}\right)$. Both characteristics occur due to the fact that the output of the describing function becomes a square wave of a peak-to-peak amplitude $2k\delta$ for large input amplitude $\mathcal{X}$.

In this thesis, these constants are used for the saturation element:

a =0.36 A

k =1

Appendix B

Magnetic Force for Bearings

In this appendix, the expression for the magnetic force of an electromagnet of a magnetic bearing on the rotor is derived in terms of the electromagnetic coil current and air gap. The numerical values are given from *Chap.4.2.*

In order to determine the magnetic force, the derivation begins with the energy stored in the air gap as the electric power, which is defined by

$$P = vi \tag{B.1}$$

where i is the coil current, and v is the coil potential from end 1 to end 2. The coil is wound in one direction in one pole, and in reverse direction in another pole (Fig.B-1). This pair of poles with coil wound acts as an electromagnet. The magnetic flux density B throughout the two poles is obtained using *Faraday's law*,

$$\int_{\mathcal{C}} E \cdot dl = -\frac{d}{dt} \int_{\mathcal{S}} B \cdot dA \tag{B.2}$$

where dl is the infinitesimal length traversing the closed contour $\mathcal{C}$, and $\mathcal{S}$ is defined as the surface where the current flows through, enclosed by $\mathcal{C}$.

Focusing in the coil windings only, the potential from end 1 to end 2 can be determined from the closed-loop contour of the electric field E as shown in Fig.B-2.

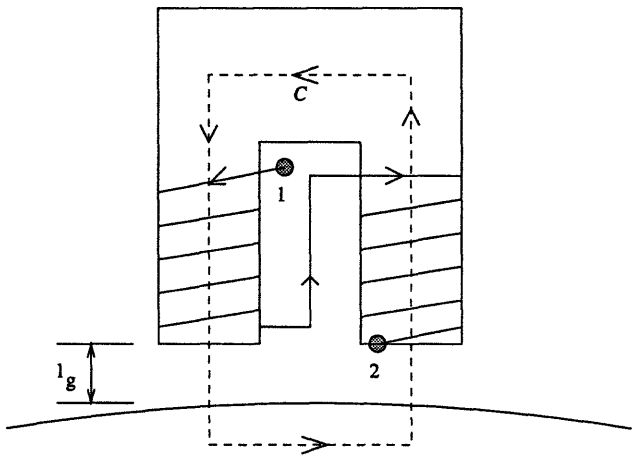

Figure B-1: Coil Windings for an Electromagnet of a Bearing

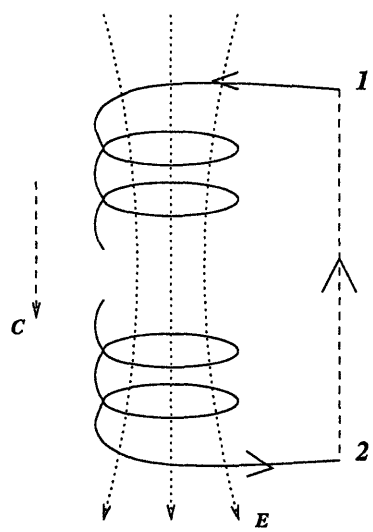

Figure B-2: Coil and Contour for Faraday's Law

Tracing the loop, the following is obtained:

$$\int_C E \cdot dl = \int_1^2 E \cdot dl + \int_2^1 E \cdot dl \tag{B.3}$$

$$= \int_2^1 E \cdot dl = -v \tag{B.4}$$

Here, the dot product means that only the projected electric field on the direction of C (shown in dashed line in Fig.B-1) is accounted for the generated potential from end 1 to end 2. The first term of the above equation is zero since the coil is assumed to be perfectly conducting, i.e. $E = 0$.

The surface area $\mathcal{S}$ is where the magnetic field is, and calculated to be $2NA_g$, where N is the number of coil turns, and A_g is the projected surface area of the gap. If the magnetic field density B_g is assumed uniform across the two poles, then

$$\int_C E \cdot dl = -v = -2NA_g \frac{dB_g}{dt} \tag{B.5}$$

$$= -0.0195 \frac{dB_g}{dt} \, (volt) \tag{B.6}$$

Assuming no power losses, the electric power is converted into the magnetic power;

$$P = vi = 2NA_g i \frac{dB_g}{dt} \tag{B.7}$$

$$= 0.0195 i \frac{dB_g}{dt} \, (watt) \tag{B.8}$$

Using *Ampere's law*,

$$\int_C H \cdot dl = \int_{\mathcal{S}} J \cdot dA \tag{B.9}$$

where the magnetic field H is defined along the contour $\mathcal{C}$ in Fig.B-1 (traversing air gap, one pole, stator, other pole, air gap, rotor). Each magnetic bearing has two poles and each of the poles has N turns. Therefore, in every bearing the coil encircles $2N$

number of times the surface $\mathcal{S}$, and the current flowing through $\mathcal{S}$ is $2N$ times i, i.e.

$$\int_{\mathcal{S}} J \cdot dA = 2Ni \tag{B.10}$$

$$= 200i\,(ampere) \tag{B.11}$$

Neglecting the iron reluctance, the magnetic field intensity along the contour $\mathcal{C}$ in the rotor, stator, and poles can be ignored. If the magnetic field intensity in the air gap is assumed to be uniform, then

$$\int_{\mathcal{C}} H \cdot dl = 2H_g l_g \tag{B.12}$$

$$= 5 \cdot 10^{-4} H_g\,(ampere) \tag{B.13}$$

where l_g is the length of the air gap.

From Eq.B.10 and Eq.B.12, the following relationship is obtained for the current, i

$$i = \frac{H_g l_g}{N} \tag{B.14}$$

$$= 2.5 \cdot 10^{-6} H_g\,(ampere) \tag{B.15}$$

Since the magnetic field intensity, H_g, is related to the magnetic flux density, B_g, by the following relationship

$$H_g = \frac{B_g}{\mu_0} \tag{B.16}$$

and substituting the expression for i, the power, P is given by

$$P = 2NA_g \left(\frac{H_g l_g}{N}\right) \frac{dB_g}{dt}$$

$$= \frac{2}{\mu_0} A_g l_g B_g \frac{dB_g}{dt} \tag{B.17}$$

$$= 0.0387\, B_g \frac{dB_g}{dt}\,(watt) \tag{B.18}$$

The energy stored in the air gap during the transition from 0 to a steady state value, B_{ss}, as the current changes from 0 to a steady state value, i_{ss}, is given by

$$\begin{aligned} W_m &= \int P\,dt \\ &= \frac{2}{\mu_0} A_g l_g \int_0^{B_{ss}} B_g d(B_g) \\ &= \frac{A_g l_g B_g^2}{\mu_0} && \text{(B.19)} \\ &= 0.0193\, B_g^2\, (Joule) && \text{(B.20)} \end{aligned}$$

Assuming no energy losses, the attractive magnetic force on the rotor due to the electromagnet is given by

$$\begin{aligned} F &= \left| -\frac{\partial W}{\partial l_g} \right| \\ &= \frac{A_g B_g^2}{\mu_0} && \text{(B.21)} \\ &= 77.3810\, B_g^2\, (newton) && \text{(B.22)} \end{aligned}$$

and using the relationship of Eq.B.14,

$$\begin{aligned} F &= \frac{A_g}{\mu_0} \left(\frac{\mu_0 N i}{l_g} \right)^2 \\ &= \frac{\mu_0 A_g N^2 i^2}{l_g^2} \\ &= K \frac{i^2}{l_g^2} && \text{(B.23)} \\ &= 19.6560\, i^2\, (newton) && \text{(B.24)} \end{aligned}$$

where $K = \mu_0 A_g N^2 = 1.23 \cdot 10^{-6}\, Nm^2/A^2$.

Appendix C

Open-loop Matrices: Numerical Results

The following are the numerical results of the open-loop transfer function matrices used in *Chap.4*:

1. from $\mathbf{u}$ to $\mathbf{x}$,

$$[s\mathbf{I}-\mathbf{A}]^{-1} = \begin{bmatrix} \mathbf{a}_1 & \mathbf{a}_2 & \mathbf{a}_3 & \mathbf{a}_4 & \mathbf{a}_5 & \mathbf{a}_6 & \mathbf{a}_7 & \mathbf{a}_8 \end{bmatrix}$$

where

$$\mathbf{a}_1 = \begin{bmatrix} \frac{s\left(s^6+8603.0s^4-13645000000.0s^2+2.5006\times10^{14}\right)}{s^8-10496.0s^6-13809000000.0s^4+5.989\times10^{14}s^2-4.7010\times10^{18}} \\ \frac{-1.0s\left(57139000.0s^2-29059000000000.0+2256.1s^4\right)}{s^8-10496.0s^6-13809000000.0s^4+5.989\times10^{14}s^2-4.7010\times10^{18}} \\ \frac{-239220.0s^4+28319000000.0s^2-4.910\times10^{14}}{s^8-10496.0s^6-13809000000.0s^4+5.989\times10^{14}s^2-4.7010\times10^{18}} \\ \frac{239220.0s^4-28319000000.0s^2+4.910\times10^{14}}{s^8-10496.0s^6-13809000000.0s^4+5.989\times10^{14}s^2-4.7010\times10^{18}} \\ \frac{19099.0s^6+164030000.0s^4-2.5983\times10^{14}s^2+4.7010\times10^{18}}{s^8-10496.0s^6-13809000000.0s^4+5.989\times10^{14}s^2-4.7010\times10^{18}} \\ \frac{\left(-57139000.0s^2+29059000000000.0-2256.1s^4\right)s^2}{s^8-10496.0s^6-13809000000.0s^4+5.989\times10^{14}s^2-4.7010\times10^{18}} \\ \frac{-1.0s\left(239220.0s^4-28319000000.0s^2+4.910\times10^{14}\right)}{s^8-10496.0s^6-13809000000.0s^4+5.989\times10^{14}s^2-4.7010\times10^{18}} \\ \frac{s\left(239220.0s^4-28319000000.0s^2+4.910\times10^{14}\right)}{s^8-10496.0s^6-13809000000.0s^4+5.989\times10^{14}s^2-4.7010\times10^{18}} \end{bmatrix}$$

$$
\mathbf{a}_2 = \begin{bmatrix}
\frac{-1.0s\left(57139000.0s^2-29059000000000.0+2256.1s^4\right)}{s^8-10496.0s^6-13809000000.0s^4+5.989\times10^{14}s^2-4.7010\times10^{18}} \\
\frac{s\left(s^6+8603.0s^4-13645000000.0s^2+2.5006\times10^{14}\right)}{s^8-10496.0s^6-13809000000.0s^4+5.989\times10^{14}s^2-4.7010\times10^{18}} \\
\frac{239220.0s^4-28318000000.0s^2+4.910\times10^{14}}{s^8-10496.0s^6-13809000000.0s^4+5.989\times10^{14}s^2-4.7010\times10^{18}} \\
\frac{-239220.0s^4+28318000000.0s^2-4.910\times10^{14}}{s^8-10496.0s^6-13809000000.0s^4+5.989\times10^{14}s^2-4.7010\times10^{18}} \\
\frac{\left(-57139000.0s^2+29059000000000.0-2256.1s^4\right)s^2}{s^8-10496.0s^6-13809000000.0s^4+5.989\times10^{14}s^2-4.7010\times10^{18}} \\
\frac{164040000.0s^4-2.5984\times10^{14}s^2+19099.0s^6+4.7010\times10^{18}}{s^8-10496.0s^6-13809000000.0s^4+5.989\times10^{14}s^2-4.7010\times10^{18}} \\
\frac{s\left(239220.0s^4-28318000000.0s^2+4.910\times10^{14}\right)}{s^8-10496.0s^6-13809000000.0s^4+5.989\times10^{14}s^2-4.7010\times10^{18}} \\
\frac{-1.0s\left(239220.0s^4-28318000000.0s^2+4.910\times10^{14}\right)}{s^8-10496.0s^6-13809000000.0s^4+5.989\times10^{14}s^2-4.7010\times10^{18}}
\end{bmatrix}
$$

$$
\mathbf{a}_3 = \begin{bmatrix}
\frac{-1442100.0s^4+170700000000.0s^2-2.4660\times10^{15}}{s^8-10496.0s^6-13809000000.0s^4+5.989\times10^{14}s^2-4.7010\times10^{18}} \\
\frac{1442100.0s^4-170700000000.0s^2+2.4660\times10^{15}}{s^8-10496.0s^6-13809000000.0s^4+5.989\times10^{14}s^2-4.7010\times10^{18}} \\
\frac{s\left(s^6-24096.0s^4-193740000.0s^2+5320900000000.0\right)}{s^8-10496.0s^6-13809000000.0s^4+5.989\times10^{14}s^2-4.7010\times10^{18}} \\
\frac{s\left(-4372300000.0s^2+115130.0s^4+40982000000000.0\right)}{s^8-10496.0s^6-13809000000.0s^4+5.989\times10^{14}s^2-4.7010\times10^{18}} \\
\frac{-1.0s\left(1442100.0s^4-170700000000.0s^2+2.4660\times10^{15}\right)}{s^8-10496.0s^6-13809000000.0s^4+5.989\times10^{14}s^2-4.7010\times10^{18}} \\
\frac{s\left(1442100.0s^4-170700000000.0s^2+2.4660\times10^{15}\right)}{s^8-10496.0s^6-13809000000.0s^4+5.989\times10^{14}s^2-4.7010\times10^{18}} \\
\frac{-13600.0s^6+13616000000.0s^4-5.458\times10^{14}s^2+4.7010\times10^{18}}{s^8-10496.0s^6-13809000000.0s^4+5.989\times10^{14}s^2-4.7010\times10^{18}} \\
\frac{\left(-4372300000.0s^2+115130.0s^4+40982000000000.0\right)s^2}{s^8-10496.0s^6-13809000000.0s^4+5.989\times10^{14}s^2-4.7010\times10^{18}}
\end{bmatrix}
$$

$$
\mathbf{a}_4 = \begin{bmatrix}
\frac{1442100.0s^4-170700000000.0s^2+2.4660\times10^{15}}{s^8-10496.0s^6-13809000000.0s^4+5.989\times10^{14}s^2-4.7010\times10^{18}} \\
\frac{-1442100.0s^4+170700000000.0s^2-2.4660\times10^{15}}{s^8-10496.0s^6-13809000000.0s^4+5.989\times10^{14}s^2-4.7010\times10^{18}} \\
\frac{s\left(-4372300000.0s^2+115130.0s^4+40982000000000.0\right)}{s^8-10496.0s^6-13809000000.0s^4+5.989\times10^{14}s^2-4.7010\times10^{18}} \\
\frac{s\left(s^6-24096.0s^4-193740000.0s^2+5320900000000.0\right)}{s^8-10496.0s^6-13809000000.0s^4+5.989\times10^{14}s^2-4.7010\times10^{18}} \\
\frac{s\left(1442100.0s^4-170700000000.0s^2+2.4660\times10^{15}\right)}{s^8-10496.0s^6-13809000000.0s^4+5.989\times10^{14}s^2-4.7010\times10^{18}} \\
\frac{-1.0s\left(1442100.0s^4-170700000000.0s^2+2.4660\times10^{15}\right)}{s^8-10496.0s^6-13809000000.0s^4+5.989\times10^{14}s^2-4.7010\times10^{18}} \\
\frac{\left(-4372300000.0s^2+115130.0s^4+40982000000000.0\right)s^2}{s^8-10496.0s^6-13809000000.0s^4+5.989\times10^{14}s^2-4.7010\times10^{18}} \\
\frac{13615000000.0s^4-13600.0s^6-5.458\times10^{14}s^2+4.7010\times10^{18}}{s^8-10496.0s^6-13809000000.0s^4+5.989\times10^{14}s^2-4.7010\times10^{18}}
\end{bmatrix}
$$

$$
\mathbf{a}_5 = \begin{bmatrix}
\frac{s^6+8352.0s^4-13615000000.0s^2+2.4962\times10^{14}}{s^8-10496.0s^6-13809000000.0s^4+5.989\times10^{14}s^2-4.7010\times10^{18}} \\
\frac{-2005.1s^4-86848000.0s^2+29487000000000.0}{s^8-10496.0s^6-13809000000.0s^4+5.989\times10^{14}s^2-4.7010\times10^{18}} \\
\frac{-1.0s\left(11.202s^4-1326100.0s^2+19157000000.0\right)}{s^8-10496.0s^6-13809000000.0s^4+5.989\times10^{14}s^2-4.7010\times10^{18}} \\
\frac{s\left(11.202s^4-1326100.0s^2+19157000000.0\right)}{s^8-10496.0s^6-13809000000.0s^4+5.989\times10^{14}s^2-4.7010\times10^{18}} \\
\frac{s\left(s^6+8352.0s^4-13615000000.0s^2+2.4962\times10^{14}\right)}{s^8-10496.0s^6-13809000000.0s^4+5.989\times10^{14}s^2-4.7010\times10^{18}} \\
\frac{-1.0s\left(2005.1s^4+86848000.0s^2-29487000000000.0\right)}{s^8-10496.0s^6-13809000000.0s^4+5.989\times10^{14}s^2-4.7010\times10^{18}} \\
\frac{\left(-11.202s^4+1326100.0s^2-19157000000.0\right)s^2}{s^8-10496.0s^6-13809000000.0s^4+5.989\times10^{14}s^2-4.7010\times10^{18}} \\
\frac{\left(11.202s^4-1326100.0s^2+19157000000.0\right)s^2}{s^8-10496.0s^6-13809000000.0s^4+5.989\times10^{14}s^2-4.7010\times10^{18}}
\end{bmatrix}
$$

$$
\mathbf{a}_6 = \begin{bmatrix}
\frac{-2005.1s^4-86848000.0s^2+29487000000000.0}{s^8-10496.0s^6-13809000000.0s^4+5.989\times10^{14}s^2-4.7010\times10^{18}} \\
\frac{s^6+8352.0s^4-13615000000.0s^2+2.4962\times10^{14}}{s^8-10496.0s^6-13809000000.0s^4+5.989\times10^{14}s^2-4.7010\times10^{18}} \\
\frac{s\left(11.202s^4-1326100.0s^2+19157000000.0\right)}{s^8-10496.0s^6-13809000000.0s^4+5.989\times10^{14}s^2-4.7010\times10^{18}} \\
\frac{-1.0s\left(11.202s^4-1326100.0s^2+19157000000.0\right)}{s^8-10496.0s^6-13809000000.0s^4+5.989\times10^{14}s^2-4.7010\times10^{18}} \\
\frac{-1.0s\left(2005.1s^4+86848000.0s^2-29487000000000.0\right)}{s^8-10496.0s^6-13809000000.0s^4+5.989\times10^{14}s^2-4.7010\times10^{18}} \\
\frac{s\left(s^6+8352.0s^4-13615000000.0s^2+2.4962\times10^{14}\right)}{s^8-10496.0s^6-13809000000.0s^4+5.989\times10^{14}s^2-4.7010\times10^{18}} \\
\frac{\left(11.202s^4-1326100.0s^2+19157000000.0\right)s^2}{s^8-10496.0s^6-13809000000.0s^4+5.989\times10^{14}s^2-4.7010\times10^{18}} \\
\frac{\left(-11.202s^4+1326100.0s^2-19157000000.0\right)s^2}{s^8-10496.0s^6-13809000000.0s^4+5.989\times10^{14}s^2-4.7010\times10^{18}}
\end{bmatrix}
$$

$$
\mathbf{a}_7 = \begin{bmatrix}
\frac{s\left(11.202s^4-1326100.0s^2+19157000000.0\right)}{s^8-10496.0s^6-13809000000.0s^4+5.989\times10^{14}s^2-4.7010\times10^{18}} \\
\frac{-1.0s\left(11.202s^4-1326100.0s^2+19157000000.0\right)}{s^8-10496.0s^6-13809000000.0s^4+5.989\times10^{14}s^2-4.7010\times10^{18}} \\
\frac{s^6-24347.0s^4-164020000.0s^2+4891800000000.0}{s^8-10496.0s^6-13809000000.0s^4+5.989\times10^{14}s^2-4.7010\times10^{18}} \\
\frac{115380.0s^4-4402200000.0s^2+41411000000000.0}{s^8-10496.0s^6-13809000000.0s^4+5.989\times10^{14}s^2-4.7010\times10^{18}} \\
\frac{\left(11.202s^4-1326100.0s^2+19157000000.0\right)s^2}{s^8-10496.0s^6-13809000000.0s^4+5.989\times10^{14}s^2-4.7010\times10^{18}} \\
\frac{\left(-11.202s^4+1326100.0s^2-19157000000.0\right)s^2}{s^8-10496.0s^6-13809000000.0s^4+5.989\times10^{14}s^2-4.7010\times10^{18}} \\
\frac{s\left(s^6-24347.0s^4-164020000.0s^2+4891800000000.0\right)}{s^8-10496.0s^6-13809000000.0s^4+5.989\times10^{14}s^2-4.7010\times10^{18}} \\
\frac{s\left(115380.0s^4-4402200000.0s^2+41411000000000.0\right)}{s^8-10496.0s^6-13809000000.0s^4+5.989\times10^{14}s^2-4.7010\times10^{18}}
\end{bmatrix}
$$

$$
\mathbf{a}_8 = \begin{bmatrix}
\frac{-1.0s\left(11.202s^4-1326100.0s^2+19157000000.0\right)}{s^8-10496.0s^6-13809000000.0s^4+5.989\times10^{14}s^2-4.7010\times10^{18}} \\
\frac{s\left(11.202s^4-1326100.0s^2+19157000000.0\right)}{s^8-10496.0s^6-13809000000.0s^4+5.989\times10^{14}s^2-4.7010\times10^{18}} \\
\frac{115380.0s^4-4402200000.0s^2+41411000000000.0}{s^8-10496.0s^6-13809000000.0s^4+5.989\times10^{14}s^2-4.7010\times10^{18}} \\
\frac{s^6-24347.0s^4-164020000.0s^2+4891800000000.0}{s^8-10496.0s^6-13809000000.0s^4+5.989\times10^{14}s^2-4.7010\times10^{18}} \\
\frac{\left(-11.202s^4+1326100.0s^2-19157000000.0\right)s^2}{s^8-10496.0s^6-13809000000.0s^4+5.989\times10^{14}s^2-4.7010\times10^{18}} \\
\frac{\left(11.202s^4-1326100.0s^2+19157000000.0\right)s^2}{s^8-10496.0s^6-13809000000.0s^4+5.989\times10^{14}s^2-4.7010\times10^{18}} \\
\frac{s\left(115380.0s^4-4402200000.0s^2+41411000000000.0\right)}{s^8-10496.0s^6-13809000000.0s^4+5.989\times10^{14}s^2-4.7010\times10^{18}} \\
\frac{s\left(s^6-24347.0s^4-164020000.0s^2+4891800000000.0\right)}{s^8-10496.0s^6-13809000000.0s^4+5.989\times10^{14}s^2-4.7010\times10^{18}}
\end{bmatrix}
$$

2. from $\mathbf{F}_d$ to $\mathbf{x}$,

$$
[s\mathbf{I}-\mathbf{A}]^{-1}\mathbf{B} = \begin{bmatrix} \mathbf{b}_1 & \mathbf{b}_2 & \mathbf{b}_3 & \mathbf{b}_4 \end{bmatrix},
$$

where

$$
\mathbf{b}_1 = \begin{bmatrix}
\frac{2.3873s^6+20504.0s^4-32479000000.0s^2+5.8760\times10^{14}}{s^8-10496.0s^6-13809000000.0s^4+5.989\times10^{14}s^2-4.7010\times10^{18}} \\
-\frac{0.28201s^6+7142.1s^4-3632300000.0s^2+1000000000.0}{s^8-10496.0s^6-13809000000.0s^4+5.989\times10^{14}s^2-4.7010\times10^{18}} \\
\frac{-2.6693s\left(11.202s^4-1326100.0s^2+19157000000.0\right)}{s^8-10496.0s^6-13809000000.0s^4+5.989\times10^{14}s^2-4.7010\times10^{18}} \\
\frac{2.6693s\left(11.202s^4-1326100.0s^2+19157000000.0\right)}{s^8-10496.0s^6-13809000000.0s^4+5.989\times10^{14}s^2-4.7010\times10^{18}} \\
\frac{\left(2.3873s^6+20504.0s^4-32479000000.0s^2+5.8760\times10^{14}\right)s}{s^8-10496.0s^6-13809000000.0s^4+5.989\times10^{14}s^2-4.7010\times10^{18}} \\
-\frac{\left(0.28201s^6+7142.1s^4-3632300000.0s^2+1000000000.0\right)s}{s^8-10496.0s^6-13809000000.0s^4+5.989\times10^{14}s^2-4.7010\times10^{18}} \\
\frac{\left(-29.901s^4+3539800.0s^2-51136000000.0\right)s^2}{s^8-10496.0s^6-13809000000.0s^4+5.989\times10^{14}s^2-4.7010\times10^{18}} \\
\frac{\left(29.901s^4-3539800.0s^2+51136000000.0\right)s^2}{s^8-10496.0s^6-13809000000.0s^4+5.989\times10^{14}s^2-4.7010\times10^{18}}
\end{bmatrix}
$$

$$
\mathrm{b}_2 = \begin{bmatrix}
-\dfrac{0.28201s^6+7142.1s^4-3632300000.0s^2+1000000000.0}{s^8-10496.0s^6-13809000000.0s^4+5.989\times10^{14}s^2-4.7010\times10^{18}} \\[2ex]
\dfrac{2.3873s^6+20504.0s^4-32479000000.0s^2+5.8760\times10^{14}}{s^8-10496.0s^6-13809000000.0s^4+5.989\times10^{14}s^2-4.7010\times10^{18}} \\[2ex]
\dfrac{2.6693s\left(11.202s^4-1326100.0s^2+19157000000.0\right)}{s^8-10496.0s^6-13809000000.0s^4+5.989\times10^{14}s^2-4.7010\times10^{18}} \\[2ex]
\dfrac{-2.6693s\left(11.202s^4-1326100.0s^2+19157000000.0\right)}{s^8-10496.0s^6-13809000000.0s^4+5.989\times10^{14}s^2-4.7010\times10^{18}} \\[2ex]
-\dfrac{\left(0.28201s^6+7142.1s^4-3632300000.0s^2+1000000000.0\right)s}{s^8-10496.0s^6-13809000000.0s^4+5.989\times10^{14}s^2-4.7010\times10^{18}} \\[2ex]
\dfrac{\left(2.3873s^6+20504.0s^4-32479000000.0s^2+5.8760\times10^{14}\right)s}{s^8-10496.0s^6-13809000000.0s^4+5.989\times10^{14}s^2-4.7010\times10^{18}} \\[2ex]
\dfrac{\left(29.901s^4-3539800.0s^2+51136000000.0\right)s^2}{s^8-10496.0s^6-13809000000.0s^4+5.989\times10^{14}s^2-4.7010\times10^{18}} \\[2ex]
\dfrac{\left(-29.901s^4+3539800.0s^2-51136000000.0\right)s^2}{s^8-10496.0s^6-13809000000.0s^4+5.989\times10^{14}s^2-4.7010\times10^{18}}
\end{bmatrix}
$$

$$
\mathrm{b}_3 = \begin{bmatrix}
\dfrac{-12.873s\left(11.202s^4-1326100.0s^2+19157000000.0\right)}{s^8-10496.0s^6-13809000000.0s^4+5.989\times10^{14}s^2-4.7010\times10^{18}} \\[2ex]
\dfrac{12.873s\left(11.202s^4-1326100.0s^2+19157000000.0\right)}{s^8-10496.0s^6-13809000000.0s^4+5.989\times10^{14}s^2-4.7010\times10^{18}} \\[2ex]
-\dfrac{1.3600s^6-1361500.0s^4+50460000000.0s^2-4.7011\times10^{14}}{s^8-10496.0s^6-13809000000.0s^4+5.989\times10^{14}s^2-4.7010\times10^{18}} \\[2ex]
\dfrac{\left(11.513s^4-437230.0s^2+4098600000.0\right)s^2}{s^8-10496.0s^6-13809000000.0s^4+5.989\times10^{14}s^2-4.7010\times10^{18}} \\[2ex]
\dfrac{\left(-144.20s^4+17071000.0s^2-246610000000.0\right)s^2}{s^8-10496.0s^6-13809000000.0s^4+5.989\times10^{14}s^2-4.7010\times10^{18}} \\[2ex]
\dfrac{\left(144.20s^4-17071000.0s^2+246610000000.0\right)s^2}{s^8-10496.0s^6-13809000000.0s^4+5.989\times10^{14}s^2-4.7010\times10^{18}} \\[2ex]
-\dfrac{\left(1.3600s^6-1361500.0s^4+50460000000.0s^2-4.7011\times10^{14}\right)s}{s^8-10496.0s^6-13809000000.0s^4+5.989\times10^{14}s^2-4.7010\times10^{18}} \\[2ex]
\dfrac{\left(11.513s^4-437230.0s^2+4098600000.0\right)s^3}{s^8-10496.0s^6-13809000000.0s^4+5.989\times10^{14}s^2-4.7010\times10^{18}}
\end{bmatrix}
$$

$$
\mathbf{b}_4 = \begin{bmatrix}
\frac{12.873s\left(11.202s^4-1326100.0s^2+19157000000.0\right)}{s^8-10496.0s^6-13809000000.0s^4+5.989\times10^{14}s^2-4.7010\times10^{18}} \\
\frac{-12.873s\left(11.202s^4-1326100.0s^2+19157000000.0\right)}{s^8-10496.0s^6-13809000000.0s^4+5.989\times10^{14}s^2-4.7010\times10^{18}} \\
\frac{\left(11.513s^4-437230.0s^2+4098600000.0\right)s^2}{s^8-10496.0s^6-13809000000.0s^4+5.989\times10^{14}s^2-4.7010\times10^{18}} \\
-\frac{1.3600s^6-1361500.0s^4+50460000000.0s^2-4.7011\times10^{14}}{s^8-10496.0s^6-13809000000.0s^4+5.989\times10^{14}s^2-4.7010\times10^{18}} \\
\frac{\left(144.20s^4-17071000.0s^2+246610000000.0\right)s^2}{s^8-10496.0s^6-13809000000.0s^4+5.989\times10^{14}s^2-4.7010\times10^{18}} \\
\frac{\left(-144.20s^4+17071000.0s^2-246610000000.0\right)s^2}{s^8-10496.0s^6-13809000000.0s^4+5.989\times10^{14}s^2-4.7010\times10^{18}} \\
\frac{\left(11.513s^4-437230.0s^2+4098600000.0\right)s^3}{s^8-10496.0s^6-13809000000.0s^4+5.989\times10^{14}s^2-4.7010\times10^{18}} \\
-\frac{\left(1.3600s^6-1361500.0s^4+50460000000.0s^2-4.7011\times10^{14}\right)s}{s^8-10496.0s^6-13809000000.0s^4+5.989\times10^{14}s^2-4.7010\times10^{18}}
\end{bmatrix}
$$

3. from $\mathbf{d}$ to $\mathbf{x}$,

$$
[s\mathbf{I}-\mathbf{A}]^{-1}\,\mathbf{L} = \begin{bmatrix} \mathbf{c}_1 & \mathbf{c}_2 \end{bmatrix}
$$

where

$$
\mathbf{c}_1 = \begin{bmatrix}
\frac{0.65305s^6+4940.9s^4-8913500000.0s^2+1.7056\times10^{14}}{s^8-10496.0s^6-13809000000.0s^4+5.989\times10^{14}s^2-4.7010\times10^{18}} \\
\frac{829.0s^4-3542700000.0s^2+83169000000000.0+0.25604s^6}{s^8-10496.0s^6-13809000000.0s^4+5.989\times10^{14}s^2-4.7010\times10^{18}} \\
\frac{-0.39701s\left(11.202s^4-1326100.0s^2+19157000000.0\right)}{s^8-10496.0s^6-13809000000.0s^4+5.989\times10^{14}s^2-4.7010\times10^{18}} \\
\frac{0.39701s\left(11.202s^4-1326100.0s^2+19157000000.0\right)}{s^8-10496.0s^6-13809000000.0s^4+5.989\times10^{14}s^2-4.7010\times10^{18}} \\
\frac{\left(0.65305s^6+4940.9s^4-8913500000.0s^2+1.7056\times10^{14}\right)s}{s^8-10496.0s^6-13809000000.0s^4+5.989\times10^{14}s^2-4.7010\times10^{18}} \\
\frac{\left(829.0s^4-3542700000.0s^2+83169000000000.0+0.25604s^6\right)s}{s^8-10496.0s^6-13809000000.0s^4+5.989\times10^{14}s^2-4.7010\times10^{18}} \\
\frac{\left(-4.4473s^4+526470.0s^2-7605500000.0\right)s^2}{s^8-10496.0s^6-13809000000.0s^4+5.989\times10^{14}s^2-4.7010\times10^{18}} \\
\frac{\left(4.4473s^4-526470.0s^2+7605500000.0\right)s^2}{s^8-10496.0s^6-13809000000.0s^4+5.989\times10^{14}s^2-4.7010\times10^{18}}
\end{bmatrix}
$$

$$
\mathbf{c}_2 = \begin{bmatrix}
\dfrac{-0.39701s\left(11.202s^4-1326100.0s^2+19157000000.0\right)}{s^8-10496.0s^6-13809000000.0s^4+5.989\times10^{14}s^2-4.7010\times10^{18}} \\[2ex]
\dfrac{0.39701s\left(11.202s^4-1326100.0s^2+19157000000.0\right)}{s^8-10496.0s^6-13809000000.0s^4+5.989\times10^{14}s^2-4.7010\times10^{18}} \\[2ex]
\dfrac{0.25604s^6+69115.0s^4-2916900000.0s^2+28296000000000.0}{s^8-10496.0s^6-13809000000.0s^4+5.989\times10^{14}s^2-4.7010\times10^{18}} \\[2ex]
\dfrac{13642.0s^4-1234200000.0s^2+13798000000000.0+0.65305s^6}{s^8-10496.0s^6-13809000000.0s^4+5.989\times10^{14}s^2-4.7010\times10^{18}} \\[2ex]
\dfrac{\left(-4.4473s^4+526470.0s^2-7605500000.0\right)s^2}{s^8-10496.0s^6-13809000000.0s^4+5.989\times10^{14}s^2-4.7010\times10^{18}} \\[2ex]
\dfrac{\left(4.4473s^4-526470.0s^2+7605500000.0\right)s^2}{s^8-10496.0s^6-13809000000.0s^4+5.989\times10^{14}s^2-4.7010\times10^{18}} \\[2ex]
\dfrac{\left(0.25604s^6+69115.0s^4-2916900000.0s^2+28296000000000.0\right)s}{s^8-10496.0s^6-13809000000.0s^4+5.989\times10^{14}s^2-4.7010\times10^{18}} \\[2ex]
\dfrac{\left(13642.0s^4-1234200000.0s^2+13798000000000.0+0.65305s^6\right)s}{s^8-10496.0s^6-13809000000.0s^4+5.989\times10^{14}s^2-4.7010\times10^{18}}
\end{bmatrix}
$$

Bibliography

[1] S.T. Ariaratnam. The vibration of unsymmetrical rotating shafts. In *Journal of Applied Mechanics*, pages 157–60, March 1965.

[2] M Athans. *Lecture Notes: Multivariable Control System II.* MIT, Cambridge, MA, Spring 1994.

[3] H.Ming Chen. Magnetic bearings and flexible rotor dynamics. In *Tribology Transactions*, volume 32, pages 9–15, January 1989.

[4] H.Ming Chen and M.S. Darlow. Design of active magnetic bearings with velocity observer. In *11th Biennial ASME Conference on Mechanical Vibration and Noise*, Boston, 1987.

[5] F.M. Dimentberg. *Flexural Vibrations of Rotating Shafts.* Butterworths, London, 1961.

[6] S. Earnshaw. On the nature of the molecular forces which regulate the constitution of the luminferous ether. In *Trans. Cambridge Phil. Soc.*, volume 7, page 79, 1842.

[7] C.D. Bradfield et al. Performance of an electromagnetic bearing of the vibration control of a supercritical shaft. In *Proceedings for Institute of Mechanical Engineers*, volume 201(C3), pages 201–212, 1987.

[8] Crandall et al. *Dynamics for Electromechanic Systems.* Krieger, Florida, 1982.

[9] J.A. Tichy et al. Geometric effects on eddy current bearing performance. In *Journal of Tribology*, volume 111, pages 209–14, April 89.

[10] Kamal Youcef-Toumi et al. *Implementation of Time Delay Control to Active Magnetic Bearings: Final Report Phase 1.* Massachusetts Institute of Technology, Cambridge, MA, 1989.

[11] R.R. Humphris et al. Effect of control algorithms on magnetic journal bearing properties. In *ASME Journal of Engineering for Gas Turbine and Power*, volume 108, pages 624–632, 1986.

[12] S. Gray S. et al. Magnetic bearings can increase availability, reduce operational and maintenance costs. In *Power Engineering*, volume 94, pages 26–9, January 90.

[13] Edgar J. Gunter Jr. *Dyamic Stability of Rotor-Bearing Systems.* Scientific and Technical Information Division, National Aeronautics and Space Administration, 1966.

[14] Robert G. Loewy and Vincent J. Piarulli. *Dynamics of Rotating Shafts.* The Shock and Vibration Information Center, United States Department of Defense, 1969.

[15] A.S. McAllister. A graphical method for finding the frequency response of non-linear closed-loop systems. In *AIEE Transactions, pt.II (Appl. Ind.)*, volume 80, pages 268–77, 1961.

[16] T. Mizuno and T. Higuchi. Compensation for unbalance in magnetic bearing system. In *Trans. Society of Instrument and Control Engineers*, volume 20 No.12, pages 1095–1101, 1984.

[17] Katsuhiko Ogata. *Modern Control Engineering.* Prentice-Hall, Englewood Cliffs, NJ, 1990.

[18] Arthur Gelb Sc.D. and Wallace E. Vander Velde Sc.D. *Multiple-Input Describing Functions and Nonlinear System Design.* McGraw-Hill Book Company, New York, 1968.

[19] Jean-Jacques E. Slotine and Weiping Li. *Applied Nonlinear Control.* Prentice-Hall, Englewood Cliffs, NJ, 1991.

[20] T.J. Yeh and Kamal Youcef-Toumi. Control and design integration for magnetic bearing systems. In *ASME winter meeting*, March 1994.